

Hyperfine interaction and spin decoherence in quantum dots

INAUGURALDISSERTATION

zur

Erlangung der Würde eines Doktors der Philosophie

vorgelegt der

Philosophisch-Naturwissenschaftlichen Fakultät

der Universität Basel

von

Daniel Joseph Klauser

aus Römerswil (LU)

Basel, 2008

Genehmigt von der Philosophisch-Naturwissenschaftlichen Fakultät auf Antrag
von

Prof. Dr. Daniel Loss
Prof. Dr. Atac Imamoğlu

Basel, den 20. Mai 2008

Prof. Dr. phil. Hans-Peter Hauri
Dekan

Acknowledgements

First of all, I would like to thank Prof. Daniel Loss for being an excellent supervisor of my thesis. Both his guidance and his deep physical understanding have been very valuable. Many ideas presented in this thesis are due to his creative mind. During a large part of my PhD I also profited a lot from the very fruitful collaboration with Bill Coish. He always had an open ear for my ever so frequent questions. His knowledge of the topics discussed in this thesis still vastly exceeds my own. Furthermore I'm grateful to have had the chance to collaborate with the Delft spin-qubit team, namely, Leo Kouwenhoven, Tristan Meunier, Katja Nowack, Ivo Vink and in particular Frank Koppens and Lieven Vandersypen. I guess it is one of the best things that can happen to a theorist, that his results are actually checked in an experiment and – even better as in my case – also confirmed. During my time in the Condensed Matter Theory Group at the University of Basel I experienced not only a stimulating scientific environment but also an active social life. My thanks go to Dan Bohr, Massoud Borhani, Bernd Braunecker, Denis Bulaev, Stefano Chesi, Charles Doiron, Mathias Duckheim, Carlos Egues, Jan Fischer, Oliver Gywat, Sarah Heizmann, Verena Körting, Joerg Lehmann, Beat Röthlisberger, Oleg Shalaev, Pascal Simon, Björn Trauzettel, Mihajlo Vanevic, Robert Zak and in particular my room-mates Mircea Trif and Dimitrije Stepanenko who taught me many things about myself and Swiss people in general. Beyond that I also profited from enlightening discussions with Prof. Guido Burkard, Hans-Andreas Engel, Patrick Maletinsky, Prof. Charles Marcus, and Amir Yacoby.

Last but not least I would like to thank Prof. Atac Imamoglu for many fruitful discussions and for co-refereeing this thesis.

Summary

Hyperfine interaction is a typical example of a topic in physics, that, due to technological advances, experiences a revival. Originally, hyperfine interaction was studied in atomic physics. In atoms, the interaction between the magnetic moments of the electrons and the nucleus leads to the hyperfine structure. The name hyperfine is historically due to the fact that the energy level splittings in atoms due to spin-orbit interaction were discovered first, and referred to as the atomic fine structure. The further splitting of these levels was then named hyperfine structure and the interaction that gives rise to it hyperfine interaction.

In recent years, with the rise of nanotechnology, new structures have been created, one of them being so-called quantum dots. Quantum dots are also called artificial atoms, since, like atoms, they confine electrons to tiny (nanometer-size) regions. As for atoms, there is also hyperfine interaction in quantum dots: the spin of an electron confined to a quantum dot interacts with the lattice nuclei. In contrast to atoms, which have properties that are “given” by nature, the properties of quantum dots can be designed and thus allow to not only study new phenomena, but also open the way for new applications. Quantum computing is one of these applications where quantum dots could play an important role. The basic building block for a quantum computer is a quantum bit (qubit). Like a classical bit a qubit is an ideal two-level system. However, a qubit is a quantum mechanical two-level system instead of a classical one. There are several requirements a quantum-mechanical two-level system has to fulfill to be a good qubit. The requirement central in this thesis is that the two states of the qubit and their superpositions should be long lived. More precisely it is crucial that coherent superpositions of the two states remain coherent for a long time compared to the manipulation time, i.e., that decoherence (the loss of coherence) is sufficiently slow.

One promising candidate for the physical implementation of a qubit is the spin of an electron confined in a quantum dot. In an applied magnetic field the spin component along the field direction forms a natural two-level system. Research in the last few years, parts of which are being presented in this thesis, has shown that the main source of decoherence for spins in quantum dots is the hyperfine interaction with the surrounding nuclei in the host material. Since the wave function of an electron confined to a quantum dot extends over many

sites of the underlying crystal lattice, the electron spin also interacts with many nuclei, in sharp contrast to an electron spin in an atom, which only interacts with a single nucleus.

In this thesis we address several aspects of hyperfine interaction and decoherence in quantum dots. First, we analyze some aspects of the decoherence that arises from the hyperfine interaction. In the case of driven single-spin oscillations we show that hyperfine interaction leads to a universal phase shift and a power-law decay. Both of these effects have been confirmed experimentally. We also find a universal phase shift and a power-law decay for the case of two electron spins in a double quantum dot in the subspace with total spin zero along the quantization axis. The appearance of these effects both in single and in double quantum dots is a consequence of the non-Markovian nature of the nuclear spin bath.

Since the main effect of hyperfine-induced decoherence can be attributed to the uncertainty in the Overhauser field, the effective magnetic field generated by the nuclei at the position of the electron, one strategy to reduce decoherence is to prepare the nuclei in a state with a narrow Overhauser field distribution, i.e., to narrow the nuclear spin state. We propose a method to measure the Overhauser field using the dynamics of the electron spins as a probe. More specifically, we propose to narrow the nuclear spin state by monitoring Rabi oscillations in a double quantum dot.

Hyperfine interaction not only leads to decoherence of the electron spin state, it also provides a mechanism for interaction between the nuclei in the quantum dot. We study the dynamics of the Overhauser field under the mutual interaction between nuclear spins that is mediated by the electron via the hyperfine interaction. At high magnetic fields we find an incomplete decay of the Overhauser field. We further show that the decay of the Overhauser field can be suppressed by measuring the Overhauser field, a clear manifestation of the quantum Zeno effect.

Contents

Acknowledgements	iii
Summary	v
1 Hyperfine interaction and spin decoherence in quantum dots reviewed	1
1.1 Introduction	1
1.2 Basics of hyperfine interaction	2
1.2.1 Isotropic hyperfine interaction	4
1.2.2 Fermi contact hyperfine interaction in quantum dots	5
1.2.3 Anisotropic hyperfine interaction	6
1.3 Structures and materials	6
1.4 Electron spin decoherence in single quantum dots	9
1.5 Singlet-triplet decoherence in double quantum dots	12
1.6 Suppression of hyperfine induced decoherence	13
1.6.1 Polarization	13
1.6.2 Spin echo	14
1.6.3 Nuclear spin state narrowing	14
1.7 Perspectives	16
2 Nuclear spin state narrowing via gate-controlled Rabi oscillations in a double quantum dot	17
2.1 Introduction	17
2.2 Oscillating exchange and ESR	19
2.2.1 Superposition of nuclear-spin eigenstates	21
2.3 State narrowing	23
2.3.1 Description of state narrowing by consecutive pseudo-spin measurements	25
2.3.2 Measurement schemes	27
2.4 Correlation functions in the $S^z = 0$ subspace	31
2.5 Analysis of $\sqrt{\text{SWAP}}$	36
2.6 Conclusion	38

3	Universal phase shift and non-exponential decay of driven single-spin oscillations	39
3.1	Introduction	39
3.2	Single-spin ESR – theory	40
3.3	Power-law decay	43
3.4	Phase shift	45
3.5	Conclusion	47
4	Nuclear spin dynamics and Zeno effect in quantum dots and defect centers	49
4.1	Introduction	49
4.2	Zeno effect	51
4.3	Hamiltonian	54
4.4	Short-time expansion	56
4.4.1	Special case: full polarization	60
4.5	Dyson-series expansion	61
4.6	Generalized master equation	64
4.7	Conclusion	66
A	Drift in δh^z	67
B	Measurement	69
C	Fit procedures	73
D	Asymptotic expansion	77
E	Estimation of dipole-dipole contribution	79
F	Measurement accuracy	81
	Bibliography	85
	Curriculum Vitae	95

Chapter 1

Hyperfine interaction and spin decoherence in quantum dots reviewed

1.1 Introduction

In this chapter we review some of the important aspects of hyperfine interaction for spins in quantum dots. Quantum dots are nanostructures that confine electrons in all spatial directions, leading to quantized energy levels like in an atom. The spin of the confined electrons plays a crucial role in many possible technological applications in the fields of quantum computation [1, 2] and spintronics [3, 4]. The successful implementation of a quantum computer demands that some basic requirements be fulfilled. These are known as the five DiVincenzo criteria [5]. One of these criteria is to have sufficient isolation of the qubit from the environment to reduce the effects of decoherence. A qubit (quantum bit) is quantum mechanical two-level system that serves as the basic building block of a quantum computer, like the bit in a classical computer. When using the spin of an electron confined to quantum dot as a qubit [1], the two spin states along the quantization axis, spin-up and spin-down, form the qubit. The state of the qubit can be destroyed by the environment in two ways: First, the environment can lead to relaxation of the qubit on a timescale T_1 , which is the timescale for spin-flip processes. Secondly, the environment can limit the lifetime of a coherent superposition of spin-up and spin-down states, and the corresponding lifetime T_2 is referred to as the decoherence time.

In the context of spin qubits in quantum dots, the environment is the host material in which the dot is created. The two main mechanisms for decoherence and relaxation in quantum dots are hyperfine interaction and spin-orbit interaction. For the relaxation of spins in quantum dots, hyperfine interaction is not an efficient mechanism since a spin-flip process between the electron spin and a nuclear spin requires the emission of a phonon due to

the difference in magnetic moments of electron and nuclei [6, 7]. The main mechanism responsible for relaxation is spin-orbit interaction. Theoretical calculations show that in GaAs T_1 varies little for B -fields larger than $\sim 5\text{T}$ and is on the order of $10 - 100\mu\text{s}$ [8]. At lower fields the spin-orbit-induced relaxation rate is suppressed by $\sim 1/B^5$ [8,9] and vanishes at $B = 0$ due to the Kramers degeneracy. The phonon-assisted electron-nuclear spin-flip processes lead to a relaxation rate that varies as $1/B^3$ at low fields. Thus, below a certain crossover field, relaxation is dominated by hyperfine-induced relaxation. The crossover was estimated to occur at $B \approx 0.3\text{T}$ and the corresponding T_1 varies between $10^2 - 10^4\text{s}$ for $B < 0.3\text{T}$ [7]. The predicted long T_1 has been confirmed in experiments with the longest T_1 time measured so far being longer than 1s at $B = 1\text{T}$ [10].

For the decoherence time T_2 the situation is very different and hyperfine interaction does play an important role. It was shown in Ref. [8] that, to leading order in spin-orbit interaction, $T_2 = 2T_1$ and thus that the decoherence time due to spin-orbit coupling is also very long. Hyperfine interaction, however, leads to much faster decoherence and it is this hyperfine-induced decoherence which is the focus of this chapter. We start introducing the basics of hyperfine interaction in quantum dots in Sec. 1.2 and discuss material issues in Sec. 1.3. In Sec. 1.4 we discuss decoherence for a single spin in a single dot and in Sec. 1.5 for a double dot with one electron in each dot. Suppression of hyperfine-induced decoherence plays an important role in this thesis and is reviewed in Sec. 1.6.

1.2 Basics of hyperfine interaction

Hyperfine interaction is well known in atomic physics: the magnetic moments of the electrons bound to a nucleus interact with the magnetic moment of that nucleus. This leads to the so-called hyperfine structure, i.e., a small shift of the electron energy levels. Quantum dots, referred to as artificial atoms [11], also confine single electrons. In contrast to atoms, where the nucleus provides the confinement for the electrons, for quantum dots, materials are artificially structured to confine the electrons. This is done by using heterostructures and/or electrostatic gates (see Sec. 1.3 for details). Since the host material for the quantum dots contains many nuclei, the electron confined in a quantum dot interacts with all these nuclei via the hyperfine interaction. The hyperfine interaction is a relativistic correction to the non-relativistic Pauli equation. To derive the relevant hyperfine Hamiltonian we start from the Dirac equation for a relativistic electron in a potential $V(\vec{r})$

$$\mathcal{H} = \vec{\alpha} \cdot \vec{\pi} + \beta mc^2 - eV(\vec{r}). \quad (1.1)$$

Here, m is the electron rest mass, $-e$ the electron charge, $\vec{\pi} = c(\mathbf{p} + e\mathbf{A})$ and

$$\vec{\alpha} = \begin{pmatrix} 0 & \vec{\sigma} \\ \vec{\sigma} & 0 \end{pmatrix}, \beta = \begin{pmatrix} \mathbf{1} & 0 \\ 0 & -\mathbf{1} \end{pmatrix}, \quad (1.2)$$

are the standard 4×4 Dirac matrices ($\vec{\sigma}$ is the vector of Pauli matrices and $\mathbf{1}$ is the 2×2 identity matrix). The Dirac Hamiltonian acts on a 4-component spinor ψ , which we write as being composed of two two-component (Pauli) spinors χ_1 and χ_2 : $\psi = (\chi_1, \chi_2)^T$. The Dirac equation $\mathcal{H}\psi = E\psi$, with energy $E = mc^2 + \epsilon$ may now be written as a pair of coupled linear equations for the Pauli spinors χ_1 and χ_2 :

$$[\epsilon + eV(\vec{r})]\chi_1 - \vec{\sigma} \cdot \vec{\pi}\chi_2 = 0, \quad (1.3)$$

$$-\vec{\sigma} \cdot \vec{\pi}\chi_1 + [2mc^2 + eV(\vec{r}) + \epsilon]\chi_2 = 0. \quad (1.4)$$

From these equations one finds immediately χ_2 in terms of χ_1

$$\chi_2 = \frac{1}{2mc^2 + eV(\vec{r}) + \epsilon} \vec{\sigma} \cdot \vec{\pi}\chi_1, \quad (1.5)$$

and for χ_1 the eigenvalue equation is

$$\left[\vec{\sigma} \cdot \vec{\pi} \frac{1}{2mc^2 + eV(\vec{r}) + \epsilon} \vec{\sigma} \cdot \vec{\pi} - eV(\vec{r}) \right] \chi_1 = \epsilon\chi_1. \quad (1.6)$$

In the non-relativistic regime χ_1 is much larger than χ_2 and they are thus referred to as large and small components, respectively. In the limit $(\epsilon + eV(\vec{r}))/mc^2 \rightarrow 0$ the small component can be neglected (i.e., χ_1 and χ_2 decouple) and by replacing $2mc^2 + eV(\vec{r}) + \epsilon \approx 2mc^2$ one obtains the Pauli equation $H_{\text{Pauli}}\chi_1 = \epsilon\chi_1$, with

$$H_{\text{Pauli}} = \frac{1}{2m} (\vec{p} + e\vec{A})^2 + \frac{e\hbar}{2m} (\vec{\nabla} \times \vec{A}) \cdot \vec{\sigma} - eV(\vec{r}). \quad (1.7)$$

In general, χ_2 is nonzero and couples with χ_1 . It is, however, possible to systematically decouple χ_1 and χ_2 order by order in $1/mc^2$ by successive unitary transformations and thus to derive a Pauli equation that takes into account relativistic corrections. The corresponding method, is known as Foldy-Wouthuysen-transformation [12, 13]. This leads to $H_{\text{FW}}\chi_1 = \epsilon\chi_1$, with

$$H_{\text{FW}} = H_{\text{Pauli}} + \frac{e\hbar}{4m^2c^2} \left[\vec{E} \times (\vec{p} + e\vec{A}) \right] \cdot \vec{\sigma} + \frac{e\hbar^2}{8m^2c^2} \vec{\nabla} \cdot \vec{E}. \quad (1.8)$$

Here, we have introduced the electric field $\vec{E} = -\vec{\nabla}V(\vec{r})$. The Hamiltonian H_{FW} contains the standard kinetic term plus three spin dependent terms

$$H_{\text{spin}} = H_{\text{ihf}} + H_{\text{ahf}} + H_{\text{so}}:$$

$$H_{\text{ihf}} = \frac{e^2 \hbar c^2}{D^2} (\vec{E} \times \vec{A}) \cdot \vec{\sigma}, \quad (1.9)$$

$$H_{\text{ahf}} = \frac{e \hbar c^2}{D} (\vec{\nabla} \times \vec{A}) \cdot \vec{\sigma}, \quad (1.10)$$

$$H_{\text{so}} = \frac{e \hbar c^2}{D^2} (\vec{E} \times \vec{p}) \cdot \vec{\sigma}, \quad (1.11)$$

with $D = 2mc^2$. These three terms describe isotropic hyperfine interaction, anisotropic hyperfine interaction and spin-orbit interaction, respectively. The last term in H_{FW} is the well known Darwin term [14].

For an electron bound to a nucleus the electrostatic potential is of the form

$$V(\vec{r}) = \frac{kZe}{r}, \quad (1.12)$$

with $k = 1/4\pi\epsilon_0$, where $\epsilon_0 \approx 8.85 \cdot 10^{-12} \text{CV}^{-1}\text{m}^{-1}$ is the dielectric constant. For distances shorter than the dimension of the nucleus the electrostatic potential deviates from Eq.(1.12), which will play an important role later on. The vector potential due to the nuclear magnetic moment $\vec{\mu}$ is

$$\vec{A} = \frac{\mu_0}{4\pi} \frac{\vec{\mu} \times \vec{r}}{r^3}, \quad (1.13)$$

with $\mu_0 = 4\pi \cdot 10^{-7} \text{VsA}^{-1}\text{m}^{-1}$. There could, of course, also be an additional term to \vec{A} due to an externally applied magnetic field, which we neglect for the moment.

A more direct but less rigorous way to derive H_{spin} is to solve Eq. (1.6) directly, using the identity $(\vec{\sigma} \cdot \vec{A})(\vec{\sigma} \cdot \vec{B}) = \vec{A} \cdot \vec{B} + i(\vec{A} \times \vec{B}) \cdot \vec{\sigma}$. This immediately yields H_{spin} with the only difference that $D = 2mc^2 + \epsilon + eV(\vec{r}) \approx 2mc^2$, where we have again assumed $(\epsilon + eV(\vec{r}))/mc^2 \ll 1$. There is one problem, though, with this direct derivation: Although it leads to the correct spin-dependent terms, it also yields a non-hermitian term. This term arises because χ_1 and χ_2 have not been decoupled and thus $|\chi_1|^2$ is not fully conserved. In the following we want to look at the two terms describing hyperfine interaction in a bit more detail. We start with the isotropic term which leads to the Fermi contact hyperfine interaction that describes the hyperfine interaction for electrons in an s-type conduction band.

1.2.1 Isotropic hyperfine interaction

To obtain an explicit form for the isotropic hyperfine term we insert the expressions $V(\vec{r})$ and \vec{A} , and use the vector identity $\vec{r} \times (\vec{\mu} \times \vec{r}) = \vec{\mu}(\vec{r} \cdot \vec{r}) - \vec{r}(\vec{\mu} \cdot \vec{r})$. For D we use the form obtained in the direct derivation of H_{spin} , i.e., $D =$

$2mc^2 + \epsilon + kZe^2/r$. By introducing the nuclear length scale $r_0 = kZe^2/2mc^2 \approx 1.5 \cdot 10^{-15} \text{Zm}$ we may write for $\epsilon \ll mc^2$

$$H_{\text{ihf}} = \frac{\mu_0 \mu_B}{4\pi r^6} \frac{r_0}{(1 + \frac{r_0}{r})^2} [r^2 \vec{\mu} \cdot \vec{\sigma} - (\vec{\sigma} \cdot \vec{r})(\vec{\mu} \cdot \vec{r})], \quad (1.14)$$

with the Bohr magneton $\mu_B = e\hbar/2m$. Evaluating the matrix elements for H_{ihf} with respect to the electron wave functions $\phi_i(\vec{r})$ and $\phi_j(\vec{r})$ gives

$$\langle \phi_i | H_{\text{ihf}} | \phi_j \rangle = \frac{\mu_0 \mu_B}{4\pi} \int_0^\infty dr \frac{r_0}{(r + r_0)^2} f(\vec{r}) \quad (1.15)$$

$$f(\vec{r}) = \int d\Omega \phi_i^*(\vec{r}) [\vec{\sigma} \cdot \vec{\mu} - (\vec{\sigma} \cdot \vec{r})(\vec{\mu} \cdot \vec{r})/r^2] \phi_j(\vec{r}). \quad (1.16)$$

Under the assumption that the wave functions $\phi_i(\vec{r})$ vary slowly on the nuclear length scale, we may write

$$\int_0^\infty dr \frac{r_0}{(r + r_0)^2} f(\vec{r}) \approx f(r=0) \int_0^\infty dr \frac{r_0}{(r + r_0)^2} = f(0). \quad (1.17)$$

The angular integrals in Eq. (1.16) give 4π and $4\pi \vec{\sigma} \cdot \vec{\mu}/3$, respectively, for s-type orbitals ϕ_i , leading to

$$\langle \phi_i | H_{\text{ihf}} | \phi_j \rangle \approx \frac{2\mu_0 \mu_B}{3} \vec{\sigma} \cdot \vec{\mu}. \quad (1.18)$$

Thus, for s-type orbitals we may rewrite H_{ihf} in a simplified form that leads to the same matrix elements and is referred to as the Fermi contact hyperfine interaction [15]:

$$H_{\text{Fhf}} = \frac{2\mu_0}{3} g_I \mu_N \mu_B \delta(\vec{r}) \vec{\sigma} \cdot \vec{I}. \quad (1.19)$$

Here, we have used $\vec{\mu} = g_I \mu_N \vec{I}$, with the nuclear g -factor g_I and the nuclear magneton $\mu_N = e\hbar/2m_p = 5.05 \times 10^{-27} \text{J/T}$. We note that for p-orbitals $f(0) = 0$ and thus $\langle \phi_i | H_{\text{ihf}} | \phi_j \rangle \approx 0$. For the derivation of H_{Fhf} we used $D = 2mc^2 + \epsilon + kZe^2/r$, as obtained in the direct derivation of H_{spin} . In this way the divergence of the Coulomb potential at small r is automatically regularized. If one works from H_{FW} this has to be done by hand by adjusting the electrostatic potential to $V(\vec{r}) = kZe/(r + r_0)$.

1.2.2 Fermi contact hyperfine interaction in quantum dots

In contrast to an atom, an electron confined to a quantum dot interacts with many lattice nuclei. Thus, the Hamiltonian describing the Fermi contact hyperfine interaction with all these nuclei is of the form ($\vec{S} = \vec{\sigma}/2$)

$$H_{\text{Fhf}} = \frac{4\mu_0}{3} g_I \mu_N \mu_B \sum_l \delta(\vec{r}_l) \vec{S} \cdot \vec{I}_l. \quad (1.20)$$

The most relevant case on which we will focus in this thesis, is an electron in the orbital ground state $\phi_0(\vec{r})$ of a quantum dot with an orbital level spacing that is much larger than the typical hyperfine energy scale. In this case, it is appropriate to derive an effective hyperfine spin Hamiltonian for the subspace of the orbital ground state

$$H_{\text{QDhf}} = \langle \phi_0 | H_{\text{ihf}} | \phi_0 \rangle = \frac{4\mu_0}{3} g_I \mu_N \mu_B \sum_l |\phi_0(\vec{r}_l)|^2 \vec{S} \cdot \vec{I}_l \quad (1.21)$$

The electron ground-state wave function $\phi_0(\vec{r})$ may now be written as the product of the $\vec{k} = 0$ Bloch function amplitude u_0 and a slowly varying envelope part $F(\vec{r})$: $\phi_0(\vec{r}_l) = u_0 F(\vec{r}_l)$, where the envelope wave function satisfies the normalization condition $\int d^3r |F(\vec{r})|^2 = 1$. With this the effective hyperfine spin Hamiltonian may be written as

$$H_{\text{QDhf}} = \vec{S} \cdot \vec{h}; \quad \vec{h} = \sum_l A_l \vec{I}_l; \quad A_l = A v_0 |F(\vec{r}_l)|^2, \quad (1.22)$$

where v_0 is the volume of a primitive crystal unit cell and the hyperfine coupling strength A is given by

$$A = \frac{4\mu_0}{3} g_I \mu_N \mu_B |u_0|^2. \quad (1.23)$$

The hyperfine interaction in a quantum dot with s-type conduction band electrons is thus of a Heisenberg form $\vec{S} \cdot \vec{h}$, where the effective magnetic field \vec{h} induced by the nuclei is referred to as the Overhauser field.

1.2.3 Anisotropic hyperfine interaction

For s-type conduction band electrons the anisotropic term H_{ahf} is small relative to the isotropic term H_{ihf} . The studies of electron spin decoherence in quantum dots have thus been focused on the effect of the Fermi contact interaction as given in H_{QDhf} . The situation is different for hole spins confined in quantum dots, since the p-type valence band both reduces the contact term and enhances the anisotropic interaction.

1.3 Structures and materials

In the last fifteen years many different types of quantum dots in various materials have been developed [16–37]. A review on quantum dots can be found in Ref. [22] and a more recent review focussing on spins in few-electron quantum dot in Ref. [37]. In the context of hyperfine interaction two properties of a quantum dot play an important role. One is the host material, which, through the nuclear magnetic moment $\mu_I = g_I I$ and the type of Bloch functions, determines the strength of the hyperfine coupling A . The other one is the spatial

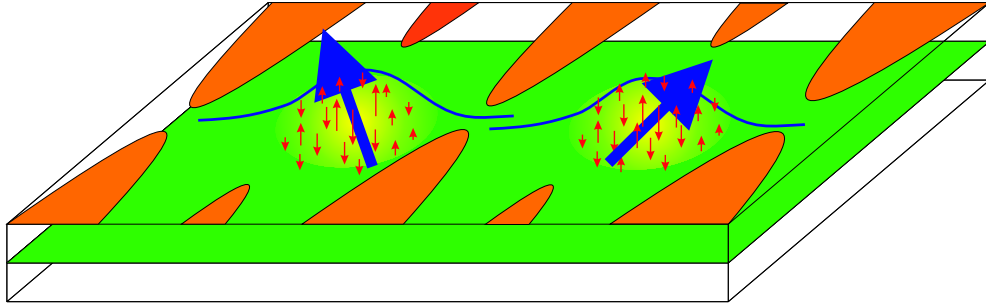


Figure 1.1: A double quantum dot. Top-gates are set to a voltage configuration that confines the electrons in the two-dimensional electron gas (green) to quantum dots (yellow). The blue line indicates the envelope wave function of the electron (blue arrow). The hyperfine interaction with a particular nuclear spins (red arrows) is proportional to the envelope wave function squared at the position of the nuclei. Thus the nuclear spins in the center are drawn bigger since they couple stronger to the electron spin.

dependence of the hyperfine coupling constants A_I . The spatial dependence of the A_I is determined by the envelope wave function of the confined electron.

Let us first dwell on the properties of the host material. In Table 1.1 we give the important properties for spin-carrying stable nuclei that are relevant to semiconductor materials [38]. Both the total nuclear spin quantum number I and the nuclear magnetic moment μ_I vary considerably. The materials most frequently used for quantum dots are GaAs and InAs. For these isotopes there are estimates [39, 40] of the hyperfine coupling constant A , also given in Table 1.1.

As mentioned above there are many different types of quantum dots. An often used structure are so called lateral quantum dots (see Fig. 1.1). A heterostructure such as GaAs/AlGaAs creates a 2-dimensional electron gas (2DEG) at the interface. Engineering electrostatic gates on the surface creates an electrostatic potential that pushes away the electrons underneath the gates and by this allows to confine single electrons. These lateral quantum dots are disk-shaped with the thickness of the disk being on the order of 10nm, while the diameter is typically on the order of 100nm. The harmonic electrostatic potential leads to a Gaussian envelope wavefunction in the plane of the 2DEG. Another often used structure are self-assembled InAs dots. These self-assembled dots are in general less symmetric and their size is a few tens of nanometers in all directions. Recently, single electron quantum dots have also been achieved in 1-dimensional structures such as nanotubes or nanowires. In nanowires the dots can either be disk-shaped or rather have the form of a cylinder. Another quantum-dot related structure are defect centers where the confinement in all three dimensions is provided by the electrostatic potential of the center.

isotope	natural abundance (%)	I	μ_I/μ_N	$A[\mu eV]$
^{13}C	1.11	1/2	0.7024	
^{14}N	99.63	1	0.4038	
^{15}N	0.37	1/2	-0.2832	
^{27}Al	100	5/2	3.6415	
^{29}Si	4.70	1/2	-0.5553	0.1
^{31}P	100	1/2	1.1316	
^{33}S	0.76	3/2	0.6433	
^{67}Zn	4.11	5/2	0.8754	
^{69}Ga	60.4	3/2	2.0166	74
^{71}Ga	39.6	3/2	2.5623	96
^{73}Ge	7.76	9/2	-0.8795	
^{75}As	100	3/2	1.4395	86
^{77}Se	7.58	1/2	0.5350	
^{111}Cd	12.75	1/2	-0.5949	
^{113}Cd	12.26	1/2	-0.6223	
^{113}In	4.28	9/2	5.5289	170
^{115}In	95.72	9/2	5.5408	170
^{121}Sb	57.25	5/2	3.3634	
^{123}Sb	42.75	7/2	2.5498	
^{123}Te	0.87	1/2	-0.7369	
^{125}Te	6.99	1/2	-0.8885	
^{199}Hg	16.84	1/2	0.5059	
^{201}Hg	13.22	3/2	-0.5602	

Table 1.1: This table gives the properties for spin-carrying stable nuclei that are relevant to semiconductor materials [38]. The materials most frequently used for quantum dots are GaAs, InAs and Si. For these isotopes there are estimates [39–41] of the hyperfine coupling constant A . For the other materials we give the nuclear spin quantum number I and the nuclear magnetic moment μ_I , which both vary considerably.

Despite the vast variety of structures quantum dots may still be grouped according to their dimension d : lateral dots are strongly confined in one direction while the movement of the electron in the plane of the 2DEG is less restricted. These dots are often referred to as 2-dimensional ($d = 2$). For

defect centers in contrast we have $d = 3$. For an isotropic electron envelope function of the form

$$\psi(\vec{r}_l) = \psi(0) \exp \left[-\frac{1}{2} \left(\frac{r_l}{r_0} \right)^q \right], \quad (1.24)$$

where r_0 is the effective Bohr radius, we define N as the number of nuclear spins within r_0 and refer to N as number of nuclear spins *within* the dot. If l is the number of nuclear spins enclosed by r_l we have in d dimensions:

$$\frac{\text{volume of } l \text{ spins}}{\text{volume of } N \text{ spins}} = \frac{v_0 l}{v_0 N} = \left(\frac{r_l}{r_0} \right)^d \quad (1.25)$$

The hyperfine coupling constants are thus of the form

$$A_l = A_0 \exp \left(-\frac{l}{N} \right)^{q/d}, \quad (1.26)$$

where A_0 is determined by the normalization condition $\sum_l A_l = A$. For a large number of nuclear spins $N \gg 1$ one may turn the sum into an integral and finds [42]

$$A_0 = \frac{A}{N^{\frac{d}{q}} \Gamma \left(\frac{d}{q} \right)}. \quad (1.27)$$

The simplest case for the coupling constants is are uniform coupling constants $A_l = A/N$.

1.4 Electron spin decoherence in single quantum dots

To discuss electron spin dynamics under the influence of hyperfine interaction we first rewrite H_{QDhf} (see Eq.(1.21)) as

$$H_{\text{QDhf}} = S_z \cdot h_z + \frac{1}{2} (S_- h_+ + S_+ h_-), \quad (1.28)$$

where the raising and lowering operators are defined as $S_{\pm} = S_x \pm iS_y$ and similarly for h_{\pm} . The first analysis of electron spin dynamics in quantum dots under H_{QDhf} showed that the long-time longitudinal spin-flip probability is $\sim 1/p^2 N$ [43], i.e., this probability is suppressed in the limit of large nuclear spin polarization p and large number N of nuclear spins in the dot. An exact solution for the case of full polarization ($p = 1$) gives, for both transverse and longitudinal electron spin components, a long-time power-law decay $\sim 1/t^{3/2}$ by a fraction $\sim 1/N$ on a timescale of $\tau \sim \hbar N/A \sim 1\mu\text{s}$ (for a GaAs dot with $N \sim 10^5$) [44]. The fact that this exact solution shows a non-exponential decay

demonstrates the non-Markovian behavior of the nuclear spin bath. For non-fully polarized systems $p < 1$ and in the limit of large magnetic fields (or high polarization $p \gg 1/\sqrt{N}$), the transverse electron spin coherence undergoes a Gaussian decay [44–46] on a timescale

$$\tau_\sigma \sim \hbar\sqrt{N}/A\sqrt{1-p^2} \quad (1.29)$$

This corresponds to $\tau_\sigma \sim 10$ ns for GaAs with $p \ll 1$ and $N \sim 10^5$) [46]. This fast initial decoherence can be seen as the major effect of hyperfine interaction and it has been confirmed in a number of experiments [28,30,47,48]. The origin of this Gaussian decay is the uncertainty in z -component h_z of the Overhauser field. The effective Zeeman splitting $\omega = \epsilon_z + h_z$, where $\epsilon_z = g\mu_B B_z$, depends on the value of h_z . Since h_z is an operator, one must take into account that the nuclear spin system generally is in a mixture or superposition of h_z eigenstates. Due to the large number of nuclear spins that contribute to the Overhauser field the eigenvalues of h_z are essentially Gaussian distributed [46] for $N \gg 1$ with a variance of $\sigma^2 = (1/\tau_\sigma)^2$, leading to the Gaussian decay. There are three main strategies to overcome this fast Gaussian decay: 1. Polarizing the nuclear spins, 2. Performing a spin echo on the electron spin, 3. Narrowing the distribution of h_z eigenvalues. We discuss these three strategies in Sec. 1.6. Assuming that one of these methods was successful the question arises what further limits the hyperfine interaction imposes to electron spin coherence. It was only shown very recently [42] that even for an initial eigenstate of h_z and effective Zeeman splitting $\omega > A$ the transverse electron spin decays exponentially with a rate

$$\frac{1}{T_2} = \frac{\pi}{4} c_+ c_- f \left(\frac{d}{q} \right) \left(\frac{A}{\omega} \right)^2 \frac{A}{N}, \quad (1.30)$$

$$f(r) = \frac{1}{r} \left(\frac{1}{3} \right)^{2r-1} \frac{\Gamma(2r-1)}{[\Gamma(r)]^3}, \quad r > 1/2, \quad (1.31)$$

with the coefficients $c_\pm = I(I+1) - \langle\langle m(m \pm 1) \rangle\rangle$ and the double angle bracket indicates an average over I_i^z eigenvalues m [42,46]. For GaAs and an external field of a few Tesla, T_2 is $\sim 1 - 10\mu$ s. In the same article [42] it was shown that for a heteronuclear system (such as GaAs or InAs) the total decay rate is the sum of decay rates per species, weighted with the square of their isotopic concentration. Thus, e.g. for GaAs with has two naturally occurring Ga isotopes, spin decay will predominantly be due to flip-flops with As spins.

Let us now look in more detail at some aspects of hyperfine-induced decoherence for a single spin in a quantum dot in the regime of large effective Zeeman splitting ω . If ω is much larger than $\sigma = [\text{Tr}\{\rho_I(h_z - h_0)^2\}]^{1/2}$, with $h_0 = \text{Tr}\{\rho_I h_z\}$ (where ρ_I is the density matrix of the nuclear spin system), we may neglect the transverse term $S_\perp \cdot h_\perp$ and find that the Hamiltonian is simply

$$H_{\text{QDhf},z} = (\epsilon_z + h_z)S_z. \quad (1.32)$$

This Hamiltonian induces precession around the z -axis with a frequency that is determined by the eigenvalue h_z^n of h_z , where $h_z|n\rangle = h_z^n|n\rangle$ and $|n\rangle$ are the eigenstates of h_z . For a large but finite number of nuclear spins ($N \sim 10^5$ for lateral GaAs dots) the eigenvalues h_z^n are Gaussian distributed (due to the central limit theorem) with mean h_0 and standard deviation $\sigma \approx \hbar A \sqrt{1-p^2}/\sqrt{N}$ [46]. Calculating the dynamics under H_0 (which is valid up to a timescale of $\sim \epsilon_z/\sigma^2 \sim 1\mu s$, where the transverse terms become relevant) leads to a Gaussian decay of the transverse electron spin state $|+\rangle = (|\uparrow\rangle + |\downarrow\rangle)/\sqrt{2}$ [46]:

$$\begin{aligned} C_{++}^{\text{QDhf},z}(t) &= \frac{1}{\sqrt{2\pi}\sigma} \int_{-\infty}^{\infty} dh_z^n e^{\left(-\frac{(h_z^n - h_0)^2}{2\sigma^2}\right)} |\langle n| \otimes \langle +| e^{(-iH_0 t)} |+\rangle \otimes |n\rangle|^2 \\ &= \frac{1}{2} + \frac{1}{2} e^{\left(-\frac{t^2}{2\tau_\sigma^2}\right)} \cos[(\epsilon_z + h_0)t]; \quad \tau_\sigma = \frac{1}{\sigma} \sim \sqrt{\frac{N}{1-p^2}} \frac{\hbar}{A}. \end{aligned} \quad (1.33)$$

Here again, p denotes the polarization, and for an unpolarized GaAs quantum dot with $N \sim 10^5$ we find $\tau_\sigma \sim 10ns$. Applying an additional ac driving field with amplitude b along the x -direction leads to electron spin resonance (ESR). Assuming again that $\epsilon_z \gg \sigma$, we have the Hamiltonian

$$H_{\text{ESR}} = H_{\text{QDhf},z} + b \cos(\omega t) S_x. \quad (1.34)$$

In a rotating-wave approximation (which is valid for $(b/\epsilon_z)^2 \ll 1$) the decay of the driven Rabi oscillations is given by [49]

$$C_{\uparrow\uparrow}^{\text{ESR}}(t) \sim 1 - C + \sqrt{\frac{b}{8\sigma^2 t}} \cos\left(\frac{b}{2}t + \frac{\pi}{4}\right) + \mathcal{O}\left(\frac{1}{t^{3/2}}\right), \quad (1.35)$$

for $t \gtrsim \max(1/\sigma, 1/b, b/2\sigma^2)$ and $\epsilon_z + h_0 - \omega = 0$. Here, $C_{\uparrow\uparrow}^{\text{ESR}}(t)$ is defined in the same way as $C_{++}^{\text{QDhf},z}(t)$ in Eq. (1.33). The time-independent constant is given by $C = \exp(b^2/8\sigma^2) \text{erfc}(b/\sqrt{8\sigma}) \sqrt{2\pi} b/8\sigma$, with $\text{erfc}(x) = 1 - \text{erf}(x)$ where $\text{erf}(x)$ is the error function. The two interesting features of the decay are the slow ($\sim 1/\sqrt{t}$) power law and the universal phase shift of $\pi/4$. The fact that the power law already becomes valid after a short time $\tau \sim 15ns$ (for $b \approx \sigma$) preserves the coherence over a long time, which makes the Rabi oscillations visible even when the Rabi period is much longer than the timescale $\tau \sim 15ns$ for transverse spin decay. Both the universal phase shift and the non-exponential decay have been recently confirmed in experiment [49]. More details on the phase shift and the power-law decay can be found in Chapter 3, where also the experimental results are also given.

1.5 Singlet-triplet decoherence in double quantum dots

We now move on to discuss hyperfine-induced decoherence in a double quantum dot. The effective Hamiltonian in the subspace of one electron on each dot is most conveniently written in terms of the sum and difference of electron spin and collective nuclear spin operators: $\mathbf{S} = \mathbf{S}_1 + \mathbf{S}_2$, $\delta\mathbf{S} = \mathbf{S}_1 - \mathbf{S}_2$ and $\mathbf{h} = \frac{1}{2}(\mathbf{h}_1 + \mathbf{h}_2)$, $\delta\mathbf{h} = \frac{1}{2}(\mathbf{h}_1 - \mathbf{h}_2)$:

$$H_{\text{dd}}(t) = \epsilon_z S_z + \mathbf{h} \cdot \mathbf{S} + \delta\mathbf{h} \cdot \delta\mathbf{S} + \frac{J}{2} \mathbf{S} \cdot \mathbf{S} - J. \quad (1.36)$$

Here, J is the Heisenberg exchange coupling between the two electron spins. Similar to the single-dot case, we assume that the Zeeman splitting is much larger than both $\langle \delta\mathbf{h} \rangle_{\text{rms}}$ and $\langle \mathbf{h}_i \rangle_{\text{rms}}$, where $\langle \mathcal{O} \rangle_{\text{rms}} = [\text{Tr}\{\rho_I(\mathcal{O} - \langle \mathcal{O} \rangle)^2\}]^{1/2}$ is the root-mean-square expectation value of the operator \mathcal{O} with respect to the nuclear spin state ρ_I . Under these conditions, the relevant spin Hamiltonian becomes block diagonal with blocks labeled by the total electron spin projection along the magnetic field S_z . In the subspace of $S_z = 0$ (singlet $|S\rangle$, and triplet $|T_0\rangle$) the Hamiltonian can be written as [50, 51]

$$H_{sz0}(t) = \frac{J}{2} \mathbf{S} \cdot \mathbf{S} + (\delta h_z + \delta b_z) \delta S_z \quad (1.37)$$

Here, δb_z is the inhomogeneity of the externally applied classical static magnetic field with $\delta b_z \ll \epsilon_z$, while the nuclear difference field δh_z is Gaussian distributed, as was h_z in the single dot case. A full account of the rich pseudospin dynamics under $H_{sz0}(t)$ can be found in Refs. [51], [50] and in Chapter 2 of this thesis. Here we only discuss the most prominent features of the SS-correlator $C_{SS}^{sz0}(t)$ (defined analogously to C_{++} in Eq. (1.33)), which gives the probability to find the singlet $|S\rangle$, if the system was initialized to $|S\rangle$ at $t = 0$. The parameters that determine the dynamics are the exchange coupling J , the expectation value of the total difference field $x_0 = \delta b_z + \delta h_0$ and the width of the difference field σ_δ (with $\delta h_0 = \langle \psi_I | \delta h_z | \psi_I \rangle$ and $\sigma_\delta = \langle \psi_I | (\delta h_z - \delta h_0)^2 | \psi_I \rangle^{1/2}$). For the asymptotics one finds that the singlet probability does not decay to zero, but goes to a finite, parameter-dependent value [50]. In the case of strong exchange coupling, $|J| \gg \max(|x_0|, \sigma_\delta)$, the singlet only decays by a small fraction quadratic in σ_δ/J or x_0/J :

$$C_{SS}^{sz0}(t \rightarrow \infty) \sim \begin{cases} 1 - 2 \left(\frac{\sigma_\delta}{J}\right)^2, & |J| \gg \sigma_\delta \gg |x_0|, \\ 1 - 2 \left(\frac{x_0}{J}\right)^2, & |J| \gg |x_0| \gg \sigma_\delta. \end{cases} \quad (1.38)$$

For short times, $t \ll |J|/4\sigma_\delta^2$, the correlator $C_{SS}^{sz0}(t)$ undergoes a Gaussian decay on a timescale $\sqrt{J^2 + 4x_0^2}/4|x_0|\sigma_\delta$, while at long times, $t \gg |J|/4\sigma_\delta^2$, we

have a power-law decay

$$C_{SS}^{sz0}(t) \sim C_{SS}^{sz0}(t \rightarrow \infty) + e^{-\frac{x_0^2}{2\sigma_\delta^2} \cos(|J|t + \frac{3\pi}{4})} \frac{1}{4\sigma_\delta \sqrt{|J|} t^{\frac{3}{2}}}. \quad (1.39)$$

As in the case of single-spin ESR, we again have a power-law decay, now with $1/t^{3/2}$ and a universal phase shift, in this case: $3\pi/4$. Measurements [52] of the correlator $C_{SS}^{sz0}(t)$ confirmed the parameter dependence of the saturation value and were consistent with the theoretical predictions concerning the decay. Using the same methods, one may also look at transverse correlators in the $S_z = 0$ subspace and find again power-law decays and a universal phase shift, albeit, with different decay power and different value of the universal phase shift [51]. Looking at the short-time behavior of the transverse correlators also allows one to analyze the fidelity of the $\sqrt{\text{SWAP}}$ gate [51].

1.6 Suppression of hyperfine induced decoherence

As discussed in Sec. 1.4, the decoherence time for the transverse electron spin is given by

$$\tau_\sigma \sim \hbar \sqrt{N}/A \sqrt{1-p^2}, \quad (1.40)$$

which for $p \ll 1$ amounts to $\tau_\sigma \sim 10\text{ns}$ in GaAs. This exceeds gating times of two-qubit gates of 180ps [28] by roughly two orders of magnitude. Standard estimates for error thresholds for quantum error correction demand a ratio of 10^{-4} [53] for gating time versus decoherence time. For non-Markovian baths it may even be 10^{-6} [54–56]. To use electron spins in quantum dots as qubits in a quantum computer thus requires to reduce hyperfine-induced decoherence in some way. As mentioned before, the three main strategies to reduce decoherence are [43, 46]: 1. Polarizing the nuclear spins, 2. Performing a spin echo on the electron spin. 3. Narrowing the distribution of h_z eigenvalues.

1.6.1 Polarization

The first strategy is the most straightforward one: since the decoherence time τ_σ scales with $1/\sqrt{1-p^2}$, where p is the degree of polarization, we see immediately that for $p \rightarrow 1$ τ_σ goes to infinity. The degree of polarization required to achieve an increase of τ_σ by a factor 100 is $p \approx 0.99995$. To induce a high degree of nuclear spin polarization in quantum dots has turned out to be experimentally challenging. In GaAs quantum dots a polarization of $\sim 60\%$ [57, 58] has been achieved by optical pumping [59] and $\sim 40\%$ by transport [60]. In self-assembled InAs dots up to 50% [61–63] have been achieved by optical pumping. There is still a long way to go to reach the required 99.995%. An alternative

method is to use a ferromagnetic phase transition at low temperatures [64,65]. Very recently it was experimentally verified in NV-Centers that indeed polarizing the spin bath leads to an extension of the decoherence time [66]. Since the spin bath considered in this experiment consist of electrons bound to impurities, it was possible to achieve a thermal spin polarization of 99.4% below 2K. For nuclear spins in GaAs this ordering occurs only at a temperature of $\sim 1\text{mK}$ at a magnetic fields of 10T or higher [67].

1.6.2 Spin echo

Spin echoes were first introduced in NMR [68] to refocus precessing nuclear spin magnetization by a π -pulse of resonant radiofrequency. In the case of a spin in a quantum dot the π -pulse is applied to the electron spin. Applying a spin-echo pulse does not alter the free-induction decay, but it allows to recover a superposition of states for a longer time than the free-induction decay time. Since the value of the nuclear field determines the precession frequency of transverse electron spin states, it is clear that by applying a π -pulse to the electron spin, which changes the sign of S_z , leads to refocussing. This, however, only applies to the fast decoherence due to the inhomogeneity in the Overhauser field. Decoherence beyond that is in general not recovered by a spin echo. Therefore, spin-echo measurements allow to investigate decoherence mechanisms beyond the initial Gaussian decay, which is what would be left if state narrowing could be successfully implemented. The first spin-echo measurements for spins in quantum dots were performed in the $S_z = 0$ subspace of two electrons in a double dot [28]. This singlet-triplet spin echo gave a spin-echo envelope decay of $\sim 1\mu\text{s}$ compared to the $\sim 10\text{ns}$ initial Gaussian decay. Theoretically it was claimed [69,70] that also the decoherence effect of electron-mediated coupling between nuclear spins can be removed with a spin-echo. Since the only decoherence mechanism left would then be direct dipolar interaction between nuclear spins, one would expect a spin-echo envelope decay that is independent of the externally applied magnetic field (for fields larger than $\sim 0.1\text{mT}$). A recent spin-echo experiment for a single spin in a single dot [71], however, showed a clear B -field dependence and the spin-echo envelope decay time found was $0.5\mu\text{s}$ at 70mT .

1.6.3 Nuclear spin state narrowing

The idea to prepare the nuclear spin system in order to prolong the electron spin coherence was put forward in Ref. [50]. Specific methods for nuclear spin state narrowing have been described in Ref. [51] in the context of a double dot with oscillating exchange interaction, in Ref. [72] for phase-estimation of a single (undriven) spin in a single dot, and in an optical setup in Ref. [73]. Here, we discuss narrowing for the case of a driven single spin in a single dot,

for which the details are very similar to the treatment in Ref. [51]. The general idea behind state narrowing is that the evolution of the electron spin system depends on the value of the nuclear field since the effective Zeeman splitting is given by $\epsilon_z + h_z^n$. This leads to a nuclear-field-dependent resonance condition $\epsilon_z + h_z^n - \omega = 0$ for ESR and thus measuring the evolution of the electron spin system determines h_z^n and thus the nuclear spin state.

We start from the Hamiltonian for single-spin ESR as given in Eq. (1.34). The electron spin is initialized to the $|\uparrow\rangle$ state at time $t = 0$ and evolves under H_{esr} up to a measurement performed at time t_m . The probability to find $|\downarrow\rangle$ for a given eigenvalue h_z^n of the nuclear field operator ($h_z|n\rangle = h_z^n|n\rangle$) is then given by

$$P_{\downarrow}^n(t) = \frac{1}{2} \frac{b^2}{b^2 + 4\delta_n^2} \left[1 - \cos \left(\frac{t}{2} \sqrt{b^2 + 4\delta_n^2} \right) \right] \quad (1.41)$$

where $\delta_n = \epsilon_z + h_z^n - \omega$ and b is the amplitude of the driving field. As mentioned above, in equilibrium we have a Gaussian distribution for the eigenvalues h_z^n , i.e., for the diagonal elements of the nuclear spin density matrix $\rho_I(h_z^n, 0) = \langle n | \rho_I | n \rangle = \exp(-(h_z^n - h_0)^2 / 2\sigma^2) / \sqrt{2\pi}\sigma$. Thus, averaged over the nuclear distribution we have the probability $P_{\downarrow}(t)$ to find the state $|\downarrow\rangle$, i.e., $P_{\downarrow}(t) = \int dh_z^n \rho_I(h_z^n, 0) P_{\downarrow}^n(t)$. After one measurement with outcome $|\downarrow\rangle$, we thus find for the diagonal of the nuclear spin density matrix [74]

$$\rho_I(h_z^n, 0) \xrightarrow{|\downarrow\rangle} \rho_I^{(1,\downarrow)}(h_z^n, t_m) = \rho_I(h_z^n, 0) \frac{P_{\downarrow}^n(t_m)}{P_{\downarrow}(t_m)}. \quad (1.42)$$

Assuming now that the measurement is performed in such a way that it gives the time-averaged value (i.e., with a time resolution less than $1/b$) we have for the probability P_{\downarrow}^n of measurement result $|\downarrow\rangle$ as a function of the nuclear field eigenvalue $P_{\downarrow}^n = \frac{1}{2} \frac{b^2}{b^2 + 4\delta_n^2}$. Thus, by performing a measurement on the electron spin (with outcome $|\downarrow\rangle$), the nuclear-spin density matrix is multiplied by a Lorentzian with width b centered around the h_z^n that satisfies the resonance condition $\epsilon_z + h_z^n - \omega = 0$. This results in a narrowed nuclear spin distribution, and thus an extension of the electron spin coherence, if $b < \sigma$. In the case of measurement outcome $|\uparrow\rangle$ we find

$$\rho_I(h_z^n, 0) \xrightarrow{|\uparrow\rangle} \rho_I^{(1,\uparrow)}(h_z^n, t_m) = \rho_I(h_z^n, 0) \frac{1 - P_{\downarrow}^n(t_m)}{1 - P_{\downarrow}(t_m)}, \quad (1.43)$$

i.e., the Gaussian nuclear spin distribution is multiplied by one minus a Lorentzian, thus reducing the probability for the nuclear field to have a value matching the resonance condition $\epsilon_z + h_z^n - \omega = 0$. Due to the slow dynamics of the nuclear spin system many such measurements of the electron spin are possible (with re-initialization of the electron spin between measurements). Under the assumption of a static nuclear field during M such initialization and measurement cycles, we find

$$\rho_I(h_z^n, 0) \longrightarrow \rho^{(M, \alpha_{\downarrow})}(h_z^n) = \frac{1}{N} \rho_I(h_z^n, 0) (P_{\downarrow}^n)^{\alpha_{\downarrow}} (1 - P_{\downarrow}^n)^{M - \alpha_{\downarrow}}, \quad (1.44)$$

where α_{\downarrow} is the number of times the measurement outcome was $|\downarrow\rangle$. The simplest way to narrow is to perform single measurements with $b \ll \sigma$. If the outcome is $|\downarrow\rangle$, narrowing has been achieved. Otherwise, the nuclear system should be allowed to re-equilibrate before the next measurement [75]. In order to achieve a systematic narrowing, one can envision adapting the driving frequency (and thus the resonance condition) depending on the outcome of the previous measurements. Such an adaptive scheme is described in detail in Refs. [73] and [51].

1.7 Perspectives

While many aspects of electron spin decoherence in quantum dots are now well understood, there still remain many open questions. An important issue is the interplay between the electron spin and the nuclear spin system and the dynamics of the nuclear spin system. On the one hand, the electron spin is important for the decay of the Overhauser field due to the electron-mediated coupling between the nuclear spins [76, 77]. Chapter 4 of this thesis studies the effect of this electron-mediated coupling on the dynamics of the Overhauser field. On the other hand the complex interplay between the nuclear spin system and the electron spin leads to hysteretic and bistable behavior, as has been observed in experiments [48, 62, 78–82]. This has triggered theoretical studies [83–86] in this direction, a detailed microscopic understanding of the processes behind these bistabilities is, however, still lacking.

Chapter 2

Nuclear spin state narrowing via gate-controlled Rabi oscillations in a double quantum dot

[D. Klauser, W.A. Coish, D. Loss, Phys. Rev. B **73**, 205302 (2006)]

In this chapter we study spin dynamics for two electrons confined to a double quantum dot under the influence of an oscillating exchange interaction. This leads to driven Rabi oscillations between the $|\uparrow\downarrow\rangle$ -state and the $|\downarrow\uparrow\rangle$ -state of the two-electron system. The width of the Rabi resonance is proportional to the amplitude of the oscillating exchange. A measurement of the Rabi resonance allows one to narrow the distribution of nuclear spin states and thereby to prolong the spin decoherence time. Further, we study decoherence of the two-electron states due to the hyperfine interaction and give requirements on the parameters of the system in order to initialize in the $|\uparrow\downarrow\rangle$ -state and to perform a $\sqrt{\text{SWAP}}$ operation with unit fidelity.

2.1 Introduction

One of the important proposals for quantum information processing in solid-state systems is the spin-qubit proposal for quantum computing with electron spins in quantum dots [1]. Much effort has been put into the realization of this proposal leading to exciting theoretical [87] and experimental achievements [28, 47, 48, 78, 88–90]. Still many challenges remain such as decoherence and the implementation of single-qubit gates.

A major obstacle to quantum computation with the quantum-dot spin qubit is decoherence due to the coupling of the qubit to its environment. The hyperfine interaction between the electron spin and the nuclear spins present in all III-V semiconductors [41] leads to the strongest decoherence effect [6, 7, 28, 43–46, 50, 91]. Experiments [28, 48, 58, 92] have yielded values for the free-

induction spin dephasing time T_2^* that are consistent with $T_2^* \sim \sqrt{N}/A \sim 10\text{ns}$ [44, 45, 91] for $N = 10^6$ and $A = 90\mu\text{eV}$ in GaAs, where N is the number of nuclei within one quantum dot Bohr radius and A characterizes the hyperfine coupling strength [39]. This is to be contrasted to potential spin-echo envelope decay, which may be much larger [70, 93, 94]. With a two-qubit switching time of $\tau_s \sim 50\text{ps}$ [43] this only allows $\sim 10^2$ gate operations within T_2^* , which falls short (by a factor of 10 to 10^2) of current requirements for efficient quantum error correction [53].

There are several ways to overcome the problem of hyperfine-induced decoherence, of which measurement and thus projection of the nuclear spin state seems to be the most promising one [46]. Other methods include polarization [43, 46, 59, 91] of the nuclear spins and spin echo techniques [28, 46, 69]. However, in order to extend the decay time by an order of magnitude through polarization of the nuclear spins, a polarization of above 99% is required [46], but the best result so far reached is only $\sim 60\%$ in quantum dots [58, 88]. With spin-echo techniques, gate operations still must be performed within the single-spin free-induction decay time, which requires faster gate operations. A projective measurement of the nuclear spin state leads to an extension of the free-induction decay time for the spin. This extension is only limited by the ability to do a strong measurement since the longitudinal nuclear spin in a quantum dot is expected to survive up to the spin diffusion time, which is on the order of seconds for nuclear spins surrounding donors in GaAs [95].

The implementation of quantum computation schemes requires coherent control of the qubits. Rabi oscillations between the two qubit states are an important signature of coherence and thus observation of controlled Rabi oscillations is an important intermediate step in the experimental implementation of quantum information processors. Despite recent experimental achievements [28, 88], there has still been no experimental observation of driven Rabi oscillations for a system of two quantum-dot spin qubits. What has been observed is electron spin resonance via g-tensor modulation in a bulk semiconductor [96].

In the quantum-dot spin qubit proposal, two-qubit gates are realized through tuning of the exchange coupling J between the two spins [1, 43]. The splitting between singlet and triplet states of the two-electron system is given by the exchange coupling J and in devices such as those in Refs. [28] and [48], J can be controlled through gate voltages. Petta *et al.* [28] have recently managed to implement the $\sqrt{\text{SWAP}}$ -gate in their setup. However, in order to implement single-qubit gates, control over local magnetic fields or g-factors is required [43].

As we will show in Sec.2.2, an oscillating exchange $J(t)$ induces Rabi oscillations between the states $|\uparrow\downarrow\rangle$ and $|\downarrow\uparrow\rangle$ of two electron spins (one electron in each dot). The amplitude of these oscillations is resonant on the splitting between $|\uparrow\downarrow\rangle$ and $|\downarrow\uparrow\rangle$ and the width of this resonance is proportional to the

amplitude j of the oscillating component of $J(t) = J_0 + j \cos(\omega t)$, where ω is the driving frequency. Since the splitting depends on the state of the nuclear system, a measurement of the resonance is also a measurement of the state of the nuclear spins and thus provides a way to narrow the quantum distribution of the nuclear spin states. This narrowing of the spin state is one possible solution to suppress hyperfine-induced decoherence in quantum-dot spin qubits [46]. It has been proposed to measure the nuclear spin polarization using a phase estimation method [72]. In the ideal case, phase estimation yields one bit of information about the nuclear-spin system for each perfectly measured electron. Optical methods have also been proposed [73]. The all-electrical method we present here can be applied with current technology.

The rest of this chapter is organized as follows. In Sec. 2.2 we show that an oscillating exchange leads to driven Rabi oscillations and calculate the resonance linewidth. In Sec. 2.3 we propose a method to narrow the distribution of the nuclear spin states. In Sec. 2.4 we consider decoherence induced through the hyperfine interaction for a static exchange coupling J . We use these results in Sec.2.5 to analyze under which conditions we reach unit fidelity for the initialization to the state $|\uparrow\downarrow\rangle$ and a $\sqrt{\text{SWAP}}$ operation [1]. Sec. 2.6 contains a summary of our results.

2.2 Oscillating exchange and ESR

In this section we show that under suitable conditions an oscillating exchange interaction may be used to induce Rabi oscillations in a system of two electrons confined to a double quantum dot like those in Refs. [28, 47, 48, 90].

We denote by $\mathbf{h}_i = (h_i^x, h_i^y, h_i^z)$, $i = 1, 2$, the collective quantum nuclear spin operator, the ‘‘Overhauser operator’’, in dot one and two, respectively, and write $\delta h^z = \frac{1}{2}(h_1^z - h_2^z)$. The collective quantum nuclear spin operator \mathbf{h}_i is defined as $\mathbf{h}_i = \sum_k A_k^i \mathbf{I}_k$, where \mathbf{I}_k is the nuclear spin operator for a nucleus of total spin I at lattice site k , and the hyperfine coupling constants are given by $A_k^i = vA|\psi_0^i(\mathbf{r}_k)|^2$, where v is the volume of a unit cell containing one nuclear spin, A characterizes the hyperfine coupling strength, and $\psi_0^i(\mathbf{r}_k)$ is the single-particle envelope wavefunction of the electron evaluated at site k . Further, $\langle \mathcal{O} \rangle_{\text{rms}} = \langle \psi_I | \mathcal{O}^2 | \psi_I \rangle^{1/2}$ is the root-mean-square expectation value of the operator \mathcal{O} with respect to the nuclear spin state $|\psi_I\rangle$. We assume that the Zeeman splitting $\epsilon_z = g\mu_B B$ induced by a uniform applied magnetic field $\mathbf{B} = (0, 0, B)$, $B > 0$, is much larger than $\langle \delta \mathbf{h} \rangle_{\text{rms}}$ and $\langle \mathbf{h}_i \rangle_{\text{rms}}$. Under these conditions the relevant spin Hamiltonian becomes block diagonal with blocks labeled by the total electron spin projection along the magnetic field S^z . In the subspace of $S^z = 0$ the Hamiltonian can be written as ($\hbar = 1$) [50]

$$H_0 = \frac{J}{2} (1 + \tau^z) + \delta h^z \tau^x + \delta b^z \tau^x. \quad (2.1)$$

Here, J is the Heisenberg exchange coupling between electron spins on the two dots and δb^z the inhomogeneity of an externally applied classical static magnetic field which we add in addition to the treatment in Ref. [50]. Further, $\boldsymbol{\tau} = (\tau^x, \tau^y, \tau^z)$ is the vector of Pauli matrices in the basis of $S^z = 0$ singlet $|S\rangle$ and triplet $|T_0\rangle$ ($|S\rangle \rightarrow |\tau^z = -1\rangle$, $|T_0\rangle \rightarrow |\tau^z = +1\rangle$). It has been proposed to use two pseudo-spin states such as $|S\rangle$ and $|T_0\rangle$ as a logical qubit [97].

We assume a time-dependent exchange of the form

$$J = J(t) = J_0 + j \cos(\omega t). \quad (2.2)$$

The operator δh^z commutes with the Hamiltonian at all times. Thus, if the nuclear-spin system is in an eigenstate $|n\rangle$ of δh^z with $\delta h^z |n\rangle = \delta h_n^z |n\rangle$, we have $H |\psi\rangle = H_n |\psi_e\rangle \otimes |n\rangle$, where in H_n the operator δh^z has been replaced by δh_n^z and $|\psi_e\rangle$ is the electron spin part of the wave function. In order to bring H_n to a form that is very similar to the standard ESR (electron spin resonance) Hamiltonian [98] ($H_{ESR} = -\frac{1}{2}\epsilon_z \sigma_z - \frac{1}{2}\Delta_x \cos(\omega t) \sigma_x$) we perform a unitary transformation $U_1 = \exp(-i\frac{\pi}{4}\tau^y)$ which is just a rotation about the y -axis in a Bloch-sphere picture. Also introducing $\Omega_n = 2(\delta h_n^z + \delta b^z)$, the above Hamiltonian becomes

$$\tilde{H}_n = U_1 H_n U_1^\dagger = \frac{J_0}{2} \tau^x + \frac{j}{2} \cos(\omega t) \tau^x - \frac{1}{2} \Omega_n \tau^z. \quad (2.3)$$

The Pauli matrices are now given in the new basis of $|\downarrow\uparrow\rangle = |\tau^z = 1\rangle = |+\rangle$ and $|\uparrow\downarrow\rangle = |\tau^z = -1\rangle = |-\rangle$. For $J_0 = 0$ this is just the standard ESR Hamiltonian. We have evaluated pseudo-spin dynamics under this Hamiltonian in a rotating wave approximation close to resonance for $j \ll \Omega_n$. When we treat the J_0 -term as a perturbation and calculate the transition probability between unperturbed eigenstates of the Hamiltonian we find that it is proportional to J_0^2/Ω_n^2 and we may thus neglect this term close to resonance and if $J_0 \ll \Omega_n$. Hence, we are left with the standard ESR Hamiltonian which leads to Rabi oscillations. Initializing the two-electron system in the state $|\downarrow\uparrow\rangle = |+\rangle$ (which can be done as proposed in Sec. 2.5) we obtain for the expectation value of $\tau^z(t)$:

$$\langle \tau^z(t) \rangle_n = \langle n | \otimes \langle + | \tau^z(t) | + \rangle \otimes | n \rangle = \frac{(\Omega_n - \omega)^2 + (j/2)^2 \cos(\omega' t)}{(\Omega_n - \omega)^2 + (j/2)^2}, \quad (2.4)$$

where

$$\omega' = \sqrt{(\Omega_n - \omega)^2 + (j/2)^2}, \quad j \ll \Omega_n, \quad J_0 \ll \Omega_n, \quad |\Omega_n - \omega| \ll \Omega_n. \quad (2.5)$$

For $\omega = \Omega_n$ the system undergoes coherent Rabi oscillations between the states $|+\rangle$ and $|-\rangle$ with a frequency of j . Averaged over time, the expectation value of τ^z is

$$\langle \langle \tau^z \rangle_n \rangle = \lim_{T \rightarrow \infty} \frac{1}{T} \int_0^T \langle \tau^z(t) \rangle_n dt = \frac{(\Omega_n - \omega)^2}{(\Omega_n - \omega)^2 + (j/2)^2}. \quad (2.6)$$

In order to measure the time-averaged value $\langle\langle\tau^z\rangle_n\rangle$ the measurement time must be much larger than the period of Rabi oscillations ($\sim 1/j$ on resonance). $1 - \langle\langle\tau^z\rangle_n\rangle$ has a Lorentzian lineshape with a full width at half maximum (FWHM) of j . Most importantly, the resonance frequency depends on the nuclear-spin eigenstate through $\Omega_n = 2(\delta h_n^z + \delta b^z)$ and thus a measurement of the resonance will determine δh_n^z .

2.2.1 Superposition of nuclear-spin eigenstates

Before a measurement on the nuclear-spin system is performed, there is no reason for the nuclear-spin system to be in an eigenstate of δh^z , but it is most likely in some generic superposition of these eigenstates. Thus, we now investigate how the resonance changes if we consider the nuclear-spin system to be in a superposition of eigenstates of the collective nuclear spin operator δh^z .

At $t = 0$ we fix the electron system in the state $|\downarrow\uparrow\rangle = |+\rangle$ while the nuclear-spin system is in an arbitrary state: $\rho(0) = \rho_e(0) \otimes \rho_I(0)$ with

$$\rho_e(0) = |+\rangle\langle+|, \quad (2.7)$$

$$\rho_I(0) = \sum_i p_i |\psi_I^i\rangle\langle\psi_I^i|; \quad |\psi_I^i\rangle = \sum_n a_n^i |n\rangle, \quad (2.8)$$

where the a_n^i satisfy the normalization condition $\sum_n |a_n^i|^2 = 1$ and $\sum_i p_i = 1$. Here, $\rho_I(n) = \sum_i p_i |a_n^i|^2$ are the diagonal elements of the nuclear-spin density operator. The Hamiltonian H_0 commutes with δh^z and thus we find

$$\overline{\langle\tau^z(t)\rangle} = \sum_n \rho_I(n) \langle\tau^z(t)\rangle_n, \quad (2.9)$$

which defines the overbar.

We assume that for a large number of nuclear spins $N \gg 1$ which are in a superposition of δh^z -eigenstates $|n\rangle$, $\rho_I(n)$ describes a continuous Gaussian distribution of δh_n^z values, with mean $\overline{\delta h^z}$ and variance $\sigma^2 = \overline{(\delta h^z - \overline{\delta h^z})^2}$. In the limit of large N the approach to a Gaussian distribution for a sufficiently randomized nuclear system is guaranteed by the central limit theorem [46]. We perform the continuum limit according to

$$\sum_n \rho_I(n) f(n) \rightarrow \int dx \rho_{I;\bar{x},\sigma}(x) f(x), \quad (2.10)$$

$$\rho_{I;\bar{x},\sigma}(x) = \frac{1}{\sqrt{2\pi}\sigma} \exp\left(-\frac{(x - \bar{x})^2}{2\sigma^2}\right), \quad (2.11)$$

where $x = \delta h_n^z$, $\bar{x} = \overline{\delta h^z}$ and $\sigma^2 = \overline{x^2} - \bar{x}^2$. The only effect of δb^z is to shift the mean value of the Overhauser field inhomogeneity to $x_0 = \bar{x} + \delta b^z$, whereas

the width is left unchanged: $\sigma_0 = \sigma$. According to this description we obtain

$$\overline{\langle \tau^z(t) \rangle} = \int_{-\infty}^{\infty} dx \rho_{I;x_0,\sigma_0}(x) (f(x) + g(x, t)), \quad (2.12)$$

$$f(x) = \frac{(2x - \omega)^2}{(2x - \omega)^2 + (j/2)^2}, \quad (2.13)$$

$$g(x, t) = \frac{(j/2)^2 \cos\left(2\sqrt{(2x - \omega)^2 + (j/2)^2}t\right)}{(2x - \omega)^2 + (j/2)^2}. \quad (2.14)$$

The second term (Eq.(2.14)) vanishes when it is averaged over time and we find

$$1 - \overline{\langle \tau^z \rangle} = \frac{1}{2\sigma_0\sqrt{2\pi}} \int_{-\infty}^{\infty} dx \exp\left(-\frac{(x - 2x_0)^2}{8\sigma_0^2}\right) \frac{(j/2)^2}{(x - \omega)^2 + (j/2)^2}. \quad (2.15)$$

This integral (a convolution of a Lorentzian and Gaussian) is the well-known Voigt function, [99] and the resulting lineshape is the so-called ‘‘Voigt profile’’. The Voigt function may be expressed as ($\tilde{\omega} = j + 4ix_0 - 2i\omega$)

$$\overline{\langle \tau^z \rangle} = 1 - \frac{j}{4\sigma_0} \sqrt{\frac{\pi}{2}} \operatorname{Re} \left[\exp\left(\frac{\tilde{\omega}^2}{32\sigma_0^2}\right) \operatorname{erfc}\left(\frac{\tilde{\omega}}{4\sqrt{2}\sigma_0}\right) \right], \quad (2.16)$$

where $\operatorname{erfc}(z)$ is the complementary error function. In the regime where $\sigma_0 \ll j$ we may approximate the Lorentzian in the convolution (Eq.(2.15)) by its value at $x = 2x_0$ and obtain

$$\overline{\langle \tau^z \rangle} \approx \frac{(2x_0 - \omega)^2}{(2x_0 - \omega)^2 + (j/2)^2}; \quad \sigma_0 \ll j. \quad (2.17)$$

In this case the resulting resonance has the same FWHM as the Lorentzian, viz. j . On the other hand, if $\sigma_0 \gg j$, we may approximate the Gaussian with its value at $x = \omega$ and thus obtain

$$\overline{\langle \tau^z \rangle} \approx 1 - \frac{j}{4\sigma_0} \sqrt{\frac{\pi}{2}} \exp\left(-\frac{(2x_0 - \omega)^2}{8\sigma_0^2}\right); \quad \sigma_0 \gg j. \quad (2.18)$$

In this regime the width is twice the width σ_0 of the Gaussian distribution of the nuclear spin states. In order to make a statement about the width of the Voigt profile in general we look at the peak-to-peak separation Δ_V of the first derivative of the Voigt profile. For a Gaussian with a standard deviation of $2\sigma_0$ we find $\Delta_G = 4\sigma_0$ for the peak-to-peak separation of the derivative and for a Lorentzian with FWHM of j we have $\Delta_L = j/\sqrt{3}$. A Padé approximant for Δ_V in terms of Δ_L and Δ_G yields [100]

$$\Delta_V = \frac{\Delta_G^2 + a_1\Delta_G\Delta_L + a_2\Delta_L^2}{\Delta_G + a_2\Delta_L} \quad (2.19)$$

where $a_1 = 0.9085$, $a_2 = 0.4621$. This approximation is accurate to better than $0.01\Delta_V$ for all values of Δ_L, Δ_G [100]. A similar formula may also be given for the half width at half maximum (HWHM) of the Voigt profile [101].

2.3 State narrowing

The general idea behind state narrowing is that the evolution of the two-electron system is dependent on the nuclear spin state and thus knowing the evolution of the two-electron system determines the nuclear spin state. Thus, in this section we describe how the Gaussian superposition $\rho_{I;\sigma_0,x_0}(x)$ of collective nuclear spin eigenstates $|n\rangle$ can be narrowed through a sequence of measurements performed on a double quantum dot on a time scale much less than the timescale of variation of δh^z and for $j \lesssim \sigma_0$. We first give a general description of how a complete measurement of the lineshape of the Rabi resonance narrows the Gaussian superposition. Such a complete measurement of the lineshape consists of many single measurements of the operator τ^z . In Sec. 2.3.1 we present a detailed analysis of such a complete measurement and in Sec. 2.3.2 we discuss different measurement schemes.

The operator δh^z was defined in Sec. 2.2 and it describes the difference in the z-components of total nuclear field in each of the two dots. The total nuclear field is the result of $N \sim 10^6$ single nuclear spins and thus the eigenvalues of δh^z will be highly degenerate. In the limit of large N the spectrum of δh^z is quasi-continuous and the probability density of eigenvalues of δh^z is given by a Gaussian distribution, as described in Sec. 2.2.1. For such a Gaussian superposition of nuclear spin eigenstates, the lineshape of the Rabi resonance is given by a Voigt profile, as described in Sec. 2.2.1. This Voigt profile can be seen as a superposition of Lorentzian lineshapes, where each Lorentzian results from a nuclear spin eigenvalue δh_n^z and is centered around $\Omega_n = 2(\delta h_n^z + \delta b^z)$. In the Voigt profile, these Lorentzian lineshapes are weighted according to the amplitude of the corresponding eigenvalue δh_n^z in the Gaussian-distributed superposition. Through a perfect complete measurement of the Rabi-resonance lineshape, the superposition of Lorentzian lineshapes collapses and we are left with one single Lorentzian (see figure 2.1).

This Lorentzian corresponds to one single eigenvalue of δh^z and thus the Gaussian distribution has been narrowed to zero width; the nuclear-spin system is in a state with fixed eigenvalue δh_n^z .

In principle, we would need to do infinitely many single measurements in order to completely measure the lineshape of the Rabi resonance with perfect accuracy, since each point on this resonance curve is a (time-averaged) expectation value of the quantum mechanical operator τ^z . Still, we may perform a finite number M of single measurements (see Sec. 2.3.1) for each of a set of driving frequencies ω and thus obtain the series of expectation values for different ω up to some error. This error depends on M . There will then in general be more than one Lorentzian which can be fit (within error) to these expectation values and thus we would not narrow to zero width. We would still have a distribution of nuclear spin eigenstates, but one with smaller width than before the measurements.

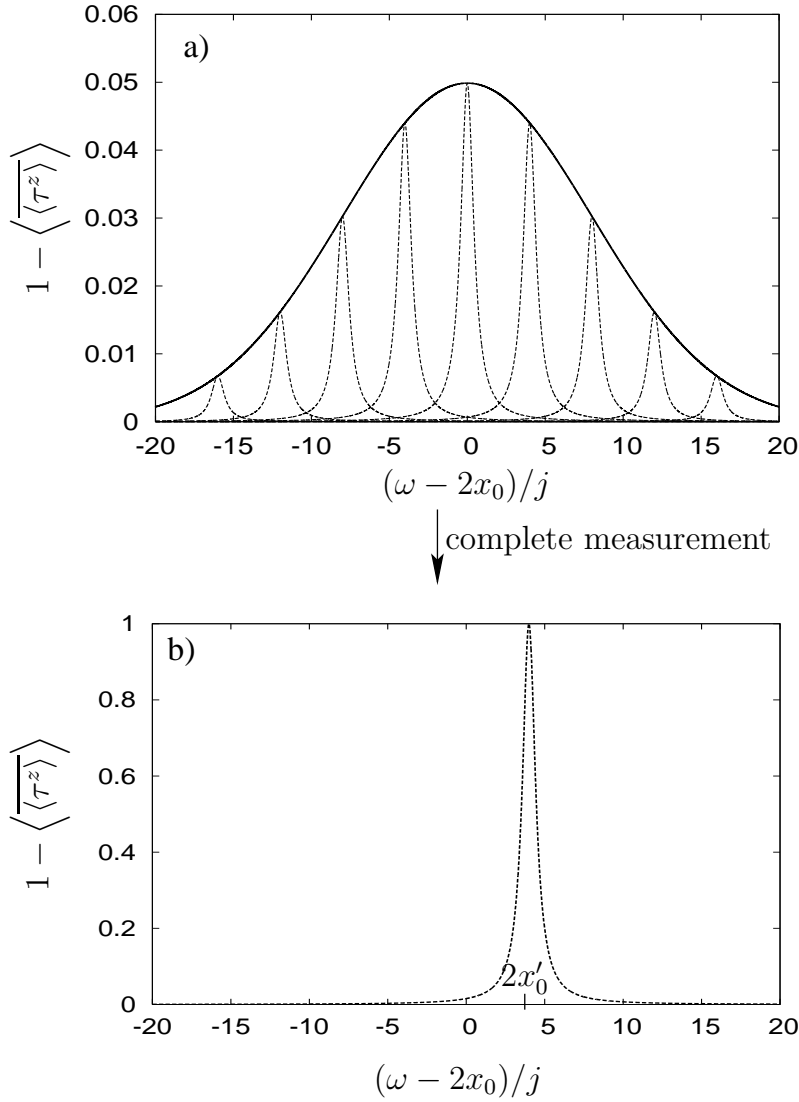


Figure 2.1: a) This figure illustrates the projection obtained through an ideal complete measurement of the Rabi-resonance lineshape. All the different Lorentzian resonances corresponding to different nuclear spin eigenstates add up to a Gaussian lineshape. b) Through a perfect complete measurement of the lineshape of the Rabi resonance, which involves many single measurements of τ^z , the superposition collapses and we are left with one single Lorentzian centered around $2x'_0 = \Omega_n$, which in general is different from $2x_0$.

For such a narrowing through measurement to be successful, the amplitude j of the oscillating exchange $J(t)$ which determines the width of the Lorentzian lineshapes should be smaller than the width σ_0 of the Gaussian distribution.

Otherwise, the Rabi resonance would be dominated by the Lorentzian (see Eq.(2.17)) and the method would not result in narrowing of the nuclear-spin distribution. The general requirements on the system parameters to narrow the distribution of nuclear spin eigenvalues are

$$j, J_0, \sigma_0 \ll x_0; \quad j \lesssim \sigma_0. \quad (2.20)$$

We note that, unlike in standard ESR, power absorption is not measured here, but instead the expectation value of the pseudo-spin τ^z , for instance via a quantum point contact (QPC) nearby one quantum dot (for a detailed description of the measurement process via such a QPC we refer the interested reader to Ref. [102]). To determine the expectation value of the pseudo-spin τ^z many single measurements of the pseudo-spin are necessary and we thus proceed to give a detailed description of the state narrowing by considering the effect of these single measurements on the nuclear spin state.

2.3.1 Description of state narrowing by consecutive pseudo-spin measurements

In this subsection we describe in detail how a single measurement of the pseudo-spin τ^z of the two-electron system affects the nuclear-spin system. Further, we give a general formula for the diagonal elements of the nuclear-spin-system density operator in the continuum limit after M measurements. The sequence of M measurements is referred to as a “complete measurement”.

At $t = 0$ the two-electron system is initialized to the state $|+\rangle = |\downarrow\uparrow\rangle$ and we assume that the electron and the nuclear system are initially factorized. Thus, the total system at $t = 0$ is described generally by the following density operator

$$\rho(0) = \rho_e(0) \otimes \rho_I(0) = |+\rangle \langle +| \otimes \sum_i p_i |\psi_I^i\rangle \langle \psi_I^i|, \quad (2.21)$$

with nuclear-spin state $|\psi_I^i\rangle = \sum_n a_n^i |n\rangle$. The diagonal elements of the nuclear-spin density operator at $t = 0$ are given by $\rho_I(n) = \rho_I(n, 0) = \sum_i p_i |a_n^i|^2$ and in the continuum limit we obtain the probability density $\rho_{I;\bar{x},\sigma}(x)$ for the eigenvalues $\delta h_n^z = x$ as given in Eq.(2.11). At time t_m a measurement of the two-electron system (at driving frequency ω , where ω is defined in Eq.(2.2)) is performed with two possible outcomes $|+\rangle$ and $|-\rangle$. The diagonal elements of the nuclear-spin density operator after the measurement are given by (see Appendix B)

$$\rho_I^{(1,\pm)}(n, t_m) = \frac{\rho_I(n, 0)}{P^\pm(t_m)} \frac{1}{2} (1 \pm \langle \tau^z(t_m) \rangle_n), \quad (2.22)$$

where $\langle \tau^z(t) \rangle_n$ is given by Eq.(2.4) and the probabilities $P^\pm(t_m)$ to measure $|\pm\rangle$ are

$$P^\pm(t_m) = \sum_i \sum_n \frac{1}{2} (1 \pm \langle \tau^z(t_m) \rangle_n) p_i |a_n^i|^2. \quad (2.23)$$

In the case where a measurement is performed with a low time resolution¹ Δt , i.e., if $\Delta t \gg 1/j$, the density operator after the measurement is the time average over the time interval Δt and the cosine term in $\langle \tau^z(t_m) \rangle_n$ averages out (note that in the case of a measurement with low time resolution, t_m is arbitrary, as long as Δt is chosen to be large enough). For the rest of this subsection we thus assume² that measurements are performed with low time resolution $\Delta t \gg 1/j$. Further, we perform the continuum limit and obtain for the probability density of eigenvalues, i.e., the diagonal part of the density operator in the continuum limit (with $x = \delta h_n^z + \delta b^z$ and $\rho_I(x) \equiv \rho_{I;x_0,\sigma_0}(x)$, see Eq.(2.11)):

$$\rho_I^{(1,+,\omega)}(x) = \rho_I(x)(1 - L_\omega(x))\frac{1}{P_\omega^+}, \quad (2.24)$$

$$\rho_I^{(1,-,\omega)}(x) = \rho_I(x)L_\omega(x)\frac{1}{P_\omega^-}, \quad (2.25)$$

where the probabilities for measuring $|+\rangle$ or $|-\rangle$ are given by

$$P_\omega^+ = \int_{-\infty}^{\infty} dx \rho_I(x)(1 - L_\omega(x)), \quad (2.26)$$

$$P_\omega^- = \int_{-\infty}^{\infty} dx \rho_I(x)L_\omega(x), \quad (2.27)$$

with

$$L_\omega(x) = \frac{1}{2} \frac{(j/4)^2}{(x - \frac{\omega}{2})^2 + (j/4)^2}. \quad (2.28)$$

After the first measurement, the two-electron system is reinitialized to the state $|+\rangle$ if necessary and a second measurement is performed. Since the initial density matrix factors out in the above results, it is clear how to generalize Eqs.(2.24) and (2.25) to the case where M consecutive measurements (without randomization of the nuclear-spin system in between measurements) are performed: every time $|+\rangle$ is measured, the diagonal elements $\rho_I(x)$ of the nuclear density matrix is multiplied by $1 - L_\omega(x)$ and every time $|-\rangle$ is measured, $\rho_I(x)$ is multiplied by $L_\omega(x)$. Thus, we obtain the diagonal elements $\rho_I^{(M,\alpha^-, \omega)}(x)$ of the nuclear density matrix after M measurements, of which α^- times the measurement outcome was $|-\rangle$ (and $(M - \alpha^-)$ -times $|+\rangle$):

$$\rho_I^{(M,\alpha^-, \omega)}(x) = \frac{\rho_I(x)}{Q_\omega(M, \alpha^-)} W_\omega(M, \alpha^-; x). \quad (2.29)$$

¹By "low time resolution", we mean that the measurement is performed at an unknown time t_m (giving rise to state $\rho(t_m)$) in the interval $\Delta t = t_b - t_a$, with a uniform probability density $1/\Delta t$. The state after the measurement is then $\frac{1}{\Delta t} \int_{t_a}^{t_b} dt_m \rho(t_m)$.

²This assumption is not necessary for our narrowing scheme. However, it does allow for the derivation of the analytical formulas in this section, which give insight into the mechanism of narrowing. In the case of perfect time resolution, one would have an additional factor of $(1 - \cos(\omega' t_m))$ in Eq. (2.28) (ω' is given in Eq.(2.5)) and would also have to take into account the time t_m at which each measurement was performed.

Here, $W_\omega(M, \alpha^-; x)$ and the normalization factor $Q_\omega(M, \alpha^-)$ are given by

$$W_\omega(M, \alpha^-; x) = L_\omega(x)^{\alpha^-} (1 - L_\omega(x))^{M - \alpha^-}, \quad (2.30)$$

$$Q_\omega(M, \alpha^-) = \int_{-\infty}^{\infty} dx \rho_I(x) W_\omega(M, \alpha^-; x). \quad (2.31)$$

The normalization factor $Q_\omega(M, \alpha^-)$ is related to P_ω^\pm through $P_\omega^- = Q_\omega(1, 1)$, $P_\omega^+ = Q_\omega(1, 0)$. In the case where measurements are performed at m_f different frequencies, Eq.(2.29) generalizes to

$$\rho_I^{\{\{M_i\}, \{\alpha_i^-\}, \{\omega_i\}\}}(x) = \rho_I(x) \prod_{i=1}^{m_f} \frac{W_{\omega_i}(M_i, \alpha_i^-; x)}{Q_{\omega_i}(M_i, \alpha_i^-)}. \quad (2.32)$$

The probability density $\rho_I^{\{\{M_i\}, \{\alpha_i^-\}, \{\omega_i\}\}}(x)$ after M measurements performed at m_f different driving frequencies depends on the frequencies $\{\omega_i\} = \{\omega_1, \dots, \omega_{m_f}\}$, the number of measurements at each frequency $\{M_i\} = \{M_1, \dots, M_{m_f}\}$, and the number of times $|-\rangle$ was measured at each frequency $\{\alpha_i^-\} = \{\alpha_1^-, \dots, \alpha_{m_f}^-\}$. Eq.(2.32) gives the distribution of nuclear spin eigenvalues for any sequence of M measurements, i.e., without randomization of the nuclear-spin system in between measurements.

2.3.2 Measurement schemes

In this subsection we describe different measurement schemes. One main characteristic of the schemes is whether we have unconditional evolution of the nuclear-spin density matrix between measurements (one waits for the nuclear-spin system to rerandomize between subsequent measurements), or whether we have conditional evolution, i.e., the nuclear-spin system is assumed to be static between measurements.

Unconditional scheme

The simplest scheme is to measure only once at one single driving frequency ω . If the outcome is $|-\rangle$, the nuclear-spin distribution after the measurement is given by Eq.(2.25); the FWHM ($2\sigma_0\sqrt{2\ln 2} \approx 2\sigma_0$) of the initial distribution will have been narrowed by a factor $\approx j/4\sigma_0$ (the nuclear-spin distribution will approximately be a Lorentzian with FWHM of $j/2$). For $j \ll \sigma_0$ and $\omega = 2x_0$, the probability P_ω^- to measure $|-\rangle$ in the first measurement is $P_{\omega=2x_0}^- \approx j/6\sigma_0$ (the exact formula is given in Eq.(2.27)). If the measurement outcome is $|-\rangle$, we stop measuring. Otherwise, we wait for the system to rerandomize (in contrast to the conditional schemes) and perform another measurement. This is repeated until $|-\rangle$ is measured for the first time. On average one needs to perform $M' \approx 6\sigma_0/j$ measurements in order to narrow by a factor of $\approx j/4\sigma_0$ (we write M' because this number of measurements should not

be confused with the number of measurements M used above in the case of measurements performed without rerandomization in between). If the driving frequency ω is far from the center x_0 of the initial Gaussian distribution, the number of required measurements increases by a factor of $\exp((x_0 - \omega/2)^2/2\sigma_0^2)$. This always leads to a narrowed distribution which is centered around $\omega/2$. Thus, with this scheme it is possible to choose the center of the nuclear-spin distribution after the measurement. This unconditional measurement scheme is the one which should be easiest to implement in an experiment since one only needs to measure once at one single frequency. However, if measurements at several different frequencies can be performed, a systematic narrowing of the distribution can be implemented as we show next.

Adaptive conditional scheme

The probability of measuring $|-\rangle$ in a measurement is determined by the overlap of the Lorentzian $L_\omega(x)$ and the probability density of eigenvalues $\rho_I^{(M, \alpha^-, \omega)}(x)$ (for the first measurement this probability is P_ω^- , which is given in Eq.(2.27)). Then, if we have the outcome $|-\rangle$ for a measurement at driving frequency ω , $\rho_I^{(M, \alpha^-, \omega)}(x)$ as a function of x becomes peaked around $\omega/2$ (since $L_\omega(x)$ is centered around $x = \omega/2$), the overlap of the Lorentzian $L_\omega(x)$ and $\rho_I^{(M, \alpha^-, \omega)}(x)$ increases and therefore the probability to measure $|-\rangle$ in a subsequent measurement also grows. If, on the other hand, we have outcome $|+\rangle$, the term $1 - L_\omega(x)$ causes a dip in $\rho_I^{(M, \alpha^-, \omega)}(x)$ at $x = \omega/2$, the overlap of the Lorentzian $L_\omega(x)$ and $\rho_I^{(M, \alpha^-, \omega)}(x)$ decreases and thus the probability to measure $|-\rangle$ in a subsequent measurement with the same driving frequency ω also decreases. Since it is the measurement outcome $|-\rangle$ that primarily leads to narrowing, the measurement scheme should maximize the probability to measure $|-\rangle$. This can be achieved by changing the driving frequency ω always in such a way that before each measurement $L_\omega(x)$ and the nuclear-spin distribution $\rho_I^{(M, \alpha^-, \omega)}(x)$ have their maximum at the same x , i.e., set $\omega/2 = x_{\max}$, where x_{\max} is the x for which $\rho_I^{(M, \alpha^-, \omega)}(x)$ has a maximum. Thanks to the adaptive driving frequency ω , the probability P_ω^- to measure $|-\rangle$ is $\approx j/6\sigma_0$ in each measurement until $|-\rangle$ is measured for the first time. Without adapting, i.e., when measuring always at the same driving frequency ω , P_ω^- decreases, as explained above (as long as we do not measure $|-\rangle$). After measuring $|-\rangle$ for the first time, the probability P_ω^- to measure $|-\rangle$ increases. Every time the measurement outcome is $|-\rangle$, the distribution $\rho_I^{(M, \alpha^-, \omega)}(x)$ is multiplied by $L_\omega(x)$ and becomes narrower (since $L_\omega(x)^{\alpha^-}$ has a FWHM of $(j/2)\sqrt{2^{1/\alpha^-} - 1}$). However, the measurement outcome $|+\rangle$, for which $\rho_I^{(M, \alpha^-, \omega)}(x)$ is multiplied by $1 - L_\omega(x)$, is still more likely and leads to a small widening of the distribution. Our simulations of this measurement scheme do, however, show that after $|-\rangle$ has been measured several times, the nuclear spin distribution is narrowed by

more than a factor $j/4\sigma_0$.

This adaptive scheme was first proposed in an optical setup by Stepanenko et al. in Ref. [73]. This scheme requires that x_{\max} can be calculated (or read from a table) between subsequent measurements and that the driving frequency ω can be tuned with a precision that is better than the width of the nuclear-spin distribution before each measurement. For this adaptive scheme (and other conditional schemes) to work, it is important that the nuclear-spin system does *not* randomize during the course of the complete measurement, i.e., the complete measurement must be carried out within a time that is shorter than the time scale for nuclear spin dynamics. We thus assume that the nuclear-spin system (viz. δh^z) has no internal dynamics between the single measurements of $\tau^z(t)$, but only changes due to the measurements performed on the two-electron system, i.e., due to single measurements of $\tau^z(t)$. We expect δh^z to vary on the time scale of nuclear spin diffusion out of the dot, which is on the order of seconds for nuclear spins surrounding donor impurities in GaAs [95]. However, there may be other sources of nuclear spin dynamics (see also Appendix A).

In Fig. 2.2 we show a typical³ sequence of nuclear spin distributions for the adaptive scheme with total number of measurements $M = 100$ and $j/\sigma_0 = 1/10$. We see (Fig. 2.2 (a)) that up to $M = 50$ the measurement outcome is never $|-\rangle$ and thus each measurement “burns a hole” into the distribution where it previously had its maximum. In the 51st measurement (Fig. 2.2(b)) the outcome is $|-\rangle$, which narrows the distribution by a factor of $\approx j/4\sigma_0$. Adapting the driving frequency ω to this peak, i.e., setting $\omega/2 = x_{\max}$ in subsequent measurements, leads to further narrowing, i.e., to a total narrowing by more than a factor $j/4\sigma_0$ (Fig. 2.2(c)). In this example we have $\alpha^- = 22$ after $M = 100$ measurements and the final FWHM is $\approx \sigma_0/100$, i.e., the distribution has been narrowed by a factor $\approx j/10\sigma_0$. In figure 2.2(d) the probability P^- to measure $|-\rangle$ before each measurement is shown. After the first time $|-\rangle$ is measured, P^- jumps up and after several more times $|-\rangle$ was measured, it saturates close to $1/2$. P^- is a good signature of the distribution’s width. As the width of the distribution goes to zero, P^- approaches $1/2$. This adaptive conditional scheme is more intricate than the unconditional scheme, but allows one to narrow by more than a factor $j/4\sigma_0$.

Other conditional schemes

Other possible measurement schemes involve measurements at several frequencies, as in the adaptive scheme. One may either choose a fixed number of frequencies within one or two σ_0 and measure several times at each frequency

³We have performed more than 60 runs of the simulation, varying M and j/σ_0

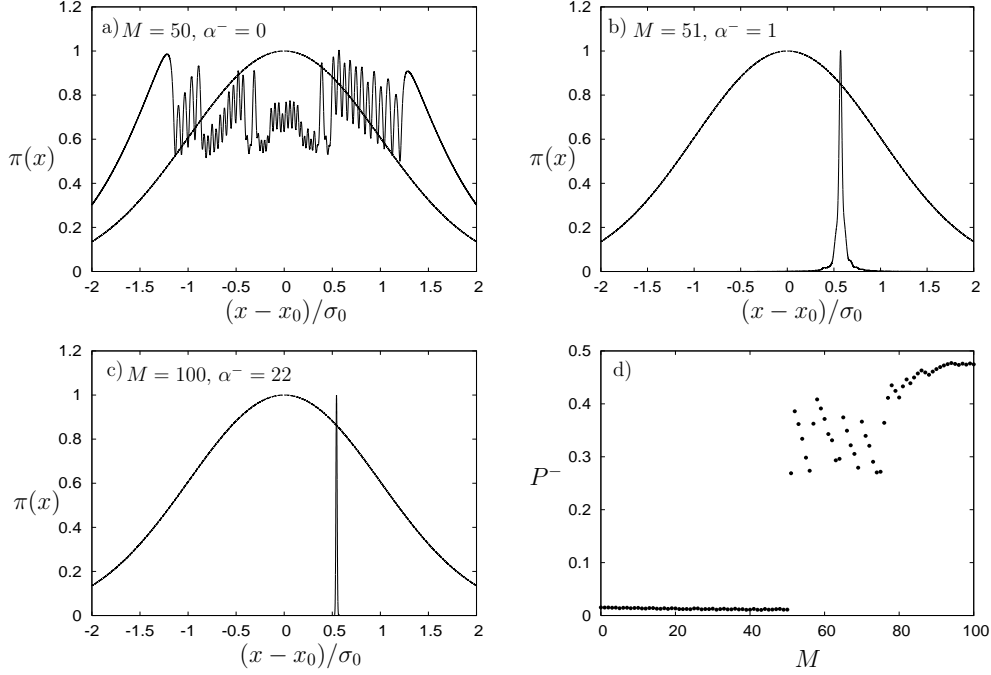


Figure 2.2: In this figure we show a typical sequence of the rescaled probability density of eigenvalues $\pi(x) = \rho_I^{\{\{M_i\}, \{\alpha_i^-\}, \{\omega_i\}\}}(x) / \max\left(\rho_I^{\{\{M_i\}, \{\alpha_i^-\}, \{\omega_i\}\}}(x)\right)$ for the adaptive conditional scheme. Here, $\rho_I^{\{\{M_i\}, \{\alpha_i^-\}, \{\omega_i\}\}}(x)$ is given in Eq.(2.32). We have $x = \delta h_n^z + \delta b^z$, $j/\sigma_0 = 1/10$ and in a)–c) the initial Gaussian distribution (with FWHM $2\sigma_0\sqrt{2\ln 2} \approx 2\sigma_0$) is plotted for reference. a) Up to $M = 50$ measurements the outcome is never $|-\rangle$ and thus each measurement “burns a hole” into the distribution where it previously had its maximum. b) In the 51st measurement the outcome is $|-\rangle$ which leads to a narrowed distribution of nuclear spin eigenvalues (peak centered at ≈ 0.5) with a FWHM that is reduced by a factor $\approx j/4\sigma_0$. c) Adapting the driving frequency ω to this peak, i.e., setting $\omega/2 = x_{\max}$ in subsequent measurements, leads to further narrowing every time $|-\rangle$ is measured. In this example the final FWHM is $\approx \sigma_0/100$, i.e., the distribution has been narrowed by a factor $\approx j/10\sigma_0$. d) The probability P^- to measure $|-\rangle$ jumps up after the 51st measurement and after $|-\rangle$ is measured several more times, this probability saturates close to $1/2$.

(without randomization between the measurements) or sweep the frequency, i.e., measure only once at each frequency but vary the frequency only in small steps. Based on numerical simulations of these schemes, we find that the typical number of measurements to narrow by a factor of j/σ_0 is greater than in the adaptive or the unconditional (single-frequency) schemes.

Time-domain measurement scheme

We note that when a complete measurement of one of the correlators discussed in Sec. 2.4 is performed with perfect resolution in time and perfect accuracy, this would also determine the state of the nuclear spin system and thus narrow the distribution of nuclear spin states. This is because the frequency of the oscillating correlators is given by $\sqrt{J^2 + 4(\delta h_n^z)^2}$ and thus measuring the frequency of the correlator determines the eigenvalue δh_n^z of the nuclear-spin system. However, it may be possible to perform a weak measurement of the decay of the correlators and thus also to see the prolongation of the decay after applying a narrowing scheme. To understand in detail the effect of measurements in the time domain, further study is required. Narrowing through measurement of the correlators is a time-domain measurement. In contrast, the narrowing schemes we have proposed above are frequency-domain measurements. If the frequency resolution is better than the time resolution, our method would most likely be more suitable.

2.4 Correlation functions in the $S^z = 0$ subspace

In this section we investigate the Hamiltonian H_0 of Eq. (2.1) with static exchange coupling J . Using this Hamiltonian we wish to calculate correlation functions for several observables in the subspace of zero total spin in the z -direction. In our previous work [50] we calculated the time evolution of a particular correlator involving the states $|S\rangle$ and $|T_0\rangle$. However, there are four additional independent correlators involving the x and y components of pseudo-spin which require a separate calculation. Quite surprisingly, it will turn out that these correlators have different decay behavior in time. The correlators we calculate here show the decoherence properties of the pseudo-spin states under the influence of the hyperfine interaction. There may be additional sources of decoherence which we do not consider here, such as orbital dephasing, corrections to the effective Hamiltonian [50], the coupling of the QPC to the dot spins [103], etc. The results of this section will help to give requirements on the parameters of the system in order to initialize in the state $|\uparrow\downarrow\rangle$ and to assess the fidelity of a $\sqrt{\text{SWAP}}$ operation with static J (see Sec. 2.5).

Diagonalizing H_0 gives the following eigenvalues and eigenvectors

$$E_n^\pm = \frac{J}{2} \pm \frac{1}{2} \sqrt{J^2 + \Omega_n^2}, \quad (2.33)$$

$$|E_n^\pm\rangle = \frac{(\Omega_n/2)|S\rangle + E_n^\pm|T_0\rangle}{\sqrt{(E_n^\pm)^2 + (\Omega_n/2)^2}} \otimes |n\rangle, \quad (2.34)$$

where again $|n\rangle$ is an eigenstate of the operator δh^z with $\delta h^z |n\rangle = \delta h_n^z |n\rangle$. At $t = 0$ we fix the electron system in an arbitrary superposition of $|T_0\rangle$ and $|S\rangle$

$$|\psi_e(t=0)\rangle = |A\rangle; \quad |A\rangle = \cos \frac{\theta_A}{2} |S\rangle + e^{i\varphi_A} \sin \frac{\theta_A}{2} |T_0\rangle. \quad (2.35)$$

The nuclear-spin system is again in a general state (see Sec. 2.2.1). As will be shown in Sec. 2.5, it is possible, in principle, to initialize to an arbitrary state in the subspace spanned by $|T_0\rangle$ and $|S\rangle$. The probability to find the electron spins in a state $|B\rangle$ at $t > 0$ is given by the correlation function:

$$C_{BA}(t) = \sum_n \rho_I(n) |\langle n | \otimes \langle B | e^{-iH_0 t} | A \rangle \otimes | n \rangle|^2, \quad (2.36)$$

where $\rho_I(n) = \sum_i p_i |a_n^i|^2$. The correlation function has the following symmetry: $C_{BA}(t) = C_{AB}(-t)$, and if $|B\rangle$ and $|D\rangle$ are orthogonal states we have $C_{BA}(t) = 1 - C_{DA}(t)$. Further, we may decompose $C_{BA}(t)$ into the sum of a time-independent term $\overline{C_{BA}^n}$ and an interference term $C_{BA}^{\text{int}}(t)$:

$$C_{BA}(t) = \overline{C_{BA}^n} + C_{BA}^{\text{int}}(t), \quad (2.37)$$

where the overbar is defined in Eq. (2.9).

We have further $C_{BA}^n = C_{BA}(\delta h_n^z) = C_{BA}(x)$. Performing the continuum limit as described in Eq. (2.10) we obtain for the correlation function

$$C_{BA}(t) = \int_{-\infty}^{\infty} dx \rho_{I;\sigma_0,x_0}(x) (C_{BA}(x) + C_{BA}^{\text{int}}(x,t)) \quad (2.38)$$

$$= C_{BA}^{\infty} + C_{BA}^{\text{int}}(t). \quad (2.39)$$

Here, C_{BA}^{∞} is the asymptotic value of the correlator $C_{BA}(t)$ for $t \rightarrow \infty$.

We have calculated correlation functions for the following states: $|S\rangle \rightarrow |\tau^z = -1\rangle$, $|T_0\rangle \rightarrow |\tau^z = +1\rangle$, $|X\rangle \rightarrow |\tau^x = +1\rangle = \frac{1}{\sqrt{2}}(|T_0\rangle + |S\rangle)$, $|Y\rangle \rightarrow |\tau^y = +1\rangle = \frac{1}{\sqrt{2}}(|T_0\rangle + i|S\rangle)$. The frequency in the interference term is always given by $s(x) = \sqrt{J^2 + 4x^2}$. In Table 2.1 we list the integrands according to the notation in Eq. (2.38). From the Heisenberg equation of motion we find $\frac{d\tau^x}{dt} = -J\tau^y$, which leads to relations for the correlators. In the notation used in Table 2.1 we obtain $\frac{dC_{XX}}{dt} = -J(C_{YX} - \frac{1}{2})$, which is satisfied by the results shown in Table 2.1. Similar relations can be derived for the other correlators and used to check the results in Table 2.1. We see that $C_{XX}(t)$ is a linear combination of other correlators: $C_{XX}(t) = C_{YY}(t) + C_{T_0S}(t)$. For C_{T_0X} and C_{T_0Y} the interference term is an odd function in x . Thus, the time dependence vanishes for $x_0 = 0$ and we have $C_{T_0X} = C_{T_0Y} = 1/2$ for all t . In general, the integral in Eq. (2.38) is difficult to solve exactly. Thus, we concentrate on

$C_{BA}(t)$	$C_{BA}(x)$	$C_{BA}^{\text{int}}(x, t)$
$C_{T_0S}(t)$	$\frac{2x^2}{s(x)^2}$	$-\frac{2x^2}{s(x)^2} \cos(s(x)t)$
$C_{T_0X}(t)$	$\frac{1}{2} + \frac{Jx}{s(x)^2}$	$-\frac{Jx}{s(x)^2} \cos(s(x)t)$
$C_{T_0Y}(t)$	$\frac{1}{2}$	$\frac{x}{s(x)} \sin(s(x)t)$
$C_{YX}(t)$	$\frac{1}{2}$	$\frac{J}{2s(x)} \sin(s(x)t)$
$C_{YY}(t)$	$\frac{1}{2}$	$\frac{1}{2} \cos(s(x)t)$
$C_{XX}(t)$	$\frac{1}{2} + \frac{2x^2}{s(x)^2}$	$\frac{J^2}{2s(x)^2} \cos(s(x)t)$

Table 2.1: Functions $C_{BA}(x)$ and $C_{BA}^{\text{int}}(x, t)$ according to the notation of Eq. (2.38) for different correlators (with $s(x) = \sqrt{J^2 + 4x^2}$). $C_{XX}(t)$ is a linear combination of other correlators.

several interesting limits. We illustrate this for the case of $C_{YX}(t)$ and give results for the other correlators. We have

$$C_{YX}(t) = \frac{1}{2} + \text{Im} \left[\tilde{C}_{YX}^{\text{int}} \right], \quad (2.40)$$

$$\tilde{C}_{YX}^{\text{int}} = \int_{-\infty}^{\infty} \rho_{I;\sigma_0,x_0}(x) \frac{J}{2s(x)} e^{is(x)t}. \quad (2.41)$$

In the regime of $|x_0| \gg \sigma_0$ the main contribution to the integral comes from a narrow region around x_0 and we may approximate $\frac{J}{2s(x)} \approx \frac{J}{2\omega_0}$ where $\omega_0 = s(x_0)$ and in the frequency term $s(x) \approx \omega_0 + \frac{4x_0}{\omega_0}(x - x_0) + \dots$. For this to be a good approximation, we require $\frac{2J^2}{\omega_0^3}(x - x_0)^2 t \ll 1$. We use $(x - x_0)^2 \approx \sigma_0^2$ and thus obtain for the correlator and the range of validity in this limit

$$C_{YX}^{\text{int}}(t) = \frac{J}{2\omega_0} e^{-\frac{1}{2} \left(\frac{t}{t_0''} \right)^2} \sin(\omega_0 t), \quad (2.42)$$

$$t_0'' = \frac{\omega_0}{4|x_0|\sigma_0}, \quad \omega_0 = \sqrt{J^2 + 4x_0^2}, \quad (2.43)$$

$$|x_0| \gg \sigma_0, \quad t \ll \frac{(J^2 + 4x_0^2)^{3/2}}{2J^2\sigma_0^2}. \quad (2.44)$$

The results for the other correlators are (with the same range of validity)

$$C_{T_0S}^{\text{int}}(t) = -\frac{2x_0^2}{\omega_0^2} e^{-\frac{1}{2}\left(\frac{t}{t_0''}\right)^2} \cos(\omega_0 t), \quad (2.45)$$

$$C_{T_0X}^{\text{int}}(t) = -\frac{Jx_0}{\omega_0^2} e^{-\frac{1}{2}\left(\frac{t}{t_0''}\right)^2} \cos(\omega_0 t), \quad (2.46)$$

$$C_{T_0Y}^{\text{int}}(t) = \frac{x_0}{\omega_0} e^{-\frac{1}{2}\left(\frac{t}{t_0''}\right)^2} \sin(\omega_0 t), \quad (2.47)$$

$$C_{YY}^{\text{int}}(t) = \frac{1}{2} e^{-\frac{1}{2}\left(\frac{t}{t_0''}\right)^2} \cos(\omega_0 t). \quad (2.48)$$

In this limit we obtain a Gaussian decay for all correlators on a time scale $t_0'' = \frac{\omega_0}{4|x_0|\sigma_0}$ which grows with the absolute value of the exchange coupling $|J|$ and with $1/\sigma_0$. The long-time saturation value is $1/2$ for C_{YX} . For some of the other correlators we find non-trivial parameter-dependent saturation values. In the limit of $|x_0| \gg \sigma_0$ we obtain these correlators by the same approximation as for the interference term, i.e. we set $C_{BA}(x) = C_{BA}(x_0)$ and obtain

$$C_{T_0S}^{\infty} = \frac{2x_0^2}{J^2 + 4x_0^2}; \quad |x_0| \gg \sigma_0, \quad (2.49)$$

$$C_{T_0X}^{\infty} = \frac{1}{2} + \frac{Jx_0}{J^2 + 4x_0^2}; \quad |x_0| \gg \sigma_0, \quad (2.50)$$

$$C_{T_0Y}^{\infty} = C_{YX}^{\infty} = C_{YY}^{\infty} = \frac{1}{2}. \quad (2.51)$$

For large J the saturation value is quadratic in x_0/J for C_{T_0S} and linear for C_{T_0X} . The saturation value for C_{T_0S} goes to zero for $|J| \gg |x_0|$ and for C_{T_0X} approaches $1/2$. $C_{T_0X}^{\infty}$ reaches extrema equal to $\frac{1}{2} + \frac{1}{4}\text{sign}(Jx_0)$ for $|J| = 2|x_0|$.

Next we consider Eq. (2.38) for $|J| \gg \max(|x_0|, \sigma_0)$ and find

$$s(x) = \sqrt{J^2 + 4x^2} \approx |J| + \frac{2x^2}{|J|}, \quad (2.52)$$

$$\frac{J}{2s(x)} = \frac{J}{2\sqrt{J^2 + 4x^2}} \approx \text{sign}(J) \left(\frac{1}{2} - \frac{x^2}{J^2} \right). \quad (2.53)$$

For Eq. (2.52) we have the additional requirement that $t \ll \frac{|J|^3}{2\max(x_0^4, \sigma_0^4)}$. Under these approximations we find the following result:

$$\tilde{C}_{YX}^{\text{int}}(t) = \text{sign}(J) \left(\frac{1}{2}\xi(t) - \frac{\sigma_0^2}{J^2}\xi^3(t) - \frac{x_0^2}{J^2}\xi^5(t) \right) \exp \left(i|J|t - \frac{x_0^2}{2\sigma_0^2} (1 - \xi^2(t)) \right), \quad (2.54)$$

with

$$\xi(t) = \left(1 - i\frac{t}{t'_0}\right)^{-1/2}, \quad t'_0 = \frac{|J|}{4\sigma_0^2}, \quad |J| \gg \max(|x_0|, \sigma_0), \quad t \ll \frac{|J|^3}{2\max(x_0^4, \sigma_0^4)}. \quad (2.55)$$

At short times we expand $\xi^2(t) \sim 1 + i\frac{t}{t'_0} - \left(\frac{t}{t'_0}\right)^2$. Keeping only lowest order in t/t'_0 in the prefactor and second order in the frequency term we obtain

$$C_{YX}^{\text{int}}(t) = \text{sign}(J) \frac{1}{2} e^{-\frac{1}{2}\left(\frac{t}{t'_0}\right)^2} \sin(\omega'_0 t), \quad (2.56)$$

$$t'_0 \approx \frac{|J|}{4|x_0|\sigma_0}, \quad \omega'_0 = |J| + \frac{2(x_0^2 + \sigma_0^2)}{|J|}, \quad (2.57)$$

$$t \ll t'_0 = \frac{|J|}{4\sigma_0^2}, \quad |J| \gg \max(|x_0|, \sigma_0). \quad (2.58)$$

The $|x_0| \gg \sigma_0$ limit of this result agrees with the $|J| \gg |x_0|$ limit of Eq. (2.42). Again, we have a Gaussian decay on the same time scale t'_0 as in Eq. (2.42) ($\omega_0 = \sqrt{J^2 + 4x_0^2} \sim |J|$ for $|J| \gg |x_0|$). One interesting feature of this correlator is the fact that there is a change of phase by π when the sign of the exchange coupling J changes. This feature offers the possibility of measuring J even for small values of J through a measurement of this correlator. We also list the other correlators in this regime:

$$C_{T_0S}^{\text{int}}(t) = -\frac{2(x_0^2 + \sigma_0^2)}{J^2} e^{-\frac{1}{2}\left(\frac{t}{t'_0}\right)^2} \cos(\omega'_0 t), \quad (2.59)$$

$$C_{T_0X}^{\text{int}}(t) = -\frac{x_0}{J} e^{-\frac{1}{2}\left(\frac{t}{t'_0}\right)^2} \cos(\omega'_0 t), \quad (2.60)$$

$$C_{T_0Y}^{\text{int}}(t) = \frac{x_0}{|J|} e^{-\frac{1}{2}\left(\frac{t}{t'_0}\right)^2} \sin(\omega'_0 t), \quad (2.61)$$

$$C_{YY}^{\text{int}}(t) = \frac{1}{2} e^{-\frac{1}{2}\left(\frac{t}{t'_0}\right)^2} \cos(\omega'_0 t). \quad (2.62)$$

Finally, we are also interested in the behavior for large t . Thus, we expand Eq. (2.54) for large times $\xi(t \gg t'_0) \sim e^{i\pi/4} \sqrt{t'_0/t}$ and obtain

$$C_{YX}^{\text{int}}(t) \sim \text{sign}(J) e^{-\frac{x_0^2}{2\sigma_0^2}} \frac{\sqrt{|J|} \sin(|J|t + \frac{\pi}{4})}{4\sigma_0 t^{\frac{1}{2}}}, \quad (2.63)$$

$$t \gg t'_0 = \frac{|J|}{4\sigma_0^2}, \quad |J| \gg \max(|x_0|, \sigma_0). \quad (2.64)$$

For the other correlators we find

$$C_{T_0S}^{\text{int}}(t) \sim -e^{-\frac{x_0^2}{2\sigma_0^2}} \frac{\cos(|J|t + \frac{3\pi}{4})}{4\sigma_0\sqrt{|J|}t^{\frac{3}{2}}}, \quad (2.65)$$

$$C_{T_0X}^{\text{int}}(t) \sim -\text{sign}(J)e^{-\frac{x_0^2}{2\sigma_0^2}} \frac{x_0\sqrt{|J|}\cos(|J|t + \frac{3\pi}{4})}{8\sigma_0^3t^{\frac{3}{2}}}, \quad (2.66)$$

$$C_{T_0Y}^{\text{int}}(t) \sim e^{-\frac{x_0^2}{2\sigma_0^2}} \frac{x_0\sqrt{|J|}\sin(|J|t + \frac{3\pi}{4})}{8\sigma_0^3t^{\frac{3}{2}}}, \quad (2.67)$$

$$C_{YY}^{\text{int}}(t) \sim e^{-\frac{x_0^2}{2\sigma_0^2}} \frac{\sqrt{|J|}\cos(|J|t + \frac{\pi}{4})}{4\sigma_0t^{\frac{1}{2}}}. \quad (2.68)$$

$$(2.69)$$

Thus, the transverse components of the pseudo-spin have a slower decay ($\sim t^{-1/2}$) than the longitudinal component ($\sim t^{-3/2}$). This results from the fact that the Hamiltonian only has fluctuations along only one direction.

2.5 Analysis of $\sqrt{\text{SWAP}}$

In this section we analyze the $\sqrt{\text{SWAP}}$ gate using the correlation functions derived in the previous section, i.e., we analyze the $\sqrt{\text{SWAP}}$ gate taking into account the hyperfine-induced decoherence. The $\sqrt{\text{SWAP}}$ gate and single-qubit operations can be used to perform the quantum XOR gate (CNOT) which, in combination with single-qubit operations, is sufficient for universal quantum computation [1, 104]. In Ref. [28] implementation of $\sqrt{\text{SWAP}}$ has been demonstrated. However, in these experiments there was a contrast reduction of $\sim 40\%$. Here we show that taking into account hyperfine induced decoherence, still near-unit fidelity can be obtained for this operation.

The Hamiltonian of Eq. (2.1) induces unitary time evolution on the states of the system: $|\psi(t)\rangle = U(t)|\psi(0)\rangle$ with $U(t) = T \exp(-i \int_0^t H(t')dt')$. We assume that J and x_0 can be switched adiabatically [105] on a time scale that is much shorter than the time required for the gate operation and thus the time evolution operator at time τ_s has the form

$$U_s = \exp(-i\tau_s H). \quad (2.70)$$

In a Bloch-sphere picture this operator induces a rotation about an axis in the plane spanned by eigenstates of τ^x and τ^z , $|X\rangle = |\uparrow\downarrow\rangle$ and $|S\rangle = (|\uparrow\downarrow\rangle - |\downarrow\uparrow\rangle)/\sqrt{2}$ [97]. The axis of rotation is determined by the parameters J and x_0 . Through such an operation any state may be rotated into any other state on the Bloch sphere. Thus, it is possible to rotate from $|S\rangle$ to any initial state in the subspace of $S^z = 0$ by a single operation. This is important since initialization to the singlet is feasible by preparing a ground-state singlet

with both electrons on the same dot and then changing the bias [28]. We now investigate initialization to the state $|X\rangle$ taking into account hyperfine-induced decoherence.

The scheme we propose here is different from the one used in Ref. [28], where adiabatic passage from the singlet to the $|\uparrow\downarrow\rangle$ -state is used. Our scheme requires control of x_0 . We assume the system to be in the singlet state $|S\rangle$ at $t = 0$ and then switch J and x_0 such that $J = -2x_0$ and $|x_0| \gg \sigma_0$. In a Bloch-sphere picture, this corresponds to a rotation about an axis that halves the angle between $|S\rangle$ and $|X\rangle$. Since $C_{XS}(t) = C_{SX}(-t) = 1 - C_{T_0X}(-t)$ we have, for the above choice of parameters, according to Eqs. (2.46) and (2.50):

$$C_{XS}(t) = \frac{1}{2} + \frac{1}{4} \left(1 - \cos(\sqrt{2}|J|t) e^{-\frac{1}{2} \left(\frac{t}{t_0} \right)^2} \right), \quad (2.71)$$

$$J = -2x_0, \quad |x_0| \gg \sigma_0, \quad (2.72)$$

$$t_0'' = \frac{1}{\sqrt{2}\sigma_0}, \quad t \ll \frac{(J^2 + 4x_0^2)^{3/2}}{2J^2x_0^2}. \quad (2.73)$$

This correlator reaches its maximum for $\sqrt{2}|J|t = \pi$, i.e., at $\tau_s = \frac{\pi}{\sqrt{2}|J|}$. The time scale for the Gaussian decay is $t'' = \frac{1}{\sqrt{2}\sigma_0}$. To approach unit fidelity we therefore require $|J| \gg \sigma_0$, which is the case in the range of validity of the above correlator since $|x_0| \gg \sigma_0$ and J and x_0 are of the same order. At $t = \tau_s$ we switch J to zero and since $|X\rangle \otimes |n\rangle$ is an eigenstate of the remaining Hamiltonian, the system remains in this product state, untouched by decoherence induced via the nuclear spins. This scheme thus provides a way to initialize the double quantum dot system to the state $|X\rangle = \frac{1}{\sqrt{2}}(|T_0\rangle + |S\rangle) = |\uparrow\downarrow\rangle$, where arrows denote the z-component of the electron spin in each dot. In the same way, it is also possible to initialize in the state $|-X\rangle = |\tau^x = -1\rangle = \frac{1}{\sqrt{2}}(|T_0\rangle - |S\rangle) = |\downarrow\uparrow\rangle$ by switching to $J = 2x_0$.

It was already proposed in Ref. [1] to implement the $\sqrt{\text{SWAP}}$ gate by pulsing the exchange interaction J between the two dots. Here we give a detailed analysis of the $\sqrt{\text{SWAP}}$ gate taking into account hyperfine-induced decoherence.

The SWAP operation acts on the basis of the two-electron system as: $|\downarrow\downarrow\rangle \rightarrow |\downarrow\downarrow\rangle, |\downarrow\uparrow\rangle \rightarrow |\uparrow\downarrow\rangle, |\uparrow\downarrow\rangle \rightarrow |\downarrow\uparrow\rangle, |\uparrow\uparrow\rangle \rightarrow |\uparrow\uparrow\rangle$. The SWAP is an operation that acts only on the subspace of $S^z = 0$ and leaves the states $|\uparrow\uparrow\rangle$ and $|\downarrow\downarrow\rangle$ unchanged. In the system we consider this is naturally implemented through the large Zeeman splitting that separates $|\uparrow\uparrow\rangle$ and $|\downarrow\downarrow\rangle$ from the singlet and the $S^z = 0$ triplet. In order to analyze the SWAP in the $S^z = 0$ subspace we consider the regime of $|J| \gg \max(x_0, \sigma_0)$. The correlator $C_{-X,X}(t)$ gives the probability of being in the state $|-X\rangle = |\downarrow\uparrow\rangle$ for a system initialized in $|X\rangle = |\uparrow\downarrow\rangle$. Due to the symmetry relations for the correlation functions we have $C_{-X,X}(t) = 1 - C_{XX}(t) = 1 - C_{YY}(t) - C_{T_0S}(t)$ and thus find (using Eqs.

(2.59) and (2.62) and neglecting terms of order $(\sigma_0^2 + x_0^2)/J^2$,

$$C_{-X,X}(t) = 1 - C_{XX}(t) \approx \frac{1}{2} - \frac{1}{2} e^{-\frac{1}{2} \left(\frac{t}{t_0''}\right)^2} \cos(|J|t), \quad (2.74)$$

$$t_0'' = \frac{|J|}{4\sigma_0|x_0|}, \quad |J| \gg \max(|x_0|, \sigma_0), \quad t \ll t_0' = \frac{|J|}{4\sigma_0^2}. \quad (2.75)$$

We obtain the maximum value for this correlator when $\tau_s = \frac{\pi}{|J|}$. The Gaussian has a decay time of $t_0'' = \frac{|J|}{4\sigma_0|x_0|}$, so for $x_0 \rightarrow 0$ the Gaussian decay is negligible and we obtain unit fidelity for this SWAP operation $|\uparrow\downarrow\rangle \rightarrow |\downarrow\uparrow\rangle$ up to a global phase factor (which is not visible in the correlator).

From the SWAP operation it is only a small step towards the $\sqrt{\text{SWAP}}$ which we obtain when we let the system evolve with the same parameter values but for only half the time. Starting in the state $|X\rangle$ we obtain $|Y\rangle$ after applying a $\sqrt{\text{SWAP}}$. For large $|J|$ we find for the correlator C_{YX} in the limit $x_0 \rightarrow 0$

$$C_{YX}(t) = \frac{1}{2} + \text{sign}(J) \frac{1}{2} e^{-\frac{1}{2} \left(\frac{t}{t_0''}\right)^2} \sin(|J|t), \quad (2.76)$$

$$t_0'' = \frac{|J|}{4\sigma_0|x_0|}, \quad |J| \gg \max(|x_0|, \sigma_0), \quad t \ll t_0' = \frac{|J|}{4\sigma_0^2}. \quad (2.77)$$

Here again the time scale of the Gaussian decay is $\frac{|J|}{4\sigma_0|x_0|}$ and approaches infinity for $x_0 \rightarrow 0$. The time during which we have to operate with these values of the parameters J and x_0 is now $\tau_s = \frac{\pi}{2|J|}$. Our calculations show that for the time during which J is pulsed high there is a regime in which unit fidelity may be approached. The reduced visibility in the experiment [28] may be due to several reasons such as reduced visibility in the readout of $|\downarrow\uparrow\rangle$ or the initialization of $|\uparrow\downarrow\rangle$.

2.6 Conclusion

We have developed a method that uses the measurement of a Rabi resonance in the quantum-dot spin qubit to narrow the distribution of the nuclear spin states. This method relies on Rabi oscillations induced via an oscillation of the singlet-triplet splitting J in the subspace $S^z = 0$ of two electrons in a double quantum dot forming a two-qubit system. Further, we have calculated several correlators in the $S^z = 0$ subspace for static J and found that the transverse components of pseudo-spin have a slower decay than the longitudinal one. We have also discussed the implementation and fidelity of the $\sqrt{\text{SWAP}}$ -gate in this system and the initialization to the $|\uparrow\downarrow\rangle, |\downarrow\uparrow\rangle$ states.

Chapter 3

Universal phase shift and non-exponential decay of driven single-spin oscillations

[F.H.L. Koppens, D.Klauser, W.A. Coish, K.C. Nowack, L.P. Kouwenhoven, D. Loss and L.M.K. Vandersypen, Phys. Rev. Lett. **99**, 106803 (2007)]

In this chapter we study, both theoretically and experimentally, driven Rabi oscillations of a single electron spin coupled to a nuclear spin bath. Due to the long correlation time of the bath, two unusual features are observed in the oscillations. The decay follows a power law, and the oscillations are shifted in phase by a universal value of $\sim \pi/4$. These properties are well understood from a theoretical expression that we derive here in the static limit for the nuclear bath. This improved understanding of the coupled electron-nuclear system is important for future experiments using the electron spin as a qubit.

3.1 Introduction

A quantum bit is engineered such that its coupling to the disturbing environment is minimized. Understanding and controlling this coupling is therefore a major subject in the field of quantum information processing. It is not solely the coupling strength but also the dynamics of the environment that governs the quantum coherence. In particular, the limit where these dynamics are slow compared to the evolution of the quantum system is interesting. The well-known Markovian Bloch equations that describe the dynamics of a driven system, including the exponential decay of the longitudinal and transverse magnetization [106], then lose their validity. Such deviations from the exponential behavior have been studied theoretically [107, 108] and experimentally, for instance in superconducting qubit systems [109].

An electron spin confined in the solid state is affected predominantly by

phonons via the spin-orbit interaction [8, 110–113], and by nuclear spins in the host material via the hyperfine interaction. At low temperature, coupling to the nuclear spins is the dominant decoherence source [28, 44–48, 50, 52]. Although this strong coupling leads to an apparent decoherence time T_2^* of the order of 20 ns when time-averaged over experimental runs, the decoherence time T_2 strongly depends on the dynamics in the nuclear spin bath. This typical nuclear spin dynamics is very slow, because the nuclear spins are only weakly coupled with each other and the bath itself is coupled very weakly to its dissipative environment (like phonons). This implies that here, the Markovian Bloch equations are not valid.

Here we study the dynamics and decoherence of an electron spin in a quantum dot that is coherently driven via pulsed magnetic resonance, and is coupled to a nuclear spin bath with a long correlation time. We find experimentally that, remarkably, the electron spin oscillates coherently, even when the Rabi period is much longer than $T_2^* = 10 - 20$ ns. In addition, the characteristics of the driven electron spin dynamics are unusual. The decay of the Rabi oscillations is not exponential but follows a power law and a universal (parameter independent) phase shift emerges.

A power-law decay is generally difficult to observe because it usually appears at long timescales. Here, the power-law decay is already valid after a short time (see below), allowing it to be observed experimentally. In this work, we present the observation of a power-law decay as well as a universal phase shift. We compare the experimental results with a theoretical expression, derived in the limit of a static nuclear spin bath.

3.2 Single-spin ESR – theory

We consider a double quantum dot with one electron in each dot and a static external magnetic field in the z -direction, resulting in a Zeeman splitting $\epsilon_z = g\mu_B B_z$. The spin transitions are driven by a burst of a transverse oscillating field along the x -direction with amplitude B_{ac} and frequency ω , which is generated by a current I_s through a microfabricated wire close to the double dot [30]. The interaction between the electron spin and the nuclear bath is described by the Fermi contact hyperfine interaction $\vec{S} \cdot \vec{h}$, where \vec{h} is the field generated by the nuclear spins at the position of the electron. For a large but finite number of nuclear spins ($N \sim 10^6$ for lateral GaAs dots) h_z is Gaussian distributed (due to the central-limit theorem) with mean $h_0 = \overline{h_z}$ and variance $\sigma^2 = \overline{(h_z - h_0)^2}$ [44–46]. For a sufficiently large external magnetic field ($\epsilon_z \gg \sigma$), we may neglect the transverse terms $S_\perp \cdot h_\perp$ of the hyperfine interaction that give rise to electron-nuclear-spin flip-flops (see below). Furthermore, if the singlet-triplet energy splitting J is much smaller than both ϵ_z and $g\mu_B B_{ac}$, we may treat the spin dynamics of the electrons in each dot independently (valid for times less than $1/J$). For each dot we thus have the

following spin Hamiltonian ($\hbar = 1$):

$$H(t) = \frac{1}{2}(\epsilon_z + h_z)\sigma_z + \frac{b}{2}\cos(\omega t)\sigma_x, \quad (3.1)$$

where σ_i (with $i = x, z$) are the Pauli matrices and $b = g\mu_B B_{ac}$ (taken to be equal in both dots).

We note two important points about this Hamiltonian. First, it contains only one decoherence source: the uncertainty of the longitudinal nuclear field h_z . Second, h_z is considered as completely static during the electron spin time evolution. This is justified because the correlation time of the fluctuations in the nuclear-spin system due to dipole-dipole and hyperfine-mediated interaction between the nuclear spins, which is predicted to be $\gtrsim 10 - 100 \mu\text{s}$ [44–46, 51, 70, 93, 114], is much larger than the timescale for electron spin dynamics considered here (up to $1 \mu\text{s}$).

In the experiment, the electron spin state is detected in a regime where electron transport through the double quantum dot occurs via transitions from spin states with one electron in each dot (denoted as $(1,1)$) to the singlet state $|S(0,2)\rangle$ with two electrons in the right dot. These transitions, governed via the tunnel coupling t_c by the tunneling Hamiltonian $H_{t_c} = t_c |S(1,1)\rangle \langle S(0,2)| + H.c.$, are only possible for anti-parallel spins, because $\langle \uparrow\uparrow | H_{t_c} | S(0,2) \rangle = \langle \downarrow\downarrow | H_{t_c} | S(0,2) \rangle = 0$, while $\langle \downarrow\uparrow | H_{t_c} | S(0,2) \rangle \neq 0$ and $\langle \uparrow\downarrow | H_{t_c} | S(0,2) \rangle \neq 0$. Therefore, the states with even spin parity (parallel spins) block transport, while the states with odd spin parity (antiparallel spins) allow for transport. If the system is initialized to an even spin-parity state, the oscillating transverse magnetic field (if on resonance) rotates one (or both) of the two spins and thus lifts the blockade [30]. Initializing to $|\uparrow\rangle$ in both dots (the case with $|\downarrow\rangle$ gives the same result), we calculate the probability for an odd spin parity P_{odd} under time evolution for each of the two spins governed by the Hamiltonian in Eq.(3.1).

Introducing the detuning from resonance $\delta_\omega = \epsilon_z + h_z - \omega$, the probability to find spin up for a single value of h_z in the rotating wave approximation (which is valid for $(b/\epsilon_z)^2 \ll 1$) is given by

$$P_{\uparrow, \delta_\omega}(t) = \frac{1}{2} \left[1 + \frac{4\delta_\omega^2}{b^2 + 4\delta_\omega^2} + \frac{b^2}{b^2 + 4\delta_\omega^2} \cos \left(\frac{t}{2} \sqrt{b^2 + 4\delta_\omega^2} \right) \right]. \quad (3.2)$$

Assuming that $\omega = h_0 + \epsilon_z$, i.e., $\delta_\omega = h_z - h_0$, we find when averaging over the Gaussian distribution of h_z values (see Appendix D)

$$P_{\uparrow}(t) \sim \frac{1}{2} + C + \sqrt{\frac{b}{8\sigma^2 t}} \cos \left(\frac{b}{2} t + \frac{\pi}{4} \right) + \mathcal{O} \left(\frac{1}{t^{3/2}} \right), \quad (3.3)$$

for $t \gg \max(\frac{1}{\sigma}, 1/b, b/2\sigma^2)$, with $C = \frac{1}{2} - \frac{\sqrt{2\pi}b}{8\sigma} \exp \left(\frac{b^2}{8\sigma^2} \right) \text{erfc} \left(\frac{b}{2\sqrt{2}\sigma} \right)$. We can now calculate the probability of finding an odd spin-parity state taking

$\omega = h_0 + \epsilon_z$ for both dots and drawing the value of h_z independently from a distribution with width σ in each dot:

$$\begin{aligned} P_{\text{odd}}(t) &= P_{\uparrow,L}(t)(1 - P_{\uparrow,R}(t)) + (1 - P_{\uparrow,L}(t))P_{\uparrow,R}(t) \\ &= \frac{1}{2} - 2C^2 - C\frac{f(t)}{\sqrt{t}} - \frac{g(t)}{t} + \mathcal{O}\left(\frac{1}{t^{3/2}}\right), \end{aligned} \quad (3.4)$$

where

$$f(t) = \sqrt{\frac{2b}{\sigma^2}} \cos\left(\frac{bt}{2} + \frac{\pi}{4}\right), \quad (3.5)$$

$$g(t) = \frac{b}{8\sigma^2} \left[1 + \cos\left(bt + \frac{\pi}{2}\right)\right]. \quad (3.6)$$

This result is valid for times $t \gtrsim \max(1/\sigma, 1/b, b/2\sigma^2) \sim 20\text{ns}$ for a 1.4 mT nuclear field (see below) and $b \leq 2\sigma$ (accessible experimental regime). The $1/t$ -term oscillates with the double Rabi frequency which is the result of both spins being rotated simultaneously (see also [30]). This term only becomes important for $b > \sigma$, because in that case for both spins most of the nuclear-spin distribution is within the Lorentzian lineshape of the Rabi resonance. The $1/\sqrt{t}$ -term oscillates with the Rabi frequency and originates from only one of the two spins being rotated [30]. This term is important when $b < \sigma$, i.e., when only a small fraction of the nuclear-spin distribution is within the lineshape of the Rabi resonance.

We also give the expression for $P_{\text{odd}}(t)$ for the case where only one of the two spins is on resonance ($\epsilon_z + h_0 - \omega = 0$), while the other is far off-resonance ($|\epsilon_z + h_0 - \omega| \gg \sigma$). In this case the spin in one dot always remains up while the spin in the other dot rotates. This leads to

$$P_{\text{odd}}^{(1)}(t) = 1 - P_{\uparrow}(t) = \frac{1}{2} - C - \frac{f(t)}{4\sqrt{t}} + \mathcal{O}\left(\frac{1}{t^{3/2}}\right), \quad (3.7)$$

with the same range of validity as in Eq.(3.4). We see that the $1/t$ -term, which oscillates with frequency b , is not present in this case.

The expressions for $P_{\text{odd}}(t)$ (Eqs. (3.4) and (3.7)) reveal two interesting features: the *power-law decay* and a universal *phase shift* of $\pi/4$ (see Eq. (3.5)) in the oscillations which is independent of all parameters. These features can both only appear if the nuclear field h_z is static during a time much longer than the Rabi period. This is crucial because only then the driven spin coherence for one fixed value of h_z is fully preserved. Because different values of h_z give different oscillation frequencies, the decay is due to averaging over the distribution in h_z .

The phase shift is closely related to the power-law decay because it also finds its origin in the off-resonant contributions. These contributions have a

higher Rabi frequency and shift the average oscillation in phase. This universal phase shift therefore also characterizes the spin decay, together with the power law. Interestingly, the specific shape of the distribution in h_z (as long as it is peaked around the resonance) is not crucial for the appearance of both the power-law decay and the phase shift (see Appendix D. The values of the decay power and the phase shift are determined by the dependence of the oscillation frequency on h_z (in this case $\sqrt{b^2 + 4\delta_\omega^2}$).

A power-law decay has previously been found theoretically in [44, 46, 115, 116] and both a power-law decay ($1/t^{3/2}$) and a universal phase shift also appear in double dot correlation functions [50, 51]. In [52] a singlet-triplet correlation function was measured, but the amplitude of the oscillations was too small for the phase shift and the power-law decay to be determined. Here, we consider driven Rabi oscillations of a single electron spin with a power-law decay of $1/\sqrt{t}$ that is already valid after a short time $1/\sigma \sim 20$ ns. Therefore, the amplitude of the driven spin oscillations is still high when the power-law behavior sets in, even for small driving fields ($b < 2\sigma$) which are experimentally easier to achieve. The power-law decay and the phase shift thus should be observable in the experiment.

3.3 Power-law decay

We now discuss the observation of the power-law decay in the experimental data of which a selection is shown in Fig. 3.1. The data are obtained with the same device and under the same experimental conditions as in [30]. A fit is carried out to the observed oscillations for four different driving fields B_{ac} (Fig. 3.1), with three different fit functions: the theoretical expressions (Eqs. (3.4) and (3.7) with b and a constant scaling factor as fit parameters) and an exponentially decaying cosine. The width of the nuclear distribution $\sigma = g\mu_B(1.4 \text{ mT})$ is obtained from a fit of the steady state value $\frac{1}{2} - 2C^2$ of $P_{odd}(t)$ to a dataset obtained at $t = 950$ ns (Fig. 3.2a).

For the range $B_{ac} \geq 1.9$ mT, we find good agreement with the model that predicts a power-law decay of $1/\sqrt{t}$ (Eq. (3.4); h_0 equal for both dots), while the fit with an exponentially decaying cosine is poor (blue lines in Fig. 3.1). The power of the decay is independently verified by means of a fit to the data with $a_1 + a_2 \cos(2\pi t/a_3 + \pi/4)/t^d$ where, besides $a_{1,2,3}$, the power d of the time t is a fit parameter as well. We find values of $d \sim 0.6$ (Fig. 3.2b), close to the predicted $1/\sqrt{t}$ -dependence.

We see much better correspondence of the data with Eq. (3.4) than with Eq. (3.7), from which we can conclude that the mean of the Gaussian distribution h_0 is comparable for both dots (in equilibrium, we expect $h_0 \sim 0$ in both dots). There might however still be a small difference in h_0 between the

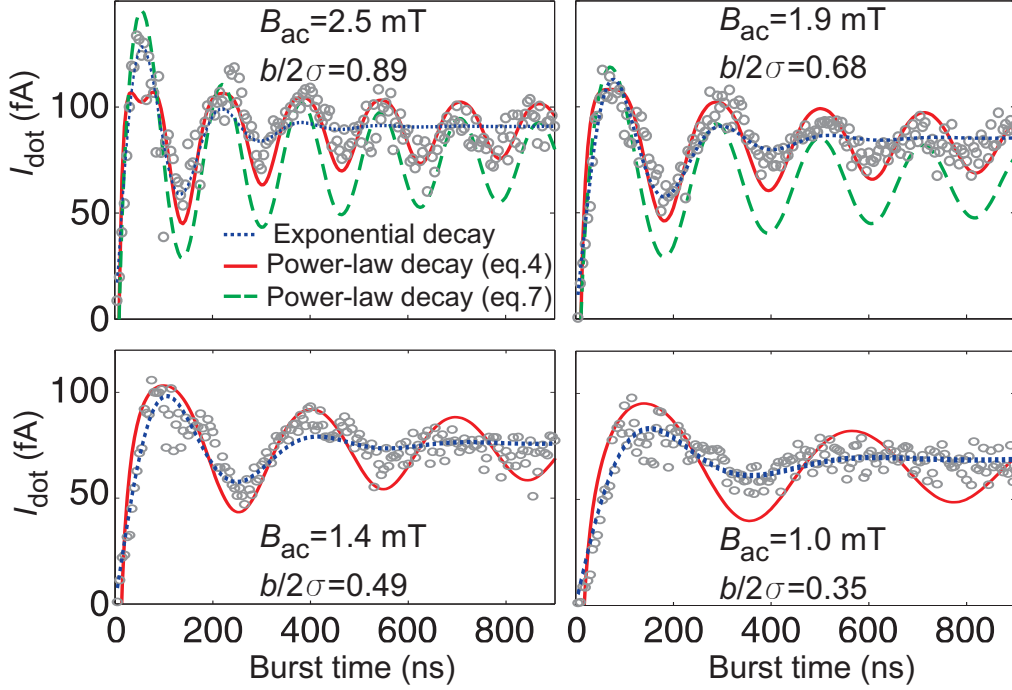


Figure 3.1: (Color online) Rabi oscillations for four different driving fields B_{ac} ($B_z = 55$ mT, $g = 0.355$ and $\sigma = g\mu_B(1.4$ mT)). The gray circles represent the experimentally measured dot current (averaged over 15 s for each value of t), which reflects the probability to find an odd spin-parity state after the RF burst that generates B_{ac} . The dotted, solid and dashed lines represent the best fit to the data of an exponentially decaying cosine function and the derived analytical expressions for $P_{odd}(t)$ and $P_{odd}^{(1)}(t)$ (Eqs. (3.4) and (3.7)) respectively. For clarity, the dashed line is shown only for the top two panels. The fit was carried out for the range 60 to 900 ns and the displayed values for B_{ac} were obtained from the fit with $P_{odd}(t)$ (Eq. (3.4)). We fit the data with an exponentially decaying cosine with a tunable phase shift that is zero at $t = 0$: $a_1 e^{-t/a_2} [\cos(\phi) - \cos(2\pi t/a_3 + \phi)] + a_4 (1 - e^{-t/a_2})$. The last term was added such that the saturation value is a fit parameter as well. We note that the fit is best for $\phi = \pi/4$, as discussed in the text.

two dots, which we cannot determine quantitatively because the two models describe only two limiting cases. If present, such a difference in h_0 could help explain the small deviation between data and model at the first oscillation for $B_{ac} = 2.5$ mT. It could originate from asymmetric feedback of the electron spins on the respective nuclear spin baths, e.g. due to unequal dot sizes, leading to different hyperfine coupling constants. Another observation is that for small driving fields, $B_{ac} < 1.9$ mT, we see that the damping is faster than predicted. Possible explanations for this effect are corrections due to

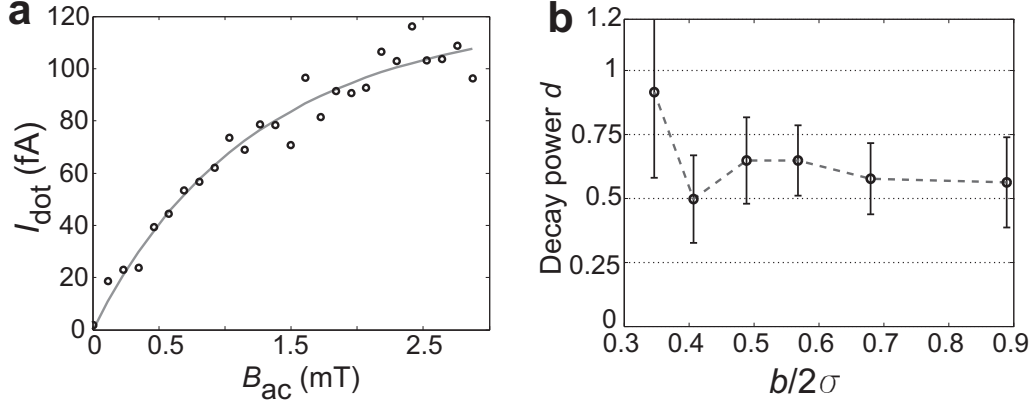


Figure 3.2: a) Dot current after an RF burst of 950 ns as a function of B_{ac} , approximately representing the steady-state value. The solid curve is the best fit with $a_1(\frac{1}{2} - 2C^2)$: the steady state expression of Eq. (3.4) with a_1 and σ as fit parameters. We find, for the 95%-confidence interval, $\sigma = g\mu_B(1.0 - 1.7$ mT). b) Decay power obtained from the best fit of the data (partially shown in Fig. 3.1) with the expression $a_1 + a_2 \cos(2\pi t/a_3 + \pi/4)/t^d$, where $a_{1,2,3}$ and d are fit parameters.

electron-nuclear flip-flops (transverse terms in the hyperfine Hamiltonian) or electric field fluctuations. Electron-nuclear flip-flops may become relevant on a timescale $\sim \epsilon_z/\sigma^2 \sim 1 \mu s$ in this experiment. Electric field fluctuations can couple to spin states via the spin-orbit interaction [103] or a finite electric-field dependent exchange coupling.

3.4 Phase shift

We continue the discussion with the experimental observation of the second theoretically predicted prominent feature of the Rabi oscillations, i.e., a phase shift of $\pi/4$ in the oscillations, which is independent of all parameters. In principle, the experimental value of this phase shift ϕ can be extracted from single traces like those in Fig. 3.1. However, the precision is poor because a small uncertainty in the Rabi frequency can lead to a large uncertainty in ϕ . A much more precise value of ϕ can be extracted from the oscillations measured for a wide range and small steps of B_{ac} , like the data shown in Fig. 3.3a. That is because the Rabi period $T_{Rabi} = 2\pi/g\mu_B(\frac{1}{2}B_{ac}) = 2\pi/g\mu_B(\frac{1}{2}KI_s)$ contains only one unknown parameter K (current to oscillating field amplitude B_{ac} conversion factor, in units of T/A) which is independent of the current through the wire I_s that generates B_{ac} [30]. The presence of a phase shift is visible in Fig. 3.3a, where the green and blue lines correspond respectively to the maxima of a cosine with and without a phase shift of $\pi/4$. The green lines match very well the yellow bands representing high data values. In contrast,

the blue lines are located on the right side of the yellow bands for small burst times and more and more on the left side of the bands for increasing burst times. Thus, a cosine without a phase shift does not match with the observed Rabi oscillations.

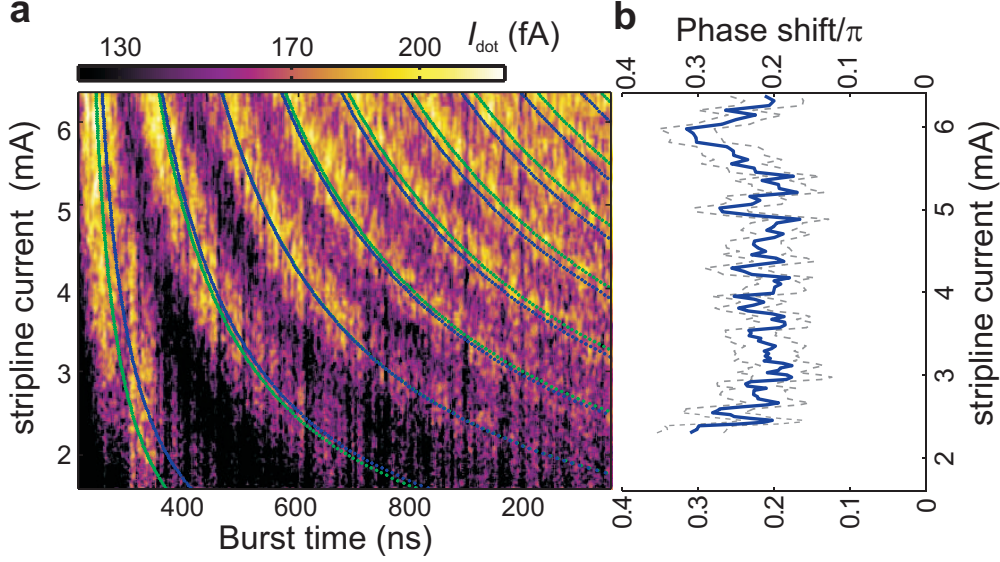


Figure 3.3: a) The dot current (represented in colorscale) is displayed over a wide range of B_{ac} (the sweep axis) and burst durations. The green and blue lines correspond respectively to the maxima of a cosine with and without a phase shift of $\pi/4$. In contrast to the green lines, the blue lines are located in advance of the maxima of the observed oscillations for small burst times, and behind the maxima for longer burst times. The current-to-field conversion factor K is fitted for both cases separately ($K=0.568$ mT/mA and $K=0.60$ mT/mA for respectively with and without phase shift; the fit range is $t = 60 - 500$ ns and $I_s = 3.6 - 6.3$ mA). b) Phase shift for a wide range of B_{ac} , displayed as a function of stripline current I_s . Values obtained from a fit of each trace of the data in a) (varying burst time, constant B_{ac}) to a damped cosine $a_1 - a_2 \cos(\frac{1}{2} K I_s g \mu_B t + a_3 \pi) / \sqrt{t}$, where $a_{1,2,3}$ are fit parameters and $K = 0.568$ mT/mA. I_s is a known value in the experiment, extracted from the applied RF power. The gray dashed lines represent the 95% confidence-interval.

In order to determine ϕ quantitatively, we perform a single two-dimensional fit of the complete dataset in Fig.3.3a with $P_{\text{odd}}(t)$ (Eq. (3.4)), excluding the $1/t$ -term (see Appendix C). The fit range is $t = 100 - 900$ ns, such that the contribution from the $1/t$ -term of Eq. (3.4) can be neglected. For the 95% confidence interval we find $\phi = (0.23 \pm 0.01)\pi$, close to the theoretical value.

The relation between ϕ and B_{ac} is visible in Fig. 3.3b, where we find no significant dependence of ϕ as a function of B_{ac} , although the accuracy decreases for smaller B_{ac} (values obtained from fits to single traces, see caption). We have not compensated for the effects of the finite rise time (<2 ns) of the bursts, which leads to a small negative phase shift, on top of the expected positive $\pi/4$ shift.

3.5 Conclusion

To conclude, we have experimentally observed a power-law decay and universal phase shift of driven single electron spin oscillations. These features are theoretically understood by taking into account the coupling of the spin to the nuclear spin bath, which is static on the timescale of the electron spin evolution time. These reported results affect the prospect of making electron-spin based qubits in GaAs quantum dots. Namely, the slow power-law decay allows spin manipulation with smaller driving fields, and knowledge of the phase-shift is relevant for determination of the correct pulse lengths. Furthermore, non-exponential coherence decay will affect error-correction schemes which usually account for exponential decays. For future investigation, it remains interesting to obtain more information about the non-static contributions of the nuclear bath or other possible decoherence mechanisms. This requires measuring the driven oscillations at larger external fields, with larger driving powers and longer evolution times than accessible in this work.

Chapter 4

Nuclear spin dynamics and Zeno effect in quantum dots and defect centers

[D. Klauser, W.A. Coish, D. Loss, arXiv:0802.2463]

In this chapter we analyze nuclear spin dynamics in quantum dots and defect centers with a bound electron under electron-mediated coupling between nuclear spins due to the hyperfine interaction (“J-coupling” in NMR). Our analysis shows that the Overhauser field generated by the nuclei at the position of the electron has short-time dynamics quadratic in time for an initial nuclear spin state without transverse coherence. The quadratic short-time behavior allows for an extension of the Overhauser field lifetime through a sequence of projective measurements (quantum Zeno effect). We analyze the requirements on the repetition rate of measurements and the measurement accuracy to achieve such an effect. Further, we calculate the long-time behavior of the Overhauser field for effective electron Zeeman splittings larger than the hyperfine coupling strength and find, both in a Dyson series expansion and a generalized master equation approach, that for a nuclear spin system with a sufficiently smooth polarization the electron-mediated interaction alone leads only to a partial decay of the Overhauser field by an amount on the order of the inverse number of nuclear spins interacting with the electron.

4.1 Introduction

Technological advancements have made it possible to confine very few electrons in a variety of nanostructures such as nanowires, quantum dots, donor impurities, or defect centers [18–20, 22–37, 117–119]. One driving force behind these achievements is a series of proposals for using the spin of an electron as a qubit for quantum computing [1, 2, 120]. This spin interacts with the nuclear

spins in the host material via the hyperfine interaction. While this interaction leads to decoherence of the electron spin state on one hand, it also provides the opportunity to create a local effective magnetic field (Overhauser field) for the electron by inducing polarization in the nuclear spin system, which could be used, e.g., for rapid single-spin rotations [121]. Polarizing the nuclear spin system is also one possible way to suppress hyperfine-induced decoherence [43, 46] or it can be used as a source of spin polarization to generate a spin-polarized current. In any case, controlling the dynamics of the Overhauser field and, in particular, to prevent its decay, is thus of vital importance in the context of spintronics and quantum computation [3].

In GaAs quantum dots the Overhauser field can become as large as 5T. The build-up, decay, and correlation time of the Overhauser field have been studied in a number of systems [48, 58, 60, 61, 77, 84–86, 95, 122–128], suggesting timescales for the decay on the order of seconds, minutes, or in one case, even hours [76].

In this article we address the question: How can a large Overhauser field be preserved? That is, how can the Overhauser-field decay be suppressed or even prevented. The dynamics of the Overhauser field are governed by the mutual interaction between the nuclear spins. There is on one hand the direct dipolar coupling between the nuclear spins. On the other hand, due to the presence of a confined electron, there is also an indirect interaction: The coupling of the nuclear spins to the electron via the hyperfine interaction leads to an effective interaction between the nuclear spins that is known as the electron-mediated interaction. While the effect of this electron-mediated interaction on the decoherence of the *electron* has been studied previously [70, 114, 121], theoretical studies of the decay of the Overhauser field have so far studied direct dipole-dipole interaction and the effect of the hyperfine interaction was taken into account through the Knight shift that the electron induces via the hyperfine interaction [129]. In this article we investigate the effect of the electron-mediated interaction between nuclear spins on the dynamics of the Overhauser field. While the direct dipolar coupling is always present, it can be weaker than the electron-mediated interaction for magnetic fields that are not too large and may be further reduced via NMR pulse sequences or by diluting the concentration of nuclear spins.¹ We find in our calculation that, for effective electron Zeeman splittings ω (sum of Zeeman splittings due to the external magnetic field and Overhauser field) larger than the hyperfine coupling strength A , the decay of the Overhauser field due to the electron-mediated interaction is incomplete, i.e., that only a small fraction of the Overhauser field decays. In a short-time expansion that is valid for ω larger than A/\sqrt{N} ,

¹Diluting reduces the dipolar coupling strongly, as it decreases with the third power of the distance between the nuclei. In contrast, the hyperfine coupling is proportional to the density of nuclei and thus for a one-dimensional (two-dimensional) system only decreases with the first (second) power of the distance between the nuclei.

where N is the number of nuclear spins with which the electron interacts, we find a quadratic initial decay on a timescale $\tau_e = N^{3/2}\omega/A^2$. We show that, by performing repeated projective measurements on the Overhauser field, a quantum Zeno effect occurs, which allows one to preserve the Overhauser field even for relatively small effective electron Zeeman splittings larger than A/\sqrt{N} . Overall, we thus obtain the following picture: The Overhauser field can be preserved either by applying a large external magnetic field (it only decays by a small fraction for $\omega \gg A$) or by performing repeated projective measurements on the Overhauser field (with our calculation for the short-time dynamics being valid for $\omega \gg A/\sqrt{N}$).

In Sec. 4.2 we briefly review the quantum Zeno effect and give the corresponding main results for the case of the Overhauser field. We start our detailed discussion in Sec. 4.3 by writing down the Hamiltonian for the hyperfine interaction and by deriving an effective Hamiltonian for the electron-mediated interaction. In Sec. 4.4 we derive an expression for the short-time behavior of the Overhauser field mean value. In Secs. 4.5 and 4.6 we address the long-time decay of the Overhauser field due to the electron-mediated interaction. Some technical details are deferred to Appendices E and F.

4.2 Zeno effect

The suppression of the decay of a quantum state due to frequently repeated measurements is known as the quantum Zeno effect. The concept of the quantum Zeno effect [130] is almost as old as quantum mechanics [74, 131] and it remains one of the most intriguing quantum effects. It has been studied intensively from the theoretical side [132–134] and also experimental evidence has been found in recent years [135].

Let us consider a two-level system initialized to the excited state and assume that a small additional perturbation (e.g. due to interaction with the environment) leads to decay from the excited state to the ground state. The survival probability P_s in the excited state as a function of the elapsed time t is initially given by $P_s(t) = 1 - c_s t^2/\tau_s^2$, with the constant c_s and the timescale τ_s being system dependent. A projective measurement at time τ_m resets the system to the excited state with probability $P_s(\tau_m)$. Repeating the measurement m times at intervals $\tau_m \ll \tau_s$, the survival probability is $P_{s,meas}(m\tau_m) = (1 - c_s \tau_m^2/\tau_s^2)^m \approx 1 - c_s m \tau_m / (\tau_s^2/\tau_m)$, for $c_s m \tau_m^2/\tau_s^2 \ll 1$. The survival probability at time $t = m\tau_m$ is thus increased due to the frequently repeated measurements: instead of a quadratic decay on a timescale τ_s without measurements, we have a linear decay on a timescale τ_s^2/τ_m .

A more complex observable such as the mean of the Overhauser-field z -component $\langle h_z(t) \rangle = \text{Tr}\{h_z \rho(t)\}$, may also show a Zeno effect. That $\langle h_z(t) \rangle$ shows an initial quadratic decay is, however, not obvious and actually depends on the initial state of the nuclear spin system $\rho_I(0)$ (see the first paragraph of

Sec. 4.4 below for details). For the short-time behavior of $\langle h_z(t) \rangle$, we expand in a Taylor series

$$\langle h_z(t) \rangle = \langle h_z(0) \rangle + t \langle h_z \rangle_1 + \frac{t^2}{2} \langle h_z \rangle_2 + \dots, \quad (4.1)$$

with $\langle h_z \rangle_n = d^n \langle h_z(t) \rangle / dt^n |_{t=0}$. If $\langle h_z \rangle_1 = 0$, the t -linear term vanishes and the initial decay is quadratic in time. In Sec. 4.4 we find that $\langle h_z \rangle_1 = 0$ under the condition that the initial nuclear spin state is diagonal in a basis of h_z -eigenstates. In this case the initial decay is of the form

$$\frac{\langle h_z(t) \rangle}{\langle h_z(0) \rangle} = 1 - c \frac{t^2}{\tau_e^2}. \quad (4.2)$$

The timescale τ_e and the constant c are given below in Eq. (4.18) and Eq. (4.19) respectively.

Let us now consider a sequence of repeated measurements of the Overhauser field $h_z(t)$. In the context of quantum dots, several proposals [51, 72, 73] to implement such measurements have been put forward. A measurement of h_z shall be performed after a time τ_m . If this measurement is projective, i.e., if it sets all the off-diagonal elements of the density matrix in a basis of h_z -eigenstates to zero (we discuss requirements on the accuracy of the measurement in Appendix F), the dynamics after τ_m again follow Eq. (4.2). Repeating the measurement at times $2\tau_m, 3\tau_m, \dots$, leads to a change of the decay of the Overhauser field in the same way as we described it for the two-level system above:

$$\frac{\langle h_z(t) \rangle_{zeno}}{\langle h_z(0) \rangle} = 1 - c \frac{t}{\tau_{zeno}}, \quad \tau_{zeno} = \frac{\tau_e^2}{\tau_m}. \quad (4.3)$$

Instead of a quadratic decay $\propto t^2/\tau_e^2$ we have a linear decay $\propto t/\tau_{zeno}$ with $\tau_{zeno} = \tau_e^2/\tau_m$. We note that the expression for $\langle h_z(t) \rangle_{zeno}$ in Eq. (4.3) is only strictly valid at times $m\tau_m$ with m being a positive integer. Between these times $\langle h_z(t) \rangle$ changes according to Eq.(4.2). The derivation of Eq. (4.3) requires $cm\tau_m^2/\tau_e^2 = ct/\tau_{zeno} \ll 1$. Fig. 4.1 shows the Zeno effect, i.e., the difference between $\langle h_z(t) \rangle / \langle h_z(0) \rangle$ and $\langle h_z(t) \rangle_{zeno} / \langle h_z(0) \rangle$.

In addition to requirements on the measurement accuracy (see Appendix F), the results in this section rest on the following separation of timescales:

$$\tau_{pm} \ll \tau_m \ll \tau_e, \tau_x, \quad (4.4)$$

where τ_{pm} is the time required to perform a single measurement and τ_x the timescale up to which the short-time expansion for $\langle h_z(t) \rangle$ is valid. In general, τ_x can be shorter than τ_e . A specific case (fully polarized nuclear state), where the short-time expansion has only a very limited range of validity, is discussed in Sec. 4.4.1. For the systems studied in experiment, we expect τ_x to be comparable to or longer than τ_e , since the experiments performed so far show

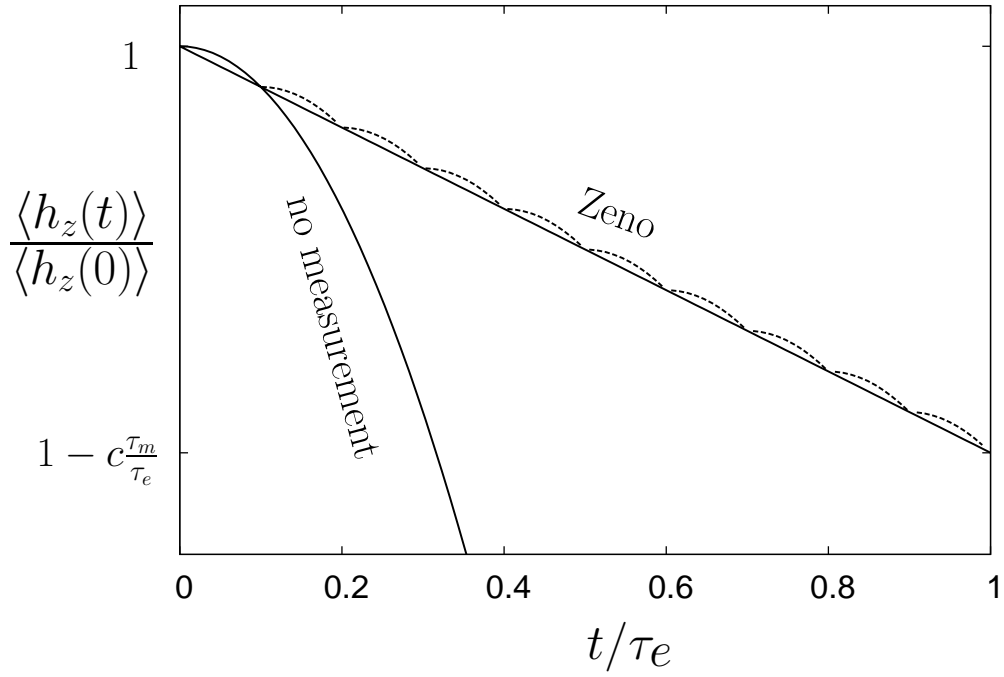


Figure 4.1: Effect of projective measurements at time intervals $\tau_m = \tau_e/10$ on the time evolution of the Overhauser field expectation value $\langle h_z(t) \rangle$. Due to the Zeno effect, the decay with measurements is $1 - ct/\tau_{zeno}$ rather than $1 - ct^2/\tau_e^2$ without measurements, where $\tau_{zeno} = \tau_e^2/\tau_m$. The formula $1 - ct/\tau_{zeno}$ for the decay with measurement is only strictly valid at times $t = m\tau_m$ with m being a positive integer. After the measurement at $t = m\tau_m$ the decay is again quadratic with time dependence $\langle h_z(m\tau_m) \rangle / \langle h_z(0) \rangle - c(t - m\tau_m)^2/\tau_e^2$ (broken lines).

timescales for the decay of $\langle h_z(t) \rangle$ on the order of seconds, minutes, or in one case, even hours [76]. We note that it may be a demanding task to perform the fast and precise measurements required to obtain a Zeno effect in the present context. Still, experimental progress in the control of the nuclear field, such as that shown in Ref. [76], suggests that such measurements may be within reach in the near future.

We continue our discussion by deriving the effective Hamiltonian we use both for calculating short-time dynamics and the long-time behavior of $\langle h_z(t) \rangle$.

4.3 Hamiltonian

We aim to describe the dynamics of many nuclear spins surrounding a central confined electron spin in a material with an s-type conduction band (e.g. GaAs, Si, etc.), where the dominant type of hyperfine interaction is the Fermi contact hyperfine interaction. The electron may be confined in many nanostructures such as nanowires, quantum dots or defect centers. Under the assumption that other possible sources of nuclear spin dynamics, such as nuclear quadrupolar splitting, are suppressed,² the two strongest interactions between nuclear spins in these nanostructures are the electron-mediated interaction (“J-coupling” in NMR [98,137]) and the direct dipole-dipole interaction. It turns out that, for a large number of nuclei N and up to magnetic fields of a few Tesla (for GaAs), the contribution of the electron-mediated interaction to the initial decay of the Overhauser field is dominant (see Appendix E). The Hamiltonian contains three parts: The electron and nuclear Zeeman energies and the Fermi contact hyperfine interaction:

$$H = H_e + H_n + H_{en} = \epsilon_z S_z + \eta_z \sum_k I_k^z + \vec{S} \cdot \vec{h}. \quad (4.5)$$

Here, the operator

$$\vec{h} = \sum_k A_k \vec{I}_k \quad (4.6)$$

is the Overhauser field. Further, \vec{S} is the electron spin and \vec{I}_k the nuclear spin at lattice site k that couples with strength $A_k = A\nu_0|\psi(r_k)|^2$ to the electron spin, where $A = \sum_k A_k$ is the total hyperfine coupling constant, ν_0 the volume occupied by a single-nucleus unit cell and $\psi(r_k)$ the electron envelope wave function. We define the number of nuclear spins N interacting with the electron as the number of nuclear spins within an envelope-function Bohr radius of the confined electron [46]. The Bohr radius a_B for an isotropic electron envelope is defined through [46] $\psi(r_k) = \psi(0)e^{-(r_k/a_B)^q/2}$, where $q = 1$ gives a hydrogen-like wave function and $q = 2$ a Gaussian. Finally, ϵ_z and η_z are the

²In high symmetry lattices, the quadrupolar splitting is often negligible [136], and is identically zero for nuclear spin $I = 1/2$.

electron and nuclear Zeeman splittings, respectively (we consider a homonuclear system). We derive an effective Hamiltonian for the electron-mediated interaction between nuclear spins, which is valid in a sufficiently large magnetic field. Using a standard Schrieffer-Wolff transformation [138] $H_{\text{eff}} = e^S H e^{-S}$, in lowest order in H_{en} , with the transformation matrix

$$S = \frac{1}{2} \sum_k A_k [(\epsilon_z + h_z - \eta_z + A_k/2)^{-1} S_+ I_k^- - (\epsilon_z + h_z - \eta_z - A_k/2)^{-1} S_- I_k^+], \quad (4.7)$$

which eliminates the off-diagonal terms between electron and nuclear spins, we find the effective Hamiltonian $H_{\text{eff}} \simeq H_0 + V$ (similar to Refs. [69, 70, 121]), where:

$$H_0 = \epsilon_z S_z + \eta_z \sum_k I_k^z + S_z h_z, \quad (4.8)$$

$$V = \frac{1}{8} \sum_{kl} A_k A_l \left[\left(\frac{1}{2} + S_z \right) (B_k^+ I_k^- I_l^+ + I_l^- I_k^+ B_k^+) - \left(\frac{1}{2} - S_z \right) (B_k^- I_k^+ I_l^- + I_l^+ I_k^- B_k^-) \right]. \quad (4.9)$$

Here, $B_k^\pm = 1/(\epsilon_z - \eta_z + h_z \pm A_k/2)$ and the raising and lowering operators are defined as $S_\pm = S_x \pm iS_y$ and similarly for h_\pm and I_k^\pm . We note that H_{eff} neglects the transfer of spin polarization from the electron to the nuclei. The electron transfers an amount of angular momentum to the nuclear system on the order $(A/\sqrt{N}\omega)^2 \ll 1$ for $\omega \gg A/\sqrt{N}$. For $\omega \sim A$ these contributions are suppressed by a factor of $O(1/N)$ compared to the decay of $\langle h_z(t) \rangle$ under H_{eff} . For very special initial states, where H_{eff} leads to no dynamics, e.g., for uniform polarization, the transfer of spin from the electron to the nuclei is the only source of nontrivial nuclear spin dynamics and therefore should be taken into account. We discuss one such initial state, namely, a fully polarized nuclear system, in Sec. 4.4.1.

In the following we assume $I = 1/2^3$ and neglect A_k in B_k^\pm which is valid up to corrections suppressed by $A_k/(\epsilon_z - \eta_z + h_z)$. We further replace h_z in the denominator of B_k^\pm by its initial expectation value $\langle h_z \rangle = \text{Tr}\{h_z \rho(0)\}$ and introduce the effective electron Zeeman splitting

$$\omega = \epsilon_z - \eta_z + \langle h_z \rangle \approx \epsilon_z + \langle h_z \rangle. \quad (4.10)$$

This replacement assumes that the initial state does not change significantly and is valid up to corrections suppressed by σ/ω , compared to the dynamics under H_{eff} . Here $\sigma = \sqrt{\langle h_z^2 \rangle - \langle h_z \rangle^2}$ is the initial width of h_z . For an unpolarized equilibrium (infinite temperature) nuclear spin state we have $\sigma \propto A/\sqrt{N}$,

³A rough estimate suggests that for $I > 1/2$ the timescales given need to be multiplied by a factor $1/(2I)^2$.

limiting the range of validity to $\omega \gg A/\sqrt{N}$.

$$V \cong \frac{1}{2\omega} \left(S_z \sum_{k \neq l} A_k A_l I_k^+ I_l^- + \frac{1}{2} \sum_k A_k^2 (S_z - I_k^z) \right), \quad (4.11)$$

where in the sum over k and l the terms $k = l$ are excluded. In the next sections we will discuss the dynamics of the Overhauser field both at short and at long times in the regimes where a perturbative treatment in V is appropriate.

4.4 Short-time expansion

With respect to the Zeno effect as discussed in Sec. 4.2, our main interest lies in the short-time behavior of the Overhauser field z -component $\langle h_z(t) \rangle$, where \vec{h} is defined in Eq. (4.6). To calculate $\langle h_z \rangle_1$ and $\langle h_z \rangle_2$ (see Eq. (4.1)), we expand

$$\langle h_z(t) \rangle = \text{Tr}\{h_z \exp(-iHt)\rho(0) \exp(iHt)\} \quad (4.12)$$

at short times. The first term $\langle h_z(0) \rangle = \text{Tr}\{h_z \rho(0)\}$ gives the expectation value at time zero, while the t -linear term is proportional to $\langle h_z \rangle_1 = -i \text{Tr}\{h_z [H, \rho(0)]\}$. Using the cyclicity of the trace we find that $\text{Tr}\{h_z [H, \rho(0)]\} = \text{Tr}\{[\rho(0), h_z] H\}$. Writing $\rho(0) = \rho_e(0) \otimes \rho_I(0)$ we have, for an initial nuclear spin state $\rho_I(0)$ without transverse coherence, $[\rho_I(0), h_z] = 0$ and thus the t -linear term vanishes. It might be possible to extend this result to more general randomly correlated initial nuclear spin states, where terms involving transverse coherence or correlations are negligibly small due to a random phase [41, 139].

To determine the frequency of projective measurements required to induce a Zeno effect, we are interested in $\langle h_z \rangle_2 = -\text{Tr}\{h_z [H, [H, \rho(0)]]\}$. We calculate $\langle h_z \rangle_2$ below using the effective Hamiltonian H_{eff} as derived in Sec. 4.3. The range of validity is limited by higher-order terms in the effective Hamiltonian which are proportional to $(h_+ h_-)^n / \omega^{(n+1)}$, $n = 2, 4, \dots$. These higher-order terms give corrections to $\langle h_z \rangle_2$ which are suppressed by a factor $(A/\sqrt{N}\omega)^n$. Thus the results for $\langle h_z(t) \rangle$ up to $O(t^2)$ given below are valid in the regime $\omega \gg A/\sqrt{N}$. Using that $[h_z, H_0] = 0$, we may simplify $\langle h_z \rangle_2$ considerably and we find for an arbitrary electron spin state:

$$\langle h_z \rangle_2 = -\frac{1}{8\omega^2} \text{Tr}_I \{h_z [\rho_I(0), h_+ h_-] h_+ h_-\}. \quad (4.13)$$

To further simplify, we assume a product initial state of the form

$$\rho(0) = \rho_e(0) \otimes \rho_I(0) = \rho_e(0) \otimes_k \rho_{I_k}, \quad (4.14)$$

$$\rho_{I_k} = 1/2 + f_k I_k^z; \quad f_k \equiv f_k(0) = 2\langle I_k^z(0) \rangle. \quad (4.15)$$

With this initial state we find

$$\langle h_z \rangle_2 = -\frac{1}{4\omega^2} \sum_{kl} f_k A_k^2 A_l^2 \text{Tr}_I \{h_z \bigotimes_{j \neq k, l} \left(\frac{1}{2} + f_j I_j^z\right) (I_k^z - I_l^z)\}. \quad (4.16)$$

Evaluating the commutators and the trace, we find for the decay of the Overhauser field mean value $\langle h_z(t) \rangle$, up to corrections of $O(t^4)$,

$$\langle h_z(t) \rangle = \langle h_z(0) \rangle - \frac{t^2}{(8\omega)^2} \sum_{kl} A_k^2 A_l^2 (A_k - A_l) (f_k - f_l). \quad (4.17)$$

We note that both for uniform coupling constants $A_k = A/N$ and for uniform polarization $f_k = p, \forall k$, the t^2 -term vanishes. This is, in fact, what one would expect, since H_{eff} only leads to a redistribution of polarization and both for uniform polarization and uniform coupling constants, such a redistribution does not affect h_z . Rewriting the sum in Eq. (4.17) we obtain (again up to corrections of $O(t^4)$)

$$\frac{\langle h_z(t) \rangle}{\langle h_z(0) \rangle} = 1 - c \frac{t^2}{\tau_e^2}, \quad \tau_e = \frac{N^{3/2} \omega}{A^2}, \quad (4.18)$$

with the numerical factor c only depending on the distribution of coupling constants through $\alpha_k = NA_k/A$ and the initial polarization distribution f_k through

$$c = \frac{1}{32Nc_0} \sum_{kl} \alpha_k^2 \alpha_l^2 (\alpha_k - \alpha_l) (f_k - f_l), \quad (4.19)$$

where $c_0 = \sum_k f_k \alpha_k$. We note that, up to the factor c (see Fig. 4.2), the timescale τ_e agrees with a previous rough estimate [51] for the timescale of nuclear-spin dynamics under the electron-mediated nuclear spin interaction. In Table 4.1 we give τ_e for a variety of values of the number of nuclear spins N and of $\omega = \epsilon_z - \eta_z + \langle h_z \rangle$.

N	$A/g\mu_B\sqrt{N}$	τ_e at $\omega = A/\sqrt{N}$	τ_e at 100mT	τ_e at 1T	τ_e at 2mT	τ_e at 5T
10^3	49mT	3ns	6ns	60ns	119ns	297ns
10^4	16mT	29ns	188ns	$2\mu\text{s}$	$4\mu\text{s}$	$9\mu\text{s}$
10^5	4.9mT	292ns	$6\mu\text{s}$	$60\mu\text{s}$	$119\mu\text{s}$	$297\mu\text{s}$
10^6	1.6mT	$3\mu\text{s}$	$188\mu\text{s}$	2ms	4ms	9ms

Table 4.1: This Table gives explicit values for the timescale τ_e of the t^2 term in the short-time expansion of $\langle h_z(t) \rangle$ (see Eq.(4.18)). We give τ_e for various values of the number of nuclear spins N and of $\omega = \epsilon_z - \eta_z + \langle h_z \rangle$ for $I = 1/2$. When $\omega = A/\sqrt{N}$ we are at the lower boundary of ω -values for which the result for τ_e is valid. The parameters used are relevant for a lateral GaAs quantum dot: $A = 90\mu\text{eV}$, $g = -0.4$.

The coupling constants A_k have a different dependence on k , depending on the dimension d and the exponent q in the electron envelope wave function through [46] $A_k = A_0 e^{-(k/N)^{q/d}}$. For a donor impurity with a hydrogen-like exponential wave function we have $d = 3, q = 1, d/q = 3$, whereas for a 2-dimensional quantum dot with a Gaussian envelope function we have $d = 2, q = 2, d/q = 1$. In Fig. 4.2 we show the constant c for the case $d/q = 1$ and a particular choice of the polarization distribution. We give the dependence on d/q in the inset of Fig. 4.2. While c is independent of N for $N \gtrsim 100$, it changes considerably depending on the initial nuclear spin state, which is parameterized by the f_k . Since there are neither experimental data nor theoretical calculations on the shape of the polarization distribution, we assume for the curves in Fig. 4.2 that it has the same shape as the distribution of coupling constants A_k , but with a different width, reflected in the number of nuclear spins N_p that are appreciably polarized. The motivation for this choice is that if polarization is introduced into the nuclear spin system via electron-nuclear spin flip-flops, the probability for these flip-flops is expected to be proportional to some power of A_k/A_0 . The degree of polarization at the center we denote by $p \in [-1, 1]$. We may thus write $f_k = p e^{-(k/N_p)^{q/d}}$. We see in Fig. 4.2 that c grows monotonically with N/N_p , i.e., a localized polarization distribution ($N/N_p > 1$) decays more quickly than a wide spread one ($N/N_p < 1$).

In the context of state narrowing, [51, 72, 73] the short-time behavior of the width of the Overhauser field $\sigma(t) = \sqrt{\langle h_z^2(t) \rangle - \langle h_z(t) \rangle^2}$ is also of interest. Nuclear spin state narrowing, i.e., the reduction of σ , extends the electron spin decoherence time. Repeating the above calculation for $\langle h_z^2(t) \rangle$ and using the result for $\langle h_z(t) \rangle$ we find (up to corrections of $O(t^4)$) for the variance of the Overhauser field

$$\sigma^2(t) = \sigma^2(0) \left(1 + c_\sigma \frac{t^2}{\tau_e^2} \right), \quad (4.20)$$

with the range of validity $\omega \gtrsim A/\sqrt{N}$, limited by higher-order corrections to the effective Hamiltonian as in the case of $\langle h_z(t) \rangle$. Here, the dimensionless constant c_σ is given by

$$c_\sigma = \frac{1}{16Nc_{\sigma 0}} \sum_{kl} \alpha_k^2 \alpha_l^2 (\alpha_k - \alpha_l) (f_k - f_l) (f_k \alpha_k + f_l \alpha_l), \quad (4.21)$$

where $c_{\sigma 0} = \sum_k \alpha_k^2 (1 - f_k^2)$. Taking the square-root of $\sigma^2(t)$ and expanding it for $c_\sigma t^2 / \tau_e^2 \ll 1$ we find for the width (up to corrections of $O(t^4)$)

$$\sigma(t) = \sigma(0) \left(1 + c_\sigma \frac{t^2}{2\tau_e^2} \right). \quad (4.22)$$

Thus, also for the width of the Overhauser field the initial dynamics are quadratic in time, with the same dependence on A , N and ω as the mean.

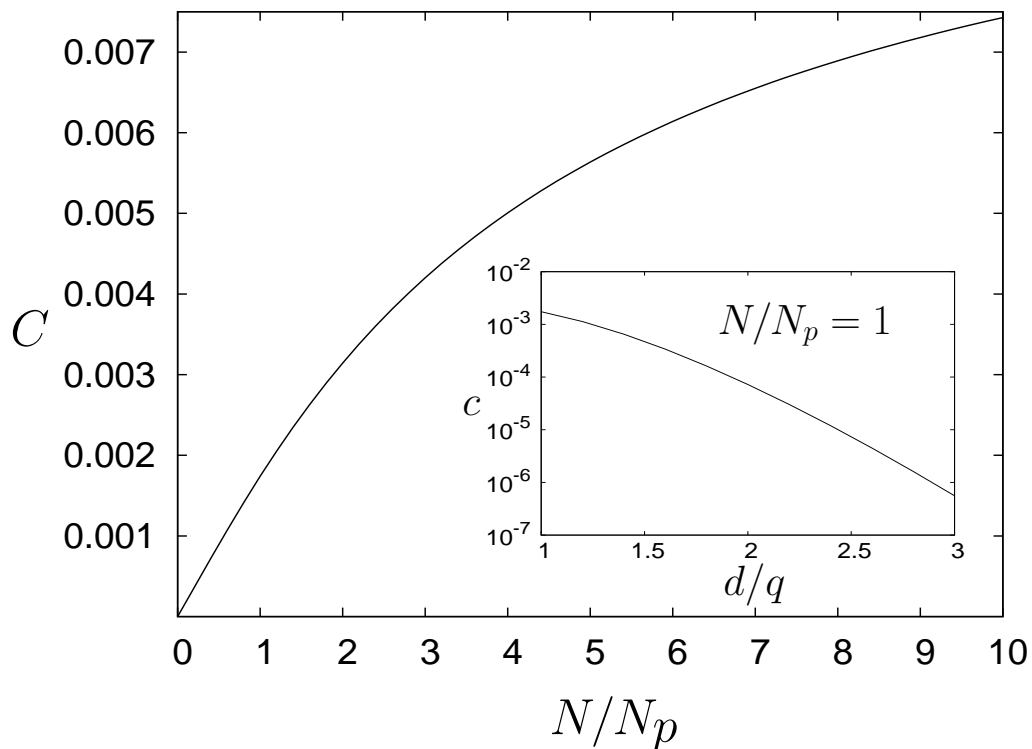


Figure 4.2: Numerical prefactor c (given in Eq. (4.19)) of the t^2 -term in the decay of the Overhauser field mean value $\langle h_z(t) \rangle$. While c turns out to be independent (for $N \gtrsim 100$ in the case shown according to numerical summation) of the number N of nuclear spins within a Bohr radius of the electron envelope wave function, it does depend on the type of structure and the initial polarization. We show the case of a 2-d quantum dot with a Gaussian electron envelope ($d/q = 1$). The dependence on the initial polarization is parameterized by N/N_p , where N_p is the number of nuclear spins that are polarized substantially (see text). Inset: dependence of c on the ratio d/q for $N/N_p = 1$. We see that, e.g., for a donor impurity with a hydrogen-like wave function ($d/q = 3$) the prefactor c is more than three orders of magnitude smaller compared to the 2-d lateral quantum dot with $d/q = 1$.

4.4.1 Special case: full polarization

In this section we analyze the special case of a fully polarized nuclear spin system, where the effective Hamiltonian derived in Sec. 4.3 gives no dynamics and thus the corrections due to the transfer of polarization from the electron to the nuclei become relevant. We thus must return to the full Hamiltonian in Eq. (4.5). Using the fact that the total spin $J_z = S_z + \sum_k I_k^z$ is a conserved quantity, we transform into a rotating frame where the Hamiltonian takes the form [46]

$$H' = (\tilde{\epsilon}_z + h_z)S_z + \frac{1}{2}(h_+S_- + h_-S_+), \quad (4.23)$$

with $\tilde{\epsilon} = \epsilon - \eta_z$. To have any dynamics for a fully polarized nuclear spin system (all spins $|\uparrow\rangle$), the initial state of the electron must be $s_\downarrow |\downarrow\rangle + s_\uparrow |\uparrow\rangle$, with $s_\downarrow \neq 0$. Since the $|\uparrow\rangle$ part gives no dynamics we consider $|\psi(0)\rangle = |\downarrow; \uparrow\uparrow \dots \uparrow\rangle$. At any later time we may thus write

$$|\psi(t)\rangle = a(t) |\psi(0)\rangle + \sum_k b_k(t) |\uparrow; \uparrow\uparrow \dots \uparrow\downarrow_k \uparrow \dots \uparrow\rangle, \quad (4.24)$$

with $a(0) = 1$ and $b_k(0) = 0, \forall k$. The same case was studied in Refs. [44, 91]. However, this study was performed from the point of view of electron spin decoherence. For the expectation value of $\langle h_z(t) \rangle$, we find, in terms of $a(t)$ and $b_k(t)$,

$$\langle h_z(t) \rangle = \langle \psi(t) | h_z | \psi(t) \rangle = \frac{A}{2} - \sum_k |b_k(t)|^2 A_k, \quad (4.25)$$

where we have used the normalization condition $|a(t)|^2 + \sum_k |b_k(t)|^2 = 1$. Using the time-dependent Schroedinger equation $i\partial_t |\psi(t)\rangle = H' |\psi(t)\rangle$, we obtain the differential equations for $a(t)$ and $b_k(t)$:

$$\dot{a}(t) = \frac{i}{4}(2\epsilon_z + A)a(t) - \frac{i}{2} \sum_k b_k(t) A_k, \quad (4.26)$$

$$\dot{b}_k(t) = -\frac{iA_k}{2}a(t) - \frac{i}{4}(2\epsilon_z + A - 2A_k)b_k(t). \quad (4.27)$$

Inserting a power-series Ansatz $a(t) = \sum_l a^{(l)} t^l$ and $b_k(t) = \sum_l b_k^{(l)} t^l$ into these equations and comparing coefficients yields recursion relations of the form

$$a^{(l+1)} = \frac{i}{4(l+1)}(2\epsilon_z + A)a^{(l)} - \frac{i}{2(l+1)} \sum_k b_k^{(l)} A_k, \quad (4.28)$$

$$b_k^{(l+1)} = -\frac{iA_k}{2(l+1)}a^{(l)} - \frac{i}{4(l+1)}(2\epsilon_z + A - 2A_k)b_k^{(l)}. \quad (4.29)$$

Iterating these recursion relations using that $a(0) = 1$ and $b_k(0) = 0, \forall k$, we find, neglecting corrections of $O(t^4)$,

$$\frac{\langle h_z(t) \rangle}{\langle h_z(0) \rangle} = 1 - \frac{1}{2A} \sum_k A_k^3 t^2. \quad (4.30)$$

For the case of a 2-d quantum dot with Gaussian envelope wave function, where we have $A_k = Ae^{-k/N}/N$, we find, evaluating $\sum_k A_k^3$ by turning it into an integral in the continuum limit $N \gg 1$, (again up to corrections of $O(t^4)$)

$$\frac{\langle h_z(t) \rangle}{\langle h_z(0) \rangle} = 1 - \frac{1}{6} \left(\frac{t}{\tau_c} \right)^2, \quad (4.31)$$

where $\tau_c = N/A$. To obtain the range of validity for this result we go to higher order in t . Again for the case of a 2-d quantum dot with Gaussian envelope wave function we find up to $O(t^4)$, neglecting terms that are suppressed by $O(1/N)$ in the t^4 -term,

$$\frac{\langle h_z(t) \rangle}{\langle h_z(0) \rangle} = 1 - \frac{1}{6} \left(\frac{t}{\tau_c} \right)^2 + \frac{1}{18} \left(\frac{t}{\tau_4} \right)^4. \quad (4.32)$$

Here, $\tau_4 = 2\sqrt{N}/\sqrt{A(2\epsilon_z + A)}$. This shows that in some cases the higher order terms in the short-time expansion can have a considerably shorter timescale. Comparing the short-time expansion with a calculation for $\langle S_z \rangle$ in the case of uniform coupling constants [91] suggests that the full dynamics contain oscillations with a frequency $\propto \epsilon_z + A/2$, thus limiting the range of validity of the short-time expansion to $t \ll (\epsilon_z + A/2)^{-1}$.

To finish our discussion of the short-time dynamics and of the Zeno effect, we point out that the main result of this section, namely the timescale τ_e and the constant c (Eqs.(4.18) and (4.19)) for the quadratic term in the short-time expansion of $\langle h_z(t) \rangle$, is what sets the condition on the repetition rate τ_m as discussed in Sec. 4.2 (see Eq. (4.4)). With this we move on to the study of the long-time behavior. We first show the results of a Dyson-series expansion in Sec. 4.5 and in Sec. 4.6 we treat the problem using the generalized master equation, showing that the Dyson-series expansion gives the leading-order contribution in A/ω .

4.5 Dyson-series expansion

In this section we calculate the expectation value of the Overhauser field $\langle h_z(t) \rangle$ in a Dyson-series expansion up to second order in the interaction V . This allows us to obtain the full time dynamics of $\langle h_z(t) \rangle$. Since the Dyson-series expansion is not a controlled expansion (it leads to secular divergences in time at higher order), we will only see from the generalized master equation

calculation in Sec. 4.6 that the Dyson series result gives the correct leading order contribution in A/ω . Thus, the results in this section are expected to be valid in the regime $\omega \gg A$. The results in this section can also be obtained from the generalized master equation approach presented in Sec. 4.6. However, the Dyson-series calculation is more accessible.

We transform all operators into the interaction picture by $\tilde{\mathcal{O}} = e^{iH_0 t} \mathcal{O} e^{-iH_0 t}$. In the interaction picture we have $\langle h_z(t) \rangle = \text{Tr}\{\tilde{h}_z \tilde{\rho}(t)\}$, with $\tilde{h}_z = h_z$ since $[H_0, h_z] = 0$. Expanding $\tilde{\rho}(t)$ in a Dyson series we find [140]

$$\begin{aligned} \tilde{\rho}(t) &= \rho(0) - i \int_0^t dt' [\tilde{V}(t'), \rho(0)] \\ &\quad - \int_0^t dt' \int_0^{t'} dt'' [\tilde{V}(t'), [\tilde{V}(t''), \rho(0)]] + O(\tilde{V}^3), \end{aligned} \quad (4.33)$$

where

$$\tilde{V}(t) \equiv e^{iH_0 t} V e^{-iH_0 t} = \frac{S_z}{2\omega} \sum_{k \neq l} e^{iS_z(A_k - A_l)t} I_k^+ I_l^-. \quad (4.34)$$

We assume again the same initial state as in Sec. 4.4 and thus the term linear in \tilde{V} will drop out under the trace as it only contains off-diagonal terms. From the remaining two terms we find

$$\langle h_z(t) \rangle = \langle h_z(0) \rangle + \frac{1}{8\omega^2} \sum_{k \neq l} \frac{A_k^2 A_l^2 (f_k - f_l)}{A_k - A_l} \left(\cos \left[(A_k - A_l) \frac{t}{2} \right] - 1 \right). \quad (4.35)$$

We first verify that this result is consistent with the short-time expansion in Sec. 4.4. For this we use that $A_k \leq A_0 \propto A/N$ and thus for times $t \ll \tau_c = N/A$ we may expand the cosine in the above expression, recovering, to second order in t , the result in Eq. (4.17). For the full time dynamics we note that the sum over cosines leads to a decay on a timescale of $\tau_c = N/A$, since for $t > \tau_c$ the different cosines interfere destructively. We illustrate this with an example: for a particular choice of the initial polarization distribution ($d/q = 1$ and $N_p = N$) we may evaluate the sum in Eq. (4.35) in the continuum limit and find

$$\frac{\langle h_z(t) \rangle}{\langle h_z(0) \rangle} = 1 - \frac{p}{8N} \frac{A^2}{\omega^2} g(t/\tau_c). \quad (4.36)$$

The function $g(t)$ is explicitly given by

$$g(t) = \frac{1}{t^4} \left[t^4 - 16t^2 + 64t \sin\left(\frac{t}{2}\right) - 256 \sin^2\left(\frac{t}{4}\right) \right], \quad (4.37)$$

with $g(0) = 0$ and $g(t \rightarrow \infty) = 1$. We thus find a power-law decay on a timescale τ_c by an amount of $O(1/N)$. Since the sum of cosines in Eq. (4.35)

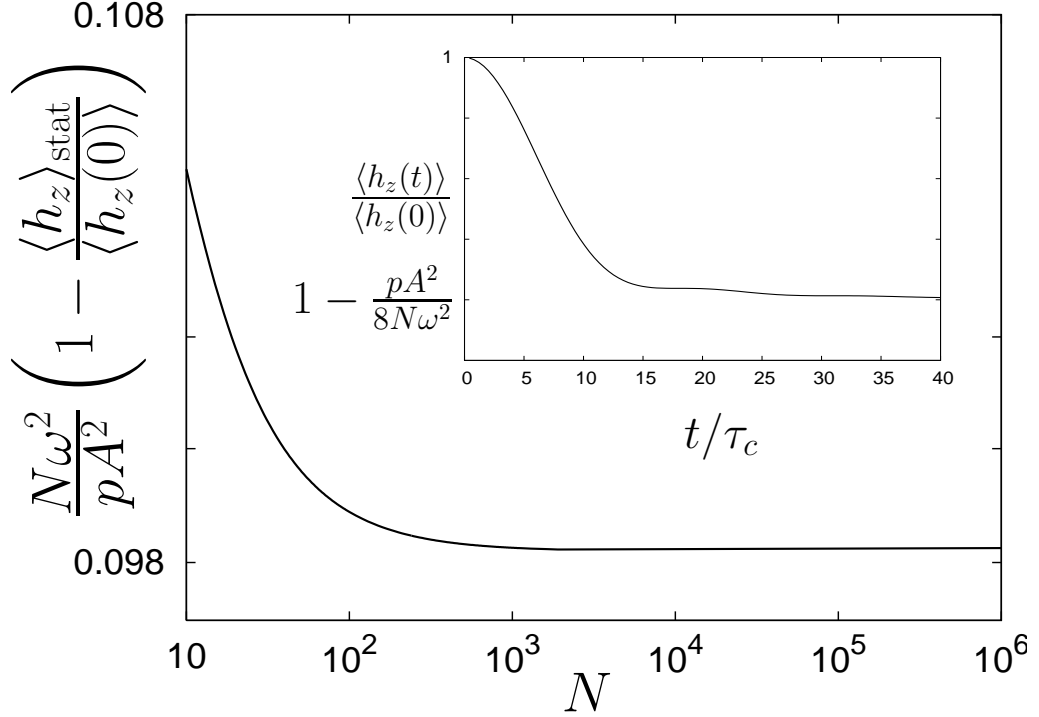


Figure 4.3: In this figure we show the N -dependence of $1 - \langle h_z \rangle_{\text{stat}} / \langle h_z(0) \rangle$ (see Eq.4.38), i.e., the part by which $\langle h_z \rangle$ decays in units of $pA^2 / N\omega^2$, in the regime $\omega \gg A$. This plot is for a 3-d defect center with a hydrogen-like electron envelope ($d/q = 3$) and the initial polarization is parameterized by $N/N_p = 0.5$ as described in Sec. 4.4. For this choice of polarization distribution the decay is of $O(1/N)$. The inset shows the full time dynamics of $\langle h_z(t) \rangle / \langle h_z(0) \rangle$ as given in Eq.(4.36) for $d/q = 1, N \gg 1, N/N_p = 1$. We see that the decay occurs on a timescale of $\tau_c = N/A$.

decays, the remaining time-independent sum gives the stationary value (up to the Poincaré recurrence time [141])

$$\frac{\langle h_z \rangle_{\text{stat}}}{\langle h_z(0) \rangle} = 1 - \left(\frac{A}{\omega} \right)^2 \frac{1}{4N^2 c_0} \sum_{k \neq l} \frac{\alpha_k^2 \alpha_l^2 (f_k - f_l)}{\alpha_k - \alpha_l}. \quad (4.38)$$

For a system with a large number of nuclear spins $N \gg 1$ and a sufficiently smooth polarization distribution, this stationary value differs only by a term of $O(1/N)$ from the initial value, i.e., $\langle h_z \rangle_{\text{stat}} / \langle h_z(0) \rangle = 1 - O(1/N)$. This can be seen in Fig. 4.3, where we show the N dependence of $1 - \langle h_z \rangle_{\text{stat}} / \langle h_z(0) \rangle$, i.e., the part by which $\langle h_z \rangle$ decays. The parameters in Fig. 4.3 are taken for a 3-d defect center with a hydrogen-like electron envelope ($d/q = 3$) and the initial polarization $N/N_p = 0.5$ as described in Sec. 4.4. For this choice of polarization distribution the decay is of $O(1/N)$. We also find a $O(1/N)$

behavior for other values of the parameters d/q and N/N_p and thus expect this to be generally true for a smoothly varying initial polarization distribution. The inset of Fig. 4.3 shows the full time dynamics of $\langle h_z(t) \rangle$ as given in Eq.(4.36) for $d/q = 1, N \gg 1, N/N_p = 1$.

We note that the 4th order of a Dyson series expansion gives secular terms (diverging in t). We thus move on to treat the long-time behavior using a master equation approach which avoids these secular terms and shows that the Dyson series result gives the correct leading-order term in A/ω .

4.6 Generalized master equation

In this section we study the decay of the Overhauser field mean value $\langle h_z(t) \rangle$ using the Nakajima-Zwanzig generalized master equation (GME) in a Born approximation. The results in this section are valid in the regime $\omega \gg A$, since higher-order corrections to the Born approximation are suppressed by a factor $(A/\omega)^2$.

We start from the GME, [141] which for $P_k \rho(0) = \rho(0)$ reads

$$P_k \dot{\rho}(t) = -i P_k L P_k \rho(t) - \int_0^t dt' P_k L e^{-i Q L (t-t')} Q L P_k \rho(t'), \quad (4.39)$$

where $L = L_0 + L_V$ is the Liouville superoperator defined as $(L_0 + L_V) \mathcal{O} = [H_0 + V, \mathcal{O}]$. The projection superoperator P_k must preserve $\langle I_k^z(t) \rangle$ and we choose it to have the form $P_k = \rho_e(0) \text{Tr}_e \otimes P_{dk} \bigotimes_{l \neq k} \rho_{I_l}(0) \text{Tr}_{I_l}$ where P_{dk} projects onto the diagonal in the subspace of nuclear spin k and is defined as $P_{dk} \mathcal{O} = \sum_{s=\uparrow, \downarrow} |s_k\rangle \langle s_k| \langle s_k| \mathcal{O} |s_k\rangle$. Further, $Q = 1 - P_k$. In a standard Born approximation and using the same initial conditions as above, i.e., a product state and no transverse coherence in the nuclear spin system, we obtain the following integro-differential equation for $\langle I_k^z(t) \rangle$

$$\langle \dot{I}_k^z(t) \rangle = -\frac{A_k^2}{8\omega^2} \int_0^t d\tau \sum_{l, l \neq k} A_l^2 \cos \left[\frac{\tau}{2} (A_k - A_l) \right] (\langle I_k^z(t - \tau) \rangle - \langle I_l^z(0) \rangle). \quad (4.40)$$

The Born approximation goes to order L_V^2 in the expansion of the self-energy. Higher-order corrections in L_V are estimated to give contributions to the right-hand side of Eq. (4.40) that are suppressed by a factor $(A/\omega)^2$. We expect the results of this section to be valid at least for $\omega \gg A$, although it could in principle happen that (as in the case of the decay of $\langle S_z(t) \rangle$ [46]) the result for the stationary value has a larger regime of validity. On the other hand, it can not be generally excluded that higher-order contributions could dominate

at sufficiently long times. Integrating Eq. (4.40) we find the formal solution

$$\begin{aligned} \langle I_k^z(t) \rangle &= \langle I_k^z(0) \rangle - \frac{A^2 \alpha_k^2}{\omega^2 8} \int_0^t dt' \int_0^{t'} d\tau \sum_{l, l \neq k} A_l^2 \\ &\quad \times \cos \left[\frac{\tau}{2} (A_k - A_l) \right] (\langle I_k^z(t' - \tau) \rangle - \langle I_l^z(0) \rangle). \end{aligned} \quad (4.41)$$

This shows that $\langle I_k^z(t) \rangle = \langle I_k^z(0) \rangle + O((A/\omega)^2)$ and we may thus iterate this equation and replace $\langle I_k^z(t' - \tau) \rangle$ in the integral by $\langle I_k^z(0) \rangle$. This implies, up to corrections of $O((A/\omega)^4)$,

$$\langle I_k^z(t) \rangle = \langle I_k^z(0) \rangle - \frac{A_k^2}{16\omega^2} \sum_{l, l \neq k} A_l^2 (f_k - f_l) \int_0^t dt' \int_0^{t'} d\tau \cos \left[\frac{\tau}{2} (A_k - A_l) \right]. \quad (4.42)$$

Performing the integrals and summing over the $\langle I_k^z(t) \rangle$ weighted by their coupling constants A_k , we recover the Dyson series result in Eq. (4.35). This shows that the Dyson series expansion gives the leading-order contribution in A/ω .

For the analytical solution of Eq. (4.40) in the stationary limit we perform a Laplace transformation, solve the resulting equation in Laplace space, and calculate the residue of the pole at $s = 0$ which yields (up to the recurrence time)

$$\begin{aligned} \langle I_k^z \rangle_{\text{stat}} &= \lim_{T \rightarrow \infty} \frac{1}{T} \int_0^T \langle I_k^z(t) \rangle dt = \lim_{s \rightarrow 0} s \langle I_k^z(s) \rangle \\ &= \frac{1}{Z_k} \sum_l P_k(l) \langle I_l^z(t=0) \rangle, \end{aligned} \quad (4.43)$$

with $Z_k = \sum_l P_k(l)$. We see that $\langle I_k^z \rangle_{\text{stat}}$ is determined by weighting the neighboring $\langle I_l^z(t=0) \rangle$ with the probability distribution $P_k(l)/Z_k$, which is explicitly given by

$$P_k(l) = \begin{cases} A_l^2 / (A_k - A_l)^2 & : l \neq k, \\ 2\omega^2 / A_k^2 & : l = k. \end{cases} \quad (4.44)$$

We point out that $\langle I_k^z \rangle_{\text{stat}}$ can be either smaller or larger than $\langle I_l^z(t=0) \rangle$ and that $\sum_k \langle I_k^z \rangle_{\text{stat}} = \sum_k \langle I_l^z(t=0) \rangle$ since the total spin is a conserved quantity. Again expanding the result in Eq.(4.43) to leading order in A/ω and summing over the nuclear spins weighted by their coupling constants A_k , we recover the same result found in the Dyson series calculation in Eq. (4.38). Intuitively one would expect a decay even at high fields (although a very slow one) to a state with uniform polarization. The fact that our calculation shows no

such decay suggests that the Knight-field gradient, i.e., the gradient in the additional effective magnetic field seen by the nuclei, due to the presence of the electron, is strong enough to suppress such a decay if the flip-flop terms are sufficiently suppressed. Applying a large magnetic field thus seems to be an efficient strategy to prevent the Overhauser field from decaying.

As a side remark, we would like to point out that in this regime of only partial decay, repeated measurements on the Overhauser field can actually enhance the decay of $\langle h_z(t) \rangle$. This occurs when the measurements are performed at intervals longer than the decay time to the stationary value ($\tau_c = N/A$, as discussed in Sec. 4.5). Performing a projective measurement at a time $t > \tau_c$ resets the initial condition and thus again a small decay occurs. Repeating these measurements at intervals longer than τ_c thus allows for a decay of $\langle h_z(t) \rangle$ to zero.

4.7 Conclusion

We have studied the dynamics of the Overhauser field generated by the nuclear spins surrounding a bound electron. We focused our analysis on the effect of the electron-mediated interaction between nuclei due to the hyperfine interaction. At short times we find a quadratic initial decay of the Overhauser field mean value $\langle h_z(t) \rangle$ on a timescale $\tau_e = N^{3/2}\omega/A^2$. Performing repeated strong measurements on h_z leads to a Zeno effect with the decay changing from quadratic to linear, with a timescale that is prolonged by a factor τ_e/τ_m , where τ_m is the time between consecutive measurements. In Secs. 4.5 and 4.6 we have addressed the long-time decay of $\langle h_z(t) \rangle$ using a Dyson series expansion and a generalized master equation approach. Both show that $\langle h_z(t) \rangle$ only decays by a fraction of $O(1/N)$ for a sufficiently smooth polarization distribution and large magnetic field.

Overall, the strategy to preserve the Overhauser field contains two tools. The first is to apply a strong external magnetic field ($\omega \gg A$) which limits the decay to a fraction of $O(1/N)$. In case such a strong magnetic field is not desirable or achievable, the second tool is to make use of the Zeno effect and perform repeated projective measurements on the Overhauser field leading to a slow-down of the decay.

It remains a subject of further study beyond the scope of this work whether, and on what timescale, the combination of electron-mediated interaction and direct dipole-dipole interaction may lead to a full decay of the Overhauser field. Another interesting question concerns the distribution of nuclear polarization within a quantum dot or defect center and its dependence on the method that is used to polarize the system.

Appendix A

Drift in δh^z

In addition to spin diffusion, driven by the nuclear dipole-dipole interaction, there may also be a change in δh^z due to corrections to the projected effective Hamiltonian considered here (see Ref. [50], Appendix B for details). After tracing out the electron pseudo-spin in state ρ_S , these correction terms give rise to an electron-mediated nuclear spin-spin interaction which, in general, takes the form of an anisotropic (XYZ) Heisenberg interaction

$$H_{mn} = \text{Tr}_S\{\rho_S H\} = \sum_{i,j,\alpha=\{x,y,z\}} J_{ij}^\alpha I_i^\alpha I_j^\alpha. \quad (\text{A.1})$$

Here, the indices i and j run over all nuclear spin sites.

We use the corrections to leading order in the inverse Zeeman splitting $1/\epsilon_z$ ($\epsilon_z = g\mu_B B$) given in Ref. [50]. This gives the typical value of the exchange constants $|J_{ij}^\alpha| \sim A^2/N^2\epsilon_z$. Assuming an unpolarized nuclear spin state, each nuclear spin will therefore precess in an effective mean field generated by all other spins in the dot of typical magnitude

$$h_{\text{eff}} \sim \sqrt{N} |J_{ij}^\alpha| \sim A^2/N^{\frac{3}{2}}\epsilon_z. \quad (\text{A.2})$$

This effective field will result in precession of the nuclear spins about an arbitrary angle (and hence, may change the value of δh^z) on a time scale

$$\tau_p \sim N^{\frac{3}{2}}\epsilon_z/A^2 \sim 10^{-2} \text{ s}, \quad (\text{A.3})$$

where we have assumed $N = 10^6$ nuclear spins within the quantum dot, and $\epsilon_z/g\mu_B = A/g\mu_B \simeq 3.5 \text{ T}$ for the time estimate. This is only a worst-case estimate, which neglects the effects, e.g., of a Knight-shift gradient (due to strong confinement of the electron), which may further weaken the dynamical effect discussed here. We expect the dipolar nuclear spin diffusion time to be the limiting time scale for nuclear spin dynamics, in light of experiments on diffusion near donor impurities in GaAs [95]. If the effect giving rise to τ_p in Eq. (A.3) were significant, it could be further suppressed by choosing a larger quantum dot size or stronger magnetic field, thus allowing many electron spin measurements on the time scale of variation of δh^z .

Appendix B

Measurement

In this appendix we describe how a single measurement of the two-electron system affects the nuclear spin state. We give the analytical expression for the diagonal elements of the nuclear spin density operator after a measurement.

At $t=0$ the system is described by the following density operator

$$\rho(0) = \rho_e(0) \otimes \rho_I(0) = |+\rangle \langle +| \otimes \sum_i p_i |\psi_I^i\rangle \langle \psi_I^i|, \quad (\text{B.1})$$

with nuclear spin state $|\psi_I^i\rangle = \sum_n a_n^i |n\rangle$. The Hamiltonian H_0 of Eq.(2.1) acts on the the nuclear-spin system as $H_0 |n\rangle = H_n |n\rangle$, where in H_n the operator δh^z has been replaced by δh_n^z (because $\delta h^z |n\rangle = \delta h_n^z |n\rangle$). Since $[H_0, \delta h^z] = 0$, only the diagonal elements of the nuclear density operator ρ_I (in the basis of δh^z) enter in matrix elements for operators acting only on the two-electron system. As described in Section 2.2.1, these diagonal elements $\rho_I(n) = \rho_I(n, 0) = \langle n | Tr_e \{ \rho(0) \} | n \rangle$ describe a continuous Gaussian distribution in the continuum limit. The trace over the electron system is defined as $Tr_e \rho(t) = \langle + | \rho(t) | + \rangle + \langle - | \rho(t) | - \rangle$ and for $\rho_I(n, 0)$ we have

$$\rho_I(n, 0) = \sum_i p_i |a_n^i|^2. \quad (\text{B.2})$$

The time evolution operators $U(t)$ and $U_n(t)$ are defined through $i\dot{U}(t) = H_0(t)U(t)$ and $i\dot{U}_n(t) = H_n(t)U_n(t)$ and thus the density operator $\rho(0)$ evolves under the Hamiltonian H_0 as

$$\begin{aligned} \rho(t) &= U(t)\rho(0)U^\dagger(t) \\ &= U(t) \left(\rho_e(0) \otimes \sum_i \sum_{n,l} p_i a_n^i a_l^{i*} |n\rangle \langle l| \right) U^\dagger(t) \\ &= \sum_{n,l} \left(U_n(t) \rho_e(0) U_l^\dagger(t) \otimes \sum_i p_i a_n^i a_l^{i*} |n\rangle \langle l| \right). \end{aligned} \quad (\text{B.3})$$

At time t_m a measurement in the basis of $|+\rangle$ and $|-\rangle$ is performed on one single two-electron system coupled to nuclear spins. Since the outcome of this measurement is known, the state of the system after the measurement is¹ (the result depends on whether $|+\rangle$ or $|-\rangle$ was measured)

$$\begin{aligned}\rho^{(1,\pm)}(t_m) &= \frac{|\pm\rangle \langle \pm| \rho(t_m) |\pm\rangle \langle \pm|}{P^\pm(t_m)} \\ &= \sum_{n,l} \left(|\pm\rangle \langle \pm| U_n(t_m) \rho_e(0) U_l^\dagger(t_m) |\pm\rangle \langle \pm| \right. \\ &\quad \left. \otimes \sum_i p_i a_n^i a_i^{i*} |n\rangle \langle l| \right) \frac{1}{P^\pm(t_m)},\end{aligned}\tag{B.4}$$

with

$$\begin{aligned}P^\pm(t_m) &= Tr_I Tr_e \{ |\pm\rangle \langle \pm| \rho(t_m) \} \\ &= \sum_i \sum_n \frac{1}{2} (1 \pm \langle \tau^z(t_m) \rangle_n) p_i |a_n^i|^2,\end{aligned}\tag{B.5}$$

where $Tr_I A = \sum_n \langle n| A |n\rangle$ and $\langle \tau^z(t) \rangle_n$ is given in Eq.(2.4). Here, $P^\pm(t_m)$ is the probability to measure $|\pm\rangle$ at time t_m . We are mainly interested in the diagonal elements of the nuclear density operator ρ_I after the measurement.

$$\begin{aligned}\rho_I^{(1,\pm)}(n, t_m) &= \langle n| Tr_e \rho^{(1,\pm)}(t_m) |n\rangle \\ &= \frac{\rho_I(n, 0)}{P^\pm(t_m)} \langle \pm| U_n(t_m) \rho_e(0) U_n^\dagger(t_m) |\pm\rangle \\ &= \frac{\rho_I(n, 0)}{P^\pm(t_m)} \frac{1}{2} (1 \pm \langle \tau^z(t_m) \rangle_n).\end{aligned}\tag{B.6}$$

Using Eq.(2.4) we find

$$\rho_I^{(1,+)}(n, t_m) = \frac{\rho_I(n, 0)}{P^+(t_m)} \frac{1}{2} \left(\frac{2(\Omega_n - \omega)^2}{(\Omega_n - \omega)^2 + (j/2)^2} + \frac{(j/2)^2(1 + \cos(\omega' t_m))}{(\Omega_n - \omega)^2 + (j/2)^2} \right)\tag{B.7}$$

and

$$\rho_I^{(1,-)}(n, t_m) = \frac{\rho_I(n, 0)}{P^-(t_m)} \frac{1}{2} \frac{(j/2)^2(1 - \cos(\omega' t_m))}{(\Omega_n - \omega)^2 + (j/2)^2},\tag{B.8}$$

¹The measurement performed at t_m is not sufficient to distinguish the different states $|\psi_I^i\rangle$. This is because it is a measurement in the two-electron system and it only has an effect on the nuclear spin system in a way that some eigenstates $|n\rangle$ gain weight and some lose. This happens for all states $|\psi_I^i\rangle$ in the same way and thus from such a measurement we cannot tell into which of the states $|\psi_I^i\rangle$ the system has collapsed.

where ω' is given in Eq.(2.5) and depends on the eigenvalue δh_n^z of the nuclear spin eigenstate through Ω_n .

Parenthetically, we note that in the case (not described in this article) where the measurement is performed on an ensemble of many different double quantum dots, the state of the ensemble after the measurement is [74]

$$\begin{aligned} \rho_{ens}^{(1)}(t_m) = & \sum_{n,l} \left(|+\rangle \langle +| U_n(t_m) \rho_e(0) U_l^\dagger(t_m) |+\rangle \langle +| \right. \\ & \left. + |-\rangle \langle -| U_n(t_m) \rho_e(0) U_l^\dagger(t_m) |+\rangle \langle +| \right) \\ & \otimes \sum_i p_i a_n^i a_l^{i*} |n\rangle \langle l|, \end{aligned} \quad (\text{B.9})$$

and the nuclear-spin distribution has not changed. If a complete measurement of the Rabi-resonance lineshape would be performed on an ensemble of double dots, the result would be the Voigt profile described in Sec. 2.2.1.

Appendix C

Fit procedures

Here, we describe the exact procedure of the two-dimensional fit from which the phase shift $\phi = (0.23 \pm 0.01)$ was obtained. The fit function is a simplification of $P_{\text{odd}}(t)$ (Eq. (4)). The first simplification is the exclusion of the $1/t$ -term because its contribution is negligible within the fit range of $t = 100 - 900$ ns. Second, both expressions for C and $0.5 - 2C^2$ are approximated as being linear in b , which is justified for the regime we consider ($I_s = 3.6 - 6.3$ mA), as can be seen in Fig. C.1. With these simplifications, we obtain the expression $y_{\text{model}} = a_1 + I_s a_2 + (a_3 + I_s a_4) \cos(\frac{1}{2} K I_s g \mu_B t / \hbar + \phi \pi) / \sqrt{t}$, where $a_{1,2,3,4}$, K and ϕ are fit parameters. The Rabi frequency ω_{Rabi} is given by $\frac{1}{2} K I_s g \mu_B / \hbar$, with I_s the current through the stripline which is known in the experiment. The constant factor $K = B_{ac} / I_s$ is not known in the experiment but can be obtained from the fit. The behavior of $y_{\text{model}} - y_{\text{data}}$ around the optimal values for the fit parameters is seen in Fig. C.2. As a cross-check, we carried out a fit for each trace of the data in Fig. 3a of the main text (varying burst time, constant B_{ac}) with a damped cosine $a_1 - a_2 \cos(\frac{1}{2} K I_s g \mu_B t / \hbar + \phi \pi) / \sqrt{t}$, where $a_{1,2}$ and ϕ are fit parameters, and K is kept at a constant value. This fit is carried out for a wide range of values for K and I_s . The best-fit values for ϕ obtained for different I_s are averaged and plotted as a function of K in Fig. C.3. (blue curve), together with the spread in ϕ (gray dotted lines) and the fit quality (green curve). The figure shows that the best fit is obtained for $\phi = 0.23\pi$, the same value we found from the two-dimensional fit.

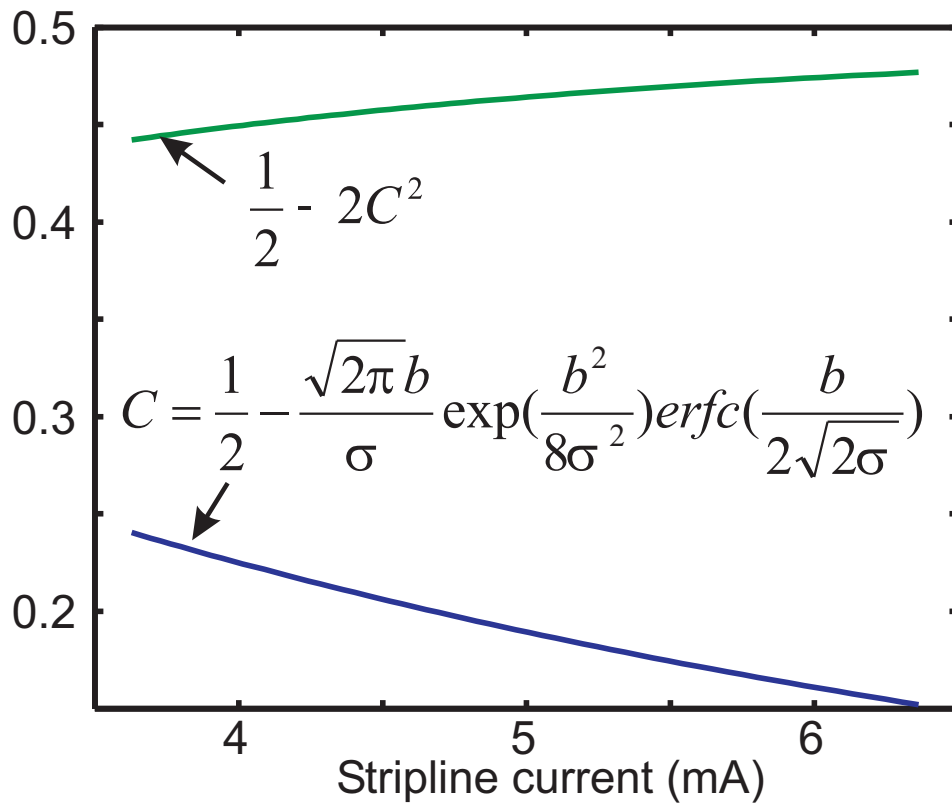


Figure C.1: C and $0.5 - 2C^2$ as a function of I_s , with $\sigma = g\mu_B(1.4 \text{ mT})$ and $b = g\mu_B K I_s$. $K = 0.56 \text{ mT/mA}$ for the curves shown here, but the curves remain linear as well for $K=0.5\text{-}0.6 \text{ mT/mA}$.

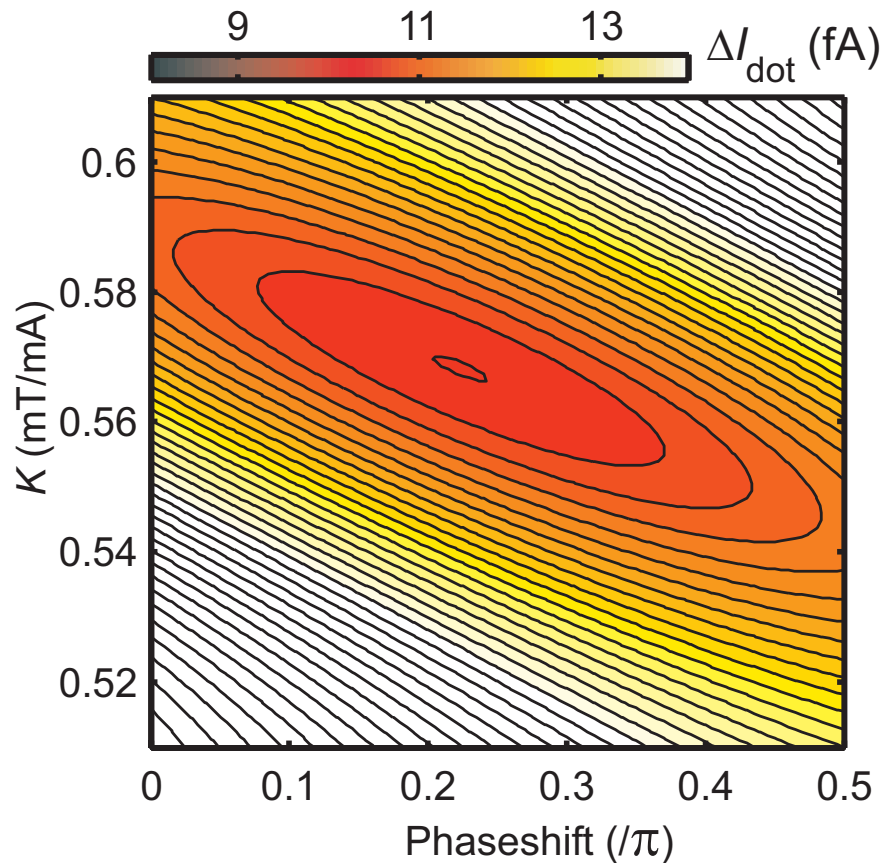


Figure C.2: Phase shift and fit quality for a range of current-to-field conversion factors K . Values obtained from a fit with a damped cosine to the single traces (constant I_s) of the data set shown in Fig. 3a of the main text, and subsequently averaged over all traces for the range $t = 100 - 900$ ns and $I_s = 3.6-6.3$ mA. The fit-quality R^2 is a measure of the correlation between the observed values y_i and the predicted values \hat{y}_i : $R^2 = \sum_{i=1}^n \frac{(\hat{y}_i - \bar{y}_i)^2}{(y_i - \bar{y}_i)^2}$, with $\bar{y} = \frac{1}{n} \sum y_i$.

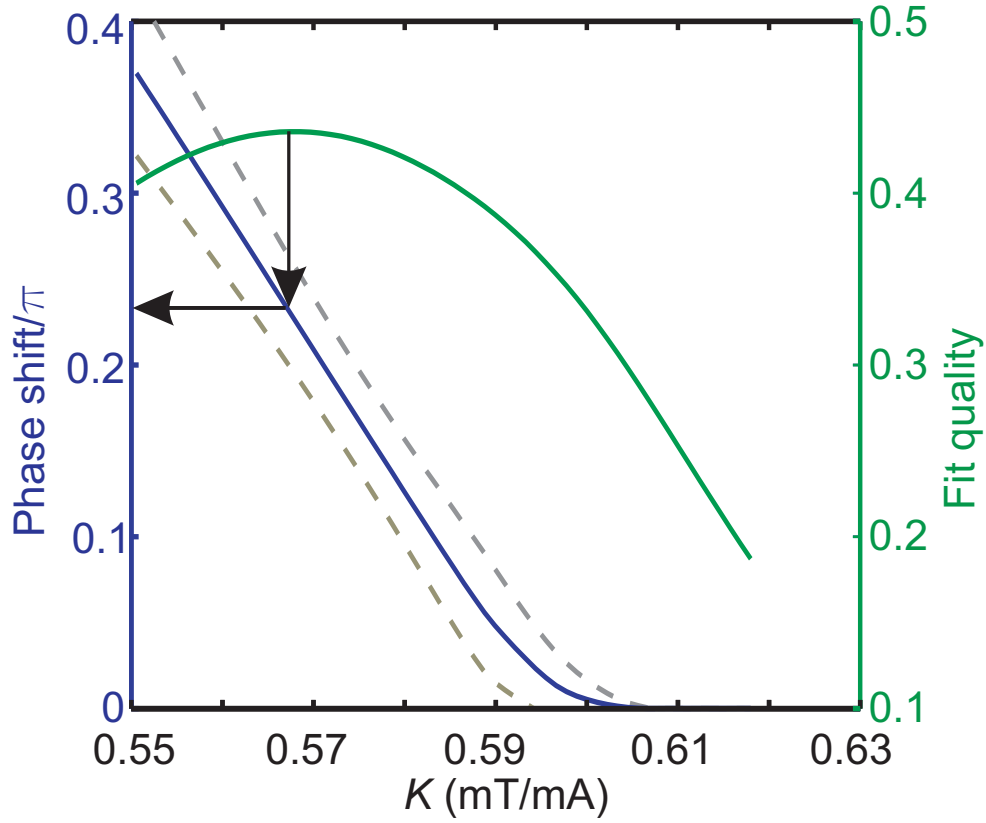


Figure C.3: Root mean square difference between the measured current y_{data} and the model y_{model} : $\left(\sum_{t, I_s} (y_{t, I_s}^{\text{data}} - y_{t, I_s}^{\text{model}})^2 \right)^{\frac{1}{2}} / N_t N_{I_s}$, for a wide range of K and ϕ . We sum over the range $t = 100 - 900$ ns and $I_s = 3.6 - 6.3$ mA.

Appendix D

Asymptotic expansion

Here we give steps and additional justification leading to the asymptotic expansion given in Eq. (3) of the main text. We consider averaging Eq. (2) from the main text over a quasicontinuous distribution of h_z values for the case where $\delta_\omega = h_z - h_0$ (with the replacement $\delta_\omega \rightarrow x$):

$$P_\uparrow(t) = \int_{-\infty}^{\infty} dx D(x) P_{\uparrow,x}(t). \quad (\text{D.1})$$

As a consequence of the central-limit theorem, for a large number of nuclear spins in a random unpolarized state, the distribution function $D(x)$ is well-approximated by a Gaussian with standard deviation σ centered at $x = 0$:

$$D(x) = \frac{1}{\sqrt{2\pi}\sigma} e^{-\frac{x^2}{2\sigma^2}}. \quad (\text{D.2})$$

Inserting Eq. (D.2) into Eq. (D.1) gives the sum of a time-independent part, which can be evaluated exactly, and a time-dependent interference term $I(t)$:

$$P_\uparrow(t) = \frac{1}{2} + C + I(t). \quad (\text{D.3})$$

Here, C is given following Eq. (3) of the main text. With the change of variables $u = (\sqrt{b^2 + 4x^2} - b)/2\sigma$, and using the fact that the integrand is an even function of x , the interference term becomes $I(t) = \text{Re}\tilde{I}(t)$, where

$$\tilde{I}(t) = \sqrt{\frac{b}{8\pi\sigma}} e^{ibt/2} \int_0^\infty du \frac{\exp\left(-\frac{u^2}{2} - \frac{bu}{2\sigma} + i\sigma t u\right)}{\sqrt{u} \sqrt{1 + \frac{\sigma u}{b}} \left(1 + \frac{2\sigma u}{b}\right)}. \quad (\text{D.4})$$

When $\sigma t \gg 1$, the time dependence of $\tilde{I}(t)$ is controlled by the region $u \lesssim 1/\sigma t$. The integrand simplifies considerably for $\sigma u/b \ll 1$, which coincides with $\sigma t \gg 1$ for

$$u \lesssim \frac{1}{\sigma t} \ll \frac{b}{\sigma}, \quad t \gg \frac{1}{\sigma}. \quad (\text{D.5})$$

Equivalently, for

$$t > \max\left(\frac{1}{b}, \frac{1}{\sigma}\right), \quad (\text{D.6})$$

we expand the integrand for $u < \min(1, b/\sigma)$:

$$\tilde{I}(t) = \sqrt{\frac{b}{8\pi\sigma}} e^{ibt/2} \int_0^\infty du \frac{\exp(-\lambda u + \mathcal{O}(u^2))}{\sqrt{u}} \left(1 + \mathcal{O}\left(\frac{\sigma u}{b}\right)\right), \quad \lambda = \frac{b}{2\sigma} - i\sigma t. \quad (\text{D.7})$$

Neglecting corrections of order u^2 in the exponential and order $\sigma u/b$ in the integrand prefactor, the remaining integral can be evaluated easily, giving

$$I(t) \sim \frac{\cos[bt/2 + \arctan(t/\tau)/2]}{2[1 + (t/\tau)^2]^{1/4}}, \quad \tau = b/2\sigma^2, \quad (\text{D.8})$$

$$t > \max(1/b, 1/\sigma). \quad (\text{D.9})$$

Eq. (D.8) is valid for the time scale indicated for an arbitrary ratio of $b/2\sigma$. Due to the exponential cutoff at $u \lesssim 2\sigma/b$ in Eq. (D.7), Eq. (D.8) is actually valid for all times in the limit $b/2\sigma \gg 1$. Expanding Eq. (D.8) to leading order for $t/\tau \gg 1$ gives the result in Eq. (3) of the main text. Higher-order contributions to the long-time expansion of Eq. (D.8) and contributions due to corrections of order $\sigma u/b$ in Eq. (D.7) both lead to more rapidly decaying behavior of order $\sim 1/t^{3/2}$. The reason for the different phase shift here ($\pi/4$) relative to that found in Ref. [50] ($3\pi/4$) is that here the fluctuations are *longitudinal*, while in Ref. [50] the fluctuations are along the transverse direction. This leads to a different integrand in Eq. (S4) and thus to a different value for the phase shift and decay power.

Since the long-time behavior of $I(t)$ is dominated by the form of the integrand near $x = 0$, the same result can be found after replacing the Gaussian distribution function by any other distribution function $\tilde{D}(x)$ which is analytic and has a single peak at $x = 0$. Specifically,

$$\tilde{D}(x) = \tilde{D}(0) \exp\left\{-\frac{x^2}{2\sigma^2} + \mathcal{O}(x^3)\right\}, \quad (\text{D.10})$$

$$\frac{1}{\sigma^2} = - \left. \frac{d^2 \ln \tilde{D}(x)}{dx^2} \right|_{x=0}. \quad (\text{D.11})$$

Thus, the universal form of the long-time power-law decay and phase shift are relatively insensitive to the specific shape of the distribution function.

Appendix E

Estimation of dipole-dipole contribution

In this appendix we estimate the timescale arising from the direct secular (terms conserving $I_{z,tot} = \sum_k I_k^z$) dipole-dipole interaction in the short-time expansion of the Overhauser field mean value $\langle h_z(t) \rangle$. This gives us the range of validity of our calculation in the main text that only took into account the electron-mediated interaction between nuclei. Let us thus consider the situation where the external magnetic field is very high, such that the electron-mediated flip-flop terms are fully suppressed. In this case the Hamiltonian has the form $H_{dd} = H_{0,dd} + V_{dd}$, with

$$H_{0,dd} = \epsilon_z S_z + \eta_z \sum_k I_k^z + S_z h_z - 2 \sum_{k \neq l} b_{kl} I_k^z I_l^z, \quad (\text{E.1})$$

$$V_{dd} = \sum_{k \neq l} b_{kl} I_k^+ I_l^-. \quad (\text{E.2})$$

Here, $b_{kl} = \gamma_I^2 (3 \cos^2(\theta_{kl}) - 1) / 4r_{kl}^3$, with θ_{kl} being the angle between a vector from nucleus k to nucleus l and the z -axis and r_{kl} being the distance between the two nuclei [98]. Further, γ_I is the nuclear gyromagnetic ratio. For the short-time expansion, only the off-diagonal terms are relevant, since $[h_z, H_0] = [\rho(0), H_0] = 0$. These off-diagonal terms in the case of the electron-mediated interaction are $S_z \sum_{k \neq l} A_k A_l I_k^+ I_l^- / 2\omega$ (see Eq. (4.11)). Replacing $A_k A_l / 2\omega$ by b_{kl} in the result for the short-time expansion in Eq.(4.17) and also taking into account the factor of 1/4 that comes from S_z^2 in the electron-mediated case we find

$$\langle h_z(t) \rangle_{\text{dip-dip}} = \langle h_z(0) \rangle - \frac{t^2}{4} \sum_{kl} b_{kl}^2 (A_k - A_l)(f_k - f_l). \quad (\text{E.3})$$

To estimate, we restrict the sum to nearest neighbors as the b_{kl} fall off with the third power of the distance between the two nuclei. Assuming $f_k =$

$(A_k/A_0)^{N/N_p}$ we find up to corrections of $O(t^4)$

$$\frac{\langle h_z(t) \rangle_{\text{dip-dip}}}{\langle h_z(0) \rangle} \approx 1 - \frac{t^2}{\tau_d^2}, \quad \tau_d = \frac{\sqrt{N_p N}}{b}, \quad (\text{E.4})$$

with b being the nearest-neighbor dipole-dipole coupling. For GaAs we have $b \sim 10^3 \text{s}^{-1}$ (with $\gamma_I/2\pi \approx 10 \text{ MHz/T}$ [142]). For $NN_p \gg 1$ we have $\tau_d \gg 10^{-3} \text{s}$. In the magnetic field range shown in Table 4.1 we thus have $\tau_d \gg \tau_e/\sqrt{c}$, which justifies neglecting the direct dipole-dipole coupling in the short-time expansion.

¹A rough estimate suggests that for $I > 1/2$ the timescales given need to be multiplied by a factor $1/(2I)^2$.

Appendix F

Measurement accuracy

The description of the Zeno effect in Sec. 4.2 relied on the assumption that the measurements on h_z set all off-diagonal elements of the density matrix to zero. This assumption requires on one hand a perfect measurement accuracy for h_z (we discuss deviations from that below), but on the other hand it also requires the h_z -eigenstates to be non-degenerate. For non-degenerate h_z eigenstates a measurement of h_z fully determines the polarization distribution f_k and we may thus write ρ_I after the measurement again as a direct product with $\rho_{I_k}(\tau_m) = 1/2 + f_k(\tau_m)I_k^z$. After the measurement, we thus again have the same time evolution for $\langle h_z(t) \rangle$ as given in Eq. (4.17), but with f_k replaced by $f_k(\tau_m)$. Iterating Eq. (4.17) for the case of m consecutive measurements at intervals τ_m one obtains Eq. (4.3).

Instead of the idealized assumption of a projective measurement we now allow for imperfect measurements. To describe these measurements we use a so-called POVM (positive operator valued measure) [74]. In a general POVM measurement the density matrix changes according to [74]

$$\rho \rightarrow \rho' = \int \sqrt{F_y} \rho \sqrt{F_y} dy, \quad (\text{F.1})$$

when averaging over all possible measurement outcomes y . The probability to measure outcome y is given by $P(y) = \text{Tr}\{\rho F_y\}$ and the condition $\int dy F_y = 1$ ensures that the probabilities sum to unity. We consider the nuclear density matrix ρ_I in a basis of h_z eigenstates $|n\rangle$ with $h_z |n\rangle = h_z^n |n\rangle$. We denote the matrix elements of ρ_I by $\rho_I(n, m) = \langle n | \rho_I | m \rangle$. For the following description we assume that the diagonal of the nuclear spin density matrix before the measurement is Gaussian distributed around its mean value $\langle h_z \rangle$ with a width σ , i.e.,

$$\rho_I(n, n) = \frac{1}{\sqrt{2\pi}\sigma} \exp \left[-\frac{(h_z^n - \langle h_z \rangle)^2}{2\sigma^2} \right]. \quad (\text{F.2})$$

For an unpolarized equilibrium (infinite temperature) state, the width is $\sigma \propto A/\sqrt{N}$. Here, σ can take any value. Let us now consider a measurement that

determines the value of h_z up to an accuracy η with a Gaussian lineshape. We refer to η as the measurement accuracy. If the outcome of the measurement is $\langle h_z \rangle + y$, the diagonal of the nuclear spin density matrix after a measurement has the form

$$\rho'_I(n, n; y) = \frac{1}{\sqrt{2\pi}\eta} \exp \left[-\frac{(h_z^n - \langle h_z \rangle - y)^2}{2\eta^2} \right]. \quad (\text{F.3})$$

Since we aim to describe measurements that at least partially project the nuclear spin state, we have $\eta < \sigma$. The POVM that describes such a measurement is given by

$$F_y = \sum_n f(n, y) |n\rangle \langle n|, \quad (\text{F.4})$$

with

$$\begin{aligned} f(n, y) &= \frac{\sigma}{\eta\sqrt{2\pi(\sigma^2 - \eta^2)}} \exp \left[-\frac{(h_z^n - \langle h_z \rangle - y)^2}{2\eta^2} \right] \\ &\times \exp \left[-\frac{(h_z^n - \langle h_z \rangle)^2}{2\sigma^2} - \frac{y^2}{2(\sigma^2 - \eta^2)} \right]. \end{aligned} \quad (\text{F.5})$$

We note that for $\eta \ll \sigma$ we have $f(n, y) \approx \exp(-(h_z^n - \langle h_z \rangle - y)^2/2\eta^2)/\sqrt{2\pi}\eta$. With $f(n, y)$, the operators F_y are fully determined and it is straightforward to calculate the probability for obtaining the measurement result $\langle h_z \rangle + y$

$$P(y) = \frac{1}{\sqrt{2\pi(\sigma^2 - \eta^2)}} \exp \left[-\frac{y^2}{2(\sigma^2 - \eta^2)} \right]. \quad (\text{F.6})$$

Clearly, the probabilities add up to one ($\int P(y)dy = 1$) as they should. Also, when weighting the $\rho'_I(n, n; y)$ with their probabilities for occurring, we find $\int \rho'_I(n, n; y)P(y)dy = \rho_I(n, n)$. Using Eq. (F.1) we thus find for the matrix elements after a measurement, when averaging over all possible measurement outcomes

$$\rho_I(n, m) \rightarrow \rho'_I(n, m) = \rho_I(n, m) \int \sqrt{f(n, y)f(m, y)}dy, \quad (\text{F.7})$$

with (for $\eta \ll \sigma$)

$$f(n, y) \approx \frac{1}{\sqrt{2\pi}\eta} \exp \left[-\frac{(h_z^n - h_{z0} - y)^2}{2\eta^2} \right]. \quad (\text{F.8})$$

Again, for $\eta \ll \sigma$, we thus have

$$\rho'_I(n, m) = \rho_I(n, m) \exp \left[-\frac{(h_z^n - h_z^m)^2}{8\eta^2} \right]. \quad (\text{F.9})$$

To reduce the off-diagonal elements, the measurement accuracy must be better than the difference in eigenvalues. In the limit $\eta \rightarrow 0$ a projective measurement is recovered, which sets all off-diagonal elements to zero. Up to t^2 in the short-time expansion, only off-diagonal elements between states that differ at most by two flip-flops can become non-zero. Thus, to have at least a partial Zeno effect, [132] resulting from the off-diagonal elements being partially reduced, the requirement on the measurement accuracy is $\eta \lesssim |h_z^n - h_z^m|$ with $|n\rangle = I_k^+ I_l^- I_p^+ I_q^- |m\rangle$. For coupling constants $A_k = Ae^{-k/N}/N$, we have typically $h_z^n - h_z^m \propto A/N$ and the minimally $h_z^n - h_z^m \gtrsim A/N^2$. Besides suppressing the off-diagonal elements of ρ_I through a measurement, there are also “natural” decoherence mechanisms, such as inhomogeneous quadrupolar splittings, electron-phonon coupling, or spin-lattice relaxation, that can lead to a reduction of the off-diagonal elements of ρ_I .

As mentioned earlier, there are several proposals [51, 72, 73] to implement a projective measurement of h_z . All of these proposed techniques rely on the fact that the dynamics of the electron spins confined in the dots depend on the Overhauser field. Thus, a measurement of the electron-spin dynamics allows one to indirectly measure h_z . The proposal in Ref. [73] is designed for optically active self-assembled quantum dots and makes use of an h_z -dependent frequency shift in an exciton transition. Numerical calculations for this method [73] show that an increase of the electron spin coherence time by a factor 100 is achievable with a preparation time of $10\mu\text{s}$, which corresponds to a measurement accuracy of $\eta = \sigma_0/100 = A/100\sqrt{N}$. The proposal in Ref. [51] considers gate-defined double quantum dots, like the ones in Refs. [28, 47, 48, 90]. The measurements of electron-spin dynamics are achieved through spin-to-charge conversion and detection of the charge by a nearby QPC. An experimental recipe in the context of the setup in Ref. [28] is presented in Ref. [75]. The narrowing (measurement accuracy) achievable with this method essentially relies on a good time-resolution of the QPC charge detection which by now has reached a few hundred nanoseconds [143].

An alternative read-out scheme is to use a double dot in the spin-blockade regime [30], where one spin, say the one in the left dot, is manipulated, while the one in the right dot is only needed for the readout. The system is initialized to the triplet $|\uparrow\uparrow\rangle$ which is spin-blocked since the triplet $T(0, 2)$ with two electrons on the right dot is energetically not accessible. The $|\downarrow\uparrow\rangle$ -state, however, may tunnel to the $S(0, 2)$ singlet and from there one electron can tunnel to the right lead if energetically allowed, leaving the two-electron system in a $(0, 1)$ -state. To describe these measurements we again use a set of POVM operators. There are two possible measurement outcomes which we denote t (tunneling) and n (no tunneling). The operators corresponding to these measurement results are $E_t = \epsilon_\downarrow |\downarrow\rangle\langle\downarrow| + (1 - \epsilon_\uparrow) |\uparrow\rangle\langle\uparrow|$ and $E_n = (1 - \epsilon_\downarrow) |\downarrow\rangle\langle\downarrow| + \epsilon_\uparrow |\uparrow\rangle\langle\uparrow|$. Here, ϵ_\downarrow is the probability to have measurement result t for the $|\downarrow\rangle$ -state, while ϵ_\uparrow is the probability to have result n for the $|\uparrow\rangle$ -state. The efficiency of this

read-out scheme generally depends on a large separation of the tunneling rates for the $|\uparrow\rangle$ state and the $|\downarrow\rangle$ state. If such a large separation, i.e., a good spin-blockade, can be achieved, this read-out method offers the potential for rapid consecutive electron-spin measurements and thus also for accurate measurements of the Overhauser field. A detailed analysis of this read-out scheme has, to our knowledge, not been undertaken yet and is beyond the scope of this work.

Bibliography

- [1] D. Loss and D. P. DiVincenzo, Phys. Rev. A **57**, 120 (1998).
- [2] A. Imamoglu, D. D. Awschalom, G. Burkard, D. P. DiVincenzo, D. Loss, M. Sherwin, and A. Small, Phys. Rev. Lett. **83**, 4204 (1999).
- [3] D. D. Awschalom, N. Samarth, and D. Loss, *Semiconductor Spintronics and Quantum Computation*, Springer, Berlin, 2002.
- [4] I. Zutic, J. Fabian, and S. D. Sarma, Rev. Mod. Phys. **76**, 323 (2004).
- [5] D. P. DiVincenzo, D. Bacon, J. Kempe, G. Burkard, and K. B. Whaley, Nature **408**, 339 (2000).
- [6] S. I. Erlingsson, Y. V. Nazarov, and V. I. Fal'ko, Phys. Rev. B **64**, 195306 (2001).
- [7] S. I. Erlingsson and Y. V. Nazarov, Phys. Rev. B **66**, 155327 (2002).
- [8] V. N. Golovach, A. Khaetskii, and D. Loss, Phys. Rev. Lett. **93**, 016601 (2004).
- [9] A. V. Khaetskii and Y. V. Nazarov, Phys. Rev. B **64**, 125316 (2001).
- [10] S. Amasha, K. Maclean, I. P. Radu, D. M. Zumbühl, M. A. Kastner, M. P. Hanson, and A. C. Gossard, Phys. Rev. Lett. **100**, 046803 (2008).
- [11] M. A. Kastner, Physics Today **46**, 24 (1993).
- [12] L. L. Foldy and S. A. Wouthuysen, Phys. Rev. **78**, 29 (1950).
- [13] R. A. Frosch and H. M. Foley, Phys. Rev. **88**, 1337 (1952).
- [14] C. G. Darwin, Proc. Roy. Soc. **118A**, 654 (1928).
- [15] E. Fermi, Zeitschrift fur Physik **60**, 320 (1930).
- [16] U. Meirav, M. A. Kastner, and S. J. Wind, Phys. Rev. Lett. **65**, 771 (1990).

-
- [17] D. Leonard, M. Krishnamurthy, C. M. Reaves, S. P. Denbaars, and P. M. Petroff, *Appl. Phys. Lett.* **63**, 3203 (1993).
- [18] S. Tarucha, D. G. Austing, T. Honda, R. J. van der Hage, and L. P. Kouwenhoven, *Phys. Rev. Lett.* **77**, 3613 (1996).
- [19] B. T. Miller, W. Hansen, S. Manus, R. J. Luyken, A. Lorke, J. P. Kotthaus, S. Huant, G. Medeiros-Ribeiro, and P. M. Petroff, *Phys. Rev. B* **56**, 6764 (1997).
- [20] M. Ciorga, A. S. Sachrajda, P. Hawrylak, C. Gould, P. Zawadzki, S. Julian, Y. Feng, and Z. Wasilewski, *Phys. Rev. B* **61**, R16315 (2000).
- [21] P. M. Petroff, A. Lorke, and A. Imamoglu, *Physics Today* **54**, 46 (2001).
- [22] L. P. Kouwenhoven, D. G. Austing, and S. Tarucha, *Rep. Prog. Phys.* **64**, 701 (2001).
- [23] J. M. Elzerman, R. Hanson, J. S. Greidanus, L. H. Willems van Beveren, S. De Franceschi, L. M. K. Vandersypen, S. Tarucha, and L. P. Kouwenhoven, *Phys. Rev. B* **67**, 161308(R) (2003).
- [24] J. R. Petta, A. C. Johnson, C. M. Marcus, M. P. Hanson, and A. C. Gossard, *Phys. Rev. Lett.* **93**, 186802 (2004).
- [25] D. M. Zumbühl, C. M. Marcus, M. P. Hanson, and A. C. Gossard, *Phys. Rev. Lett.* **93**, 256801 (2004).
- [26] R. Schleser, E. Ruh, T. Ihn, K. Ensslin, D. C. Driscoll, and A. C. Gossard, *Appl. Phys. Lett.* **85**, 2005 (2004).
- [27] N. Mason, M. J. Biercuk, and C. M. Marcus, *Science* **303**, 655 (2004).
- [28] J. R. Petta, A. C. Johnson, J. M. Taylor, E. A. Laird, A. Yacoby, M. D. Lukin, C. M. Marcus, M. P. Hanson, and A. C. Gossard, *Science* **309**, 2180 (2005).
- [29] P. Jarillo-Herrero, J. Kong, H. S. J. van der Zant, C. Dekker, L. P. Kouwenhoven, and S. De Franceschi, *Phys. Rev. Lett.* **94**, 156802 (2005).
- [30] F. H. L. Koppens, C. Buizert, K. J. Tielrooij, I. T. Vink, K. C. Nowack, T. Meunier, L. P. Kouwenhoven, and L. M. K. Vandersypen, *Nature* **442**, 766 (2006).
- [31] M. R. Gräber, W. A. Coish, C. Hoffmann, M. Weiss, J. Furer, S. Oberholzer, D. Loss, and C. Schönenberger, *Phys. Rev. B* **74**, 075427 (2006).
- [32] I. Shorubalko, A. Pfund, R. Leturcq, M. T. Borgström, F. Gramm, E. Müller, E. Gini, and K. Ensslin, *Nanotechnology* **18**, 4014 (2007).

-
- [33] C. Fasth, A. Fuhrer, L. Samuelson, V. N. Golovach, and D. Loss, *Phys. Rev. Lett.* **98**, 266801 (2007).
- [34] C. B. Simmons, M. Thalakulam, N. Shaji, L. J. Klein, H. Qin, R. H. Blick, D. E. Savage, M. G. Lagally, S. N. Coppersmith, and M. A. Eriksson, *Appl. Phys. Lett.* **91**, 3103 (2007).
- [35] Y. Hu, H. O. H. Churchill, D. J. Reilly, J. Xiang, C. M. Lieber, and C. M. Marcus, *Nature Nanotechnology* **2**, 622 (2007).
- [36] H. Ingerslev Jørgensen, K. Grove-Rasmussen, K.-Y. Wang, A. M. Blackburn, K. Flensberg, P. E. Lindelof, and D. A. Williams, arXiv:0711.3245 (2007).
- [37] R. Hanson, L. P. Kouwenhoven, J. R. Petta, S. Tarucha, and L. M. K. Vandersypen, *Rev. Mod. Phys.* **79**, 1217 (2007).
- [38] N. J. Stone, *Atomic Data and Nuclear Data Tables* **90**, 75 (2005).
- [39] D. Paget, G. Lampel, B. Sapoval, and V. I. Safarov, *Phys. Rev. B* **15**, 5780 (1977).
- [40] R.-B. Liu, W. Yao, and L. J. Sham, *New Journal of Physics* **9**, 226 (2007).
- [41] J. Schliemann, A. Khaetskii, and D. Loss, *J. Phys.: Condens. Matter* **15**, 1809 (2003).
- [42] W. A. Coish, J. Fischer, and D. Loss, *Phys. Rev. B* **77**, 125329 (2008).
- [43] G. Burkard, D. Loss, and D. P. DiVincenzo, *Phys. Rev. B* **59**, 2070 (1999).
- [44] A. V. Khaetskii, D. Loss, and L. Glazman, *Phys. Rev. Lett.* **88**, 186802 (2002).
- [45] I. A. Merkulov, A. L. Efros, and M. Rosen, *Phys. Rev. B* **65**, 205309 (2002).
- [46] W. A. Coish and D. Loss, *Phys. Rev. B* **70**, 195340 (2004).
- [47] A. C. Johnson, J. R. Petta, J. M. Taylor, A. Yacoby, M. D. Lukin, C. M. Marcus, M. P. Hanson, and A. C. Gossard, *Nature* **435**, 925 (2005).
- [48] F. H. L. Koppens, J. A. Folk, J. M. Elzerman, R. Hanson, L. H. W. van Beveren, I. T. Vink, H. P. Tranitz, W. Wegscheider, L. P. Kouwenhoven, and L. M. K. Vandersypen, *Science* **309**, 1346 (2005).

-
- [49] F. H. L. Koppens, D. Klauser, W. A. Coish, K. C. Nowack, L. P. Kouwenhoven, D. Loss, and L. M. K. Vandersypen, *Phys. Rev. Lett.* **99**, 106803 (2007).
- [50] W. A. Coish and D. Loss, *Phys. Rev. B* **72**, 125337 (2005).
- [51] D. Klauser, W. A. Coish, and D. Loss, *Phys. Rev. B* **73**, 205302 (2006).
- [52] E. A. Laird, J. R. Petta, A. C. Johnson, C. M. Marcus, A. Yacoby, M. P. Hanson, and A. C. Gossard, *Phys. Rev. Lett.* **97**, 056801 (2006).
- [53] A. M. Steane, *Phys. Rev. A* **68**, 042322 (2003).
- [54] B. M. Terhal and G. Burkard, *Phys. Rev. A* **71**, 012336 (2005).
- [55] D. Gottesman, *quant-ph/0701112* (2007).
- [56] P. Aliferis and J. Preskill, *arXiv:0710.1301* (2007).
- [57] D. Gammon, A. L. Efros, T. A. Kennedy, M. Rosen, D. S. Katzer, D. Park, S. W. Brown, V. L. Korenev, and I. A. Merkulov, *Phys. Rev. Lett.* **86**, 5176 (2001).
- [58] A. S. Bracker, E. A. Stinaff, D. Gammon, M. E. Ware, J. G. Tischler, A. Shabaev, A. L. Efros, D. Park, D. Gershoni, V. L. Korenev, and I. A. Merkulov, *Phys. Rev. Lett.* **94**, 047402 (2005).
- [59] A. Imamoglu, E. Knill, L. Tian, and P. Zoller, *Phys. Rev. Lett.* **91**, 017402 (2003).
- [60] J. Baugh, Y. Kitamura, K. Ono, and S. Tarucha, *Phys. Rev. Lett.* **99**, 096804 (2007).
- [61] C. W. Lai, P. Maletinsky, A. Badolato, and A. Imamoglu, *Phys. Rev. Lett.* **96**, 167403 (2006).
- [62] P.-F. Braun, B. Urbaszek, T. Amand, X. Marie, O. Krebs, B. Eble, A. Lemaître, and P. Voisin, *Phys. Rev. B* **74**, 245306 (2006).
- [63] B. Urbaszek, P.-F. Braun, T. Amand, O. Krebs, T. Belhadj, A. Lemaître, P. Voisin, and X. Marie, *Phys. Rev. B* **76**, 201301 (2007).
- [64] P. Simon and D. Loss, *Phys. Rev. Lett.* **98**, 156401 (2007).
- [65] P. Simon, B. Braunecker, and D. Loss, *Phys. Rev. B* **77**, 045108 (2008).
- [66] S. Takahashi, R. Hanson, J. van Tol, M. S. Sherwin, and D. D. Awschalom, *arXiv:0804.1537* (2008).

-
- [67] S. Chesi and D. Loss, arXiv:0804.3332 (2008).
- [68] E. L. Hahn, Phys. Rev. **80**, 580 (1950).
- [69] N. Shenvi, R. de Sousa, and K. B. Whaley, Phys. Rev. B **71**, 144419 (2005).
- [70] W. Yao, R.-B. Liu, and L. J. Sham, Phys. Rev. B **74**, 195301 (2006).
- [71] F. H. L. Koppens, K. C. Nowack, and L. M. K. Vandersypen, arXiv:0711:0479 (2007).
- [72] G. Giedke, J. M. Taylor, D. D'Alessandro, M. D. Lukin, and A. Imamoglu, Phys. Rev. A **74**, 032316 (2006).
- [73] D. Stepanenko, G. Burkard, G. Giedke, and A. Imamoglu, Phys. Rev. Lett. **96**, 136401 (2006).
- [74] A. Peres, *Quantum Theory: Concepts and Methods*, Kluwer Academic Publishers, New York, 1993.
- [75] D. Klauser, W. A. Coish, and D. Loss, Adv. in solid state physics **46**, 17 (2007).
- [76] A. Greilich, A. Shabaev, D. R. Yakovlev, A. L. Efros, I. A. Yugova, D. Reuter, A. D. Wieck, and M. Bayer, Science **317**, 1896 (2007).
- [77] P. Maletinsky, A. Badolato, and A. Imamoglu, Phys. Rev. Lett. **99**, 056804 (2007).
- [78] K. Ono and S. Tarucha, Phys. Rev. Lett. **92**, 256803 (2004).
- [79] P. Maletinsky, C. W. Lai, A. Badolato, and A. Imamoglu, Phys. Rev. B **75**, 035409 (2007).
- [80] A. I. Tartakovskii, T. Wright, A. Russell, V. I. Fal'Ko, A. B. van'Kov, J. Skiba-Szymanska, I. Drouzas, R. S. Kolodka, M. S. Skolnick, P. W. Fry, A. Tahraoui, H.-Y. Liu, and M. Hopkinson, Phys. Rev. Lett. **98**, 026806 (2007).
- [81] A. Russell, V. I. Fal'Ko, A. I. Tartakovskii, and M. S. Skolnick, Phys. Rev. B **76**, 195310 (2007).
- [82] R. Kaji, S. Adachi, H. Sasakura, and S. Muto, Phys. Rev. B **77**, 115345 (2008).
- [83] J. Iñarrea, C. Lopez-Monis, A. H. MacDonald, and G. Platero, Appl. Phys. Lett. **91**, 2112 (2007).

-
- [84] M. S. Rudner and L. S. Levitov, Phys. Rev. Lett. **99**, 036602 (2007).
- [85] M. S. Rudner and L. S. Levitov, Phys. Rev. Lett. **99**, 246602 (2007).
- [86] J. Danon and Y. V. Nazarov, Phys. Rev. Lett. **100**, 056603 (2008).
- [87] H.-A. Engel and D. Loss, Science **309**, 586 (2005).
- [88] V. Cerletti, W. A. Coish, O. Gywat, and D. Loss, Nanotechnology **16**, R27 (2005).
- [89] K. Ono, D. G. Austing, Y. Tokura, and S. Tarucha, Science **297**, 1313 (2002).
- [90] T. Hatano, M. Stopa, and S. Tarucha, Science **309**, 268 (2005).
- [91] A. Khaetskii, D. Loss, and L. Glazman, Phys. Rev. B **67**, 195329 (2003).
- [92] M. V. Dutt, J. Cheng, B. Li, X. Xu, X. Li, P. R. Berman, D. G. Steel, A. S. Bracker, D. Gammon, S. E. Economou, R.-B. Liu, and L. J. Sham, Phys. Rev. Lett. **94**, 227403 (2005).
- [93] R. de Sousa and S. Das Sarma, Phys. Rev. B **67**, 033301 (2003).
- [94] N. Shenvi, R. de Sousa, and K. B. Whaley, Phys. Rev. B **71**, 224411 (2005).
- [95] D. Paget, Phys. Rev. B **25**, 4444 (1982).
- [96] Y. Kato, R. C. Myers, D. C. Driscoll, A. C. Gossard, J. Levy, and D. D. Awschalom, Science **299**, 1201 (2003).
- [97] J. Levy, Phys. Rev. Lett. **89**, 147902 (2002).
- [98] C. P. Slichter, *Principles of Magnetic Resonance*, Springer Verlag, Berlin, 1989.
- [99] B. H. Armstrong, J. Quant. Spectrosc. Radiat. Transfer **7**, 61 (1967).
- [100] A. M. Stoneham, J. Phys. D: Appl. Phys. **5**, 670 (1972).
- [101] P. Minguzzi and A. di Lieto, J. Mol. Spectrosc. **109**, 388 (1985).
- [102] H.-A. Engel, V. N. Golovach, D. Loss, L. M. K. Vandersypen, J. M. Elzerman, R. Hanson, and L. P. Kouwenhoven, Phys. Rev. Lett. **93**, 106804 (2004).
- [103] M. Borhani, V. N. Golovach, and D. Loss, Phys. Rev. B **73**, 155311 (2006).

-
- [104] A. Barenco, C. H. Bennett, R. Cleve, D. P. DiVincenzo, N. Margolus, P. Shor, T. Sleator, J. A. Smolin, and H. Weinfurter, *Phys. Rev. A* **52**, 3457 (1995).
- [105] R. Requist, J. Schliemann, A. G. Abanov, and D. Loss, *Phys. Rev. B* **71**, 115315 (2005).
- [106] F. Bloch, *Phys. Rev.* **70**, 460 (1946).
- [107] D. P. Divincenzo and D. Loss, *Phys. Rev. B* **71**, 035318 (2005).
- [108] J. M. Taylor, J. R. Petta, A. C. Johnson, A. Yacoby, C. M. Marcus, and M. D. Lukin, *Phys. Rev. B* **76**, 035315 (2007).
- [109] G. Ithier, E. Collin, P. Joyez, P. J. Meeson, D. Vion, D. Esteve, F. Chiarello, A. Shnirman, Y. Makhlin, J. Schrieffer, and G. Schön, *Phys. Rev. B* **72**, 134519 (2005).
- [110] A. V. Khaetskii and Y. V. Nazarov, *Phys. Rev. B* **61**, 12639 (2000).
- [111] J. M. Elzerman, R. Hanson, L. H. Willems van Beveren, B. Witkamp, L. M. K. Vandersypen, and L. P. Kouwenhoven, *Nature* **430**, 431 (2004).
- [112] M. Kroutvar, Y. Ducommun, D. Heiss, M. Bichler, D. Schuh, G. Abstreiter, and J. J. Finley, *Nature* **432**, 81 (2004).
- [113] S. Amasha, K. MacLean, I. Radu, D. M. Zumbuhl, M. A. Kastner, M. P. Hanson, and A. C. Gossard, *arXiv:cond-mat/0607110* (2006).
- [114] C. Deng and X. Hu, *Phys. Rev. B* **73**, 241303(R) (2006), Erratum: *Phys. Rev. B* **74**, 129902(E) (2006).
- [115] V. V. Dobrovitski, H. A. de Raedt, M. I. Katsnelson, and B. N. Harmon, *Phys. Rev. Lett.* **90**, 210401 (2003).
- [116] R.-S. Huang, V. Dobrovitski, and B. Harmon, *arXiv:cond-mat/0504449* (2005).
- [117] F. Jelezko, T. Gaebel, I. Popa, A. Gruber, and J. Wrachtrup, *Phys. Rev. Lett.* **92**, 076401 (2004).
- [118] R. Hanson, O. Gywat, and D. D. Awschalom, *Phys. Rev. B* **74**, 161203(R) (2006).
- [119] L. Childress, M. V. G. Dutt, J. M. Taylor, A. S. Zibrov, F. Jelezko, J. Wrachtrup, P. R. Hemmer, and M. D. Lukin, *Science* **314**, 281 (2006).
- [120] J. Wrachtrup, S. Y. Kilin, and A. P. Nizovtsev, *Optics and Spectroscopy* **91**, 429 (2001).

-
- [121] W. A. Coish and D. Loss, Phys. Rev. B **75**, 161302(R) (2007).
- [122] A. K. Hüttel, J. Weber, A. W. Holleitner, D. Weinmann, K. Eberl, and R. H. Blick, Phys. Rev. B **69**, 073302 (2004).
- [123] D. J. Reilly, J. M. Taylor, E. A. Laird, J. R. Petta, C. M. Marcus, M. P. Hanson, and A. C. Gossard, arXiv:0712.4033 (2007).
- [124] M. N. Makhonin, A. I. Tartakovskii, I. Drouzas, A. B. Van'kov, T. Wright, J. Skiba-Szymanska, A. Russell, V. I. Fal'ko, M. S. Skolnick, H.-Y. Liu, and M. Hopkinson, arXiv:0708.2792 (2007).
- [125] J. R. Petta, J. M. Taylor, A. C. Johnson, A. Yacoby, M. D. Lukin, C. M. Marcus, M. P. Hanson, and A. C. Gossard, Phys. Rev. Lett. **100**, 067601 (2008).
- [126] S. Foletti, J. Martin, M. Dolev, D. Mahalu, V. Umansky, and A. Yacoby, arXiv:0801.3613 (2008).
- [127] D. J. Reilly, J. M. Taylor, J. R. Petta, C. M. Marcus, M. P. Hanson, and A. C. Gossard, arXiv:0803.3082 (2008).
- [128] H. Christ, J. I. Cirac, and G. Giedke, Phys. Rev. B **75**, 155324 (2007).
- [129] C. Deng and X. Hu, Phys. Rev. B **72**, 165333 (2005).
- [130] B. Misra and E. C. G. Sudarshan, J. Math. Phys. **18**, 756 (1977).
- [131] J. von Neumann, *Mathematische Grundlagen der Quantenmechanik*, , Springer, Berlin, 1932, [transl. by E.T. Beyer: *Mathematical Foundations of Quantum Mechanics*, Princeton Univ. Press (1955)].
- [132] K. Koshino and A. Shimizu, Phys. Rep. **412**, 191 (2005).
- [133] F. Helmer, M. Mariantoni, E. Solano, and F. Marquardt, arXiv:0712.1908 (2007).
- [134] J. Gambetta, A. Blais, M. Boissonneault, A. A. Houck, D. I. Schuster, and S. M. Girvin, Phys. Rev. A **77**, 012112 (2008).
- [135] W. M. Itano, D. J. Heinzen, J. J. Bollinger, and D. J. Wineland, Phys. Rev. A **41**, 2295 (1990).
- [136] R. G. Shulman, B. J. Wyluda, and P. W. Anderson, Phys. Rev. **107**, 953 (1957).
- [137] N. F. Ramsey and E. M. Purcell, Phys. Rev. **85**, 143 (1952).
- [138] J. R. Schrieffer and P. A. Wolff, Phys. Rev. **149**, 491 (1966).

-
- [139] J. Schliemann, A. V. Khaetskii, and D. Loss, *Phys. Rev. B* **66**, 245303 (2002).
- [140] K. Blum, *Density Matrix Theory and Applications*, Plenum, New York, 1996.
- [141] E. Fick and G. Sauermaun, *The Quantum Statistics of Dynamic Processes*, Springer-Verlag, Berlin, 1990.
- [142] D. Mao and P. C. Taylor, *Phys. Rev. B* **52**, 5665 (1995).
- [143] D. J. Reilly, C. M. Marcus, M. P. Hanson, and A. C. Gossard, *Appl. Phys. Lett.* **91**, 2101 (2007).

Curriculum Vitae

von Daniel Joseph Klauser
Geboren am 14. Oktober 1981 in Römerswil, Schweiz
Staatsangehörigkeit: Schweizer

Ausbildung

- | | |
|-----------|--|
| 1994–1995 | Sekundarschule in Beromünster (LU). |
| 1995–1997 | Gymnasium in Beromünster (LU). |
| 1998 | Schüleraustauschjahr am Wellington College, Wellington, Neuseeland. |
| 1999–2000 | Gymnasium in Beromünster (LU). |
| Juni 2000 | Matura (Typus B). |
| 2000–2004 | Studium der Physik, Mathematik und Philosophie an der Universität Bern. |
| Dez. 2004 | Msc. in Physik.
Masterarbeit “Relativistic quantum mechanics of interacting particles” in theoretischer Physik unter der Leitung von Prof. U.-J. Wiese. |
| 2005–2008 | Promotionsstudium in Theoretischer Physik an der Universität Basel. Dissertation “Hyperfine interaction and spin decoherence in quantum dots” unter der Anleitung von Prof. Daniel Loss. |

Publikationen

Nuclear spin dynamics and Zeno effect in quantum dots and defect centers

D. Klauser, W.A. Coish, Daniel Loss

arXiv:0802.2463v1, submitted to Phys. Rev. B

Electron and hole spin dynamics and decoherence in quantum dots

D. Klauser, D.V. Bulaev, W.A. Coish and Daniel Loss

arXiv:0706.1514v1, Chapter 10 in Semiconductor Quantum Bits, eds. O. Benson and F. Henneberger, World Scientific, (2008). ISBN 978-981-4241-05-2.

Universal phase shift and non-exponential decay of driven single-spin oscillations

F.H.L. Koppens, D. Klauser, W.A. Coish, K.C. Nowack, L.P. Kouwenhoven, D. Loss, L.M.K. Vandersypen

Phys. Rev. Lett. 99, 106803 (2007)

Quantum-dot spin qubit and hyperfine interaction

D.Klauser, W.A. Coish and Daniel Loss

Advances in Solid State Physics 46, p.17-29, (2007)

Nuclear spin state narrowing via gate-controlled Rabi oscillations in a double quantum dot

D. Klauser, W.A. Coish, Daniel Loss

Phys. Rev. B 73, 205302 (2006)